

**DIELECTRIC AND ELECTRICAL CHARACTERISTICS OF
PALM OIL-BASED NANOFLUID AS HIGH VOLTAGE
INSULATION MATERIAL**

MOHAMAD ZUL HILMEY BIN MAKMUD

**FACULTY OF ENGINEERING
UNIVERSITY OF MALAYA
KUALA LUMPUR**

2019

**DIELECTRIC AND ELECTRICAL CHARACTERISTICS
OF PALM OIL-BASED NANOFLUID AS HIGH
VOLTAGE INSULATION MATERIAL**

MOHAMAD ZUL HILMEY BIN MAKMUD

**THESIS SUBMITTED IN FULFILMENT OF THE
REQUIREMENTS FOR THE DEGREE OF DOCTOR OF
PHILOSOPHY**

**FACULTY OF ENGINEERING
UNIVERSITY OF MALAYA
KUALA LUMPUR**

2019

UNIVERSITY OF MALAYA
ORIGINAL LITERARY WORK DECLARATION

Name of Candidate: **MOHAMAD ZUL HILMEY BIN MAKMUD**

Matric No: **KHA150068**

Name of Degree: **DOCTOR OF PHILOSOPHY**

Title of Project Paper/Research Report/Dissertation/Thesis ("this Work"):

DIELECTRIC AND ELECTRICAL CHARACTERISTICS OF PALM OIL-BASED NANOFLUID AS HIGH VOLTAGE INSULATION MATERIAL Field of Study:

HIGH VOLTAGE ENGINEERING

I do solemnly and sincerely declare that:

- (1) I am the sole author/writer of this Work;
- (2) This Work is original;
- (3) Any use of any work in which copyright exists was done by way of fair dealing and for permitted purposes and any excerpt or extract from, or reference to or reproduction of any copyright work has been disclosed expressly and sufficiently and the title of the Work and its authorship have been acknowledged in this Work;
- (4) I do not have any actual knowledge nor do I ought reasonably to know that the making of this work constitutes an infringement of any copyright work;
- (5) I hereby assign all and every rights in the copyright to this Work to the University of Malaya ("UM"), who henceforth shall be owner of the copyright in this Work and that any reproduction or use in any form or by any means whatsoever is prohibited without the written consent of UM having been first had and obtained;
- (6) I am fully aware that if in the course of making this Work I have infringed any copyright whether intentionally or otherwise, I may be subject to legal action or any other action as may be determined by UM.

Candidate's Signature

Date:

Subscribed and solemnly declared before,

Witness's Signature

Date:

Name:

Designation:

ABSTRACT

High voltage (HV) transformer is one of the most important apparatus in power industries. With an increase of power demand, the rated power of a HV transformer is also increasing rapidly. Hence, the need to provide insulation material for a transformer without any risk of failure is essential. Nowadays, nanofluid is one of the insulation materials most widely studied. Although many researches have been done on nanofluid breakdown strength in the past, there is still lack of work on the influence of nanoparticle types and concentrations on dielectric characteristics of palm oil-based nanofluids as HV insulation in coming future. Therefore, in this work, investigation on the effects of conductive and semiconductive nanoparticles towards dielectric responses of palm oil-based nanofluids has been conducted. Iron (II,III) oxide, Fe_3O_4 (conductive) and Titanium dioxide, TiO_2 (semiconductive) are utilized as the nanoparticle due to their capabilities to trap electrons and have higher dissolution rate in a neutral suspension. The responses of electrical characteristics such as; dielectric properties, current-voltage (I-V) curves, partial discharge (PD) activities and breakdown voltage (BDV) were measured from base oil and six types of nanofluid samples. A stability analysis was also performed to investigate the influence of nanoparticles and their amount of concentrations on dispersion characteristics of nanofluid insulation. As overall, the findings from this research indicate that palm oil with conductive nanoparticles at a very low amount of concentration (in this work, 0.01 g/L) is the most effective nanofluid insulation. In terms of reliability, palm oil with semiconductive nanoparticles is more practical as insulating material due to its aggregation stability and consistency as electrons trap although in higher amount of particle concentration (in this case, 1.0 g/L).

Keywords: High voltage engineering, nanofluid insulation, dielectric characteristics, breakdown voltage, partial discharge.

ABSTRAK

Transformer voltan tinggi adalah merupakan salah satu peralatan terpenting di dalam industri tenaga. Dengan peningkatan bilangan permintaan tenaga, maka kadaran kuasa untuk transformer voltan tinggi turut meningkat dengan pesat. Dengan demikian, keperluan untuk menyediakan bahan penebatan bagi transformer tanpa berlakunya risiko kegagalan adalah mustahak. Hari ini, nanobendalir adalah salah satu bahan penebatan yang banyak dikaji. Walaupun banyak penyelidikan telah dibuat berkaitan kekuatan pecah-tebat bagi nanobendalir pada masa lalu, tetapi di sana masih terlalu sedikit rujukan terhadap pengaruh jenis nanopartikel serta kepekatan pada ciri-ciri dielektrik bagi nanobendalir berasaskan minyak sawit sebagai penebatan voltan tinggi pada masa akan datang. Maka di dalam kajian ini, penyiasatan mengenai kesan-kesan nanopartikel konduktif dan semikonduktif terhadap tindak balas dielektrik bagi nanobendalir berasaskan minyak sawit telah dijalankan. Iron (II,III) oksida, Fe_3O_4 (konduktif) dan Titanium dioksida, TiO_2 (semikonduktif) digunakan sebagai nanopartikel disebabkan kebolehan bahan ini memerangkap elektron dan kadar penguraianya yang tinggi di dalam larutan neutral. Tindak balas bagi ciri-ciri elektrik seperti; sifat dielektrik, lekuk arus-voltan (I-V), aktiviti nyahcas separa (PD), dan kekuatan pecah-tebat (BDV) telah diukur dari minyak asas dan enam jenis sampel nanobendalir. Satu analisis kestabilan juga dilaksanakan bagi menyiasat kesan nanopartikel dan amaun kepekatan pada ciri serakan nanobendalir. Secara keseluruhan, dapatan dari kajian ini menunjukkan bahawa minyak sawit dengan nanopartikel konduktif pada amaun kepekatan yang terendah (dalam kajian ini, 0.01 g/L) adalah paling efektif sebagai penebatan nanobendalir. Dari segi kebolehpercayaan, minyak sawit dengan nanopartikel semikonduktif adalah lebih praktikal sebagai bahan penebatan disebabkan kestabilan agregasinya dan konsisten sebagai pemerangkap elektron walaupun dalam kadar kepekatan partikel yang tinggi (dalam kes ini, 1.0 g/L).

Kata kunci: Kejuruteraan voltan tinggi, penebat nanobendalir, ciri-ciri dielektrik, voltan pecah-tebat, nyahcas separa.

University of Malaya

ACKNOWLEDGEMENTS

All praise is due to Allah, the Most Gracious and the Most Merciful.

First and foremost, I would like to express my gratitude to my supervisors, Associate Professor Ir. Dr. Hazlee Azil Illias and Associate Professor Ir. Dr. Ching Yern Chee for their countless guidance, advice and support throughout my PhD journey. Their professionalism always inspires me. Their expertise always impresses me. Their enthusiasm always motivates me.

I am thankful to all the staffs, graduate students of University Malaya High Voltage Research Group (UMHVRG) and my colleague; Sameh Dabbak, Gamil Al-Tamimi, Fuad Erman, and Tuan Ahmad Zahidi for their help on testing, discussion, opinion and technical assistance throughout my study.

I could not have completed this work without the support and help of many people. I am highly indebted to Universiti Malaysia Sabah (UMS) and University of Malaya (UM) for the sponsorship through Skim Latihan Bumiputera (SLAB) and Postgraduate Research Fund (PG236-2016A).

Last but not least, I would also like to extend my deepest gratitude to my father; Makmud Abdullah (alm), my mother; Siti Arbe Hj Mokhtar, brothers, sisters, my wife Nur Izzati Ishak and my children; Ahmad Yassin, Umar Mukhtar, Kauthar Hana, and Maryam Busyra for all their endless love, prayers and support, which have provided me strength and courage to complete my PhD journey.

Appreciate the efforts and contributions shared by individuals whose names are not mentioned above. Thank you!

TABLE OF CONTENTS

Abstract	iii
Abstrak	iv
Acknowledgements	vi
Table of Contents	vii
List of Figures	xii
List of Tables	xv
List of Symbols and Abbreviations	xvi
 CHAPTER 1: INTRODUCTION	 1
1.1 Background of the study	1
1.2 Problem statement	3
1.3 Aim and objectives	5
1.4 Contributions of the research	5
1.5 Research scope	6
1.6 Thesis outline	6
 CHAPTER 2: LITERATURE REVIEW	 8
2.1 Introduction	8
2.2 High voltage insulation material	8
2.2.1 Conventional mineral oil and related hazards	8
2.2.2 Natural ester-based liquid insulation	9
2.2.3 Vegetable oils	12
2.2.4 Methods to improve the vegetable oil as insulation oil	13
2.2.4.1 Antioxidant	14
2.2.4.2 Chemical additive	15

2.2.4.3	Esterification and trans-esterification.....	16
2.2.4.4	Addition of nanoparticles	16
2.3	Nanofluid as high voltage insulation material	17
2.3.1	Synthesis and nanofluid characterization	18
2.3.1.1	One-step synthesis method.....	19
2.3.1.2	Two-step synthesis method	20
2.3.2	Stability treatment techniques	21
2.3.2.1	Physical treatment	21
2.3.2.2	Chemical treatment	23
2.3.3	Stability characterization method	24
2.3.3.1	Sedimentation analysis	24
2.3.3.2	Electron microscopy.....	25
2.3.3.3	Light scattering.....	26
2.3.3.4	Zeta potential.....	27
2.4	Dielectric and electrical performance of nanofluid insulation	28
2.4.1	Measurement of dielectric permittivity and losses.....	34
2.4.2	Measurement of electrical conductivity	36
2.4.3	Measurement of partial discharge activities	38
2.4.4	Measurement of breakdown strength	42
2.5	Effects of nanoparticles on enhancement mechanism of nanofluid insulation.....	45
2.5.1	Effect of nanoparticle properties	45
2.5.2	Effect of mass fraction	47
2.5.3	Effect of interfacial layers	48
2.6	Summary.....	49
CHAPTER 3: METHODOLOGY		51
3.1	Introduction.....	51

3.2	Material preparation.....	52
3.2.1	Base oil	52
3.2.2	Nanoparticles	52
3.2.3	Drying process.....	53
3.3	Synthesis of nanofluid	54
3.3.1	Amount of nanoparticles	54
3.3.2	Ultrasonication	55
3.4	Dispersion characterization techniques	55
3.4.1	Crystallinity test	56
3.4.2	Sedimentation analysis	56
3.4.3	Agglomeration size.....	57
3.4.4	Particle distribution	57
3.5	Dielectric and electrical measurements	58
3.5.1	Dielectric properties	58
3.5.1.1	Experiment setup.....	58
3.5.1.2	Test chamber	59
3.5.1.3	Dielectric constant and losses	59
3.5.1.4	Current-voltage (I-V)	60
3.5.2	Partial discharge	61
3.5.2.1	Experiment setup.....	61
3.5.2.2	PD test chamber	62
3.5.2.3	Charge calibration	63
3.5.2.4	Partial discharge inception voltage (PDIV).....	64
3.5.2.5	Phase resolved partial discharge (PRPD) pattern.....	64
3.5.3	Breakdown voltage.....	66
3.5.3.1	Experiment setup.....	66

3.5.3.2	BDV test chamber	66
3.5.3.3	Weibull distribution.....	67
3.6	Electric field simulation.....	68
3.6.1	Model geometry and parameters	68
3.6.2	Boundary condition	69
3.6.3	Meshing	71
3.7	Summary.....	72
CHAPTER 4: RESULTS AND DISCUSSION		73
4.1	Introduction.....	73
4.2	Dispersion characteristics of palm oil-based nanofluid insulation.....	73
4.2.1	Crystalline size of dispersed nanoparticles.....	73
4.2.2	Sedimentation analysis with elapsed time.....	74
4.2.3	Agglomeration size observation under SEM.....	76
4.2.4	Particles distribution assessment using Zetasizer.....	77
4.2.5	Discussion	78
4.3	Dielectric properties of palm oil-based nanofluid insulation	79
4.3.1	Effect of nanoparticles on dielectric constant	80
4.3.2	Effect of nanoparticles on dielectric loss	82
4.3.3	Effect of nanoparticles on dielectric conduction	84
4.3.4	Discussion	86
4.4	Resistance to PD of palm oil-based nanofluid insulation.....	89
4.4.1	PD activities at inception condition.....	89
4.4.2	PD activities at steady state condition.....	91
4.4.2.1	Effect of nanoparticle type on PD resistance	91
4.4.2.2	Effect of applied voltage amplitude on PD activity	94
4.4.2.3	Effect of nanoparticles concentration on PD activity.....	96

4.4.3	Discussion	98
4.5	Breakdown strength of palm oil-based nanofluid insulation.....	100
4.5.1	Effect of nanoparticle type on breakdown strength.....	101
4.5.2	Effect of nanoparticle weight fraction on breakdown voltage	102
4.5.3	Effect of nanoparticles treatment on breakdown voltage	105
4.5.4	Discussion	107
4.6	Electric field distribution	109
4.7	Summary.....	112
CHAPTER 5: CONCLUSIONS AND FUTURE WORK		114
5.1	Conclusions	114
5.2	Future work.....	116
References		117
List of Publications and Papers Presented		130

LIST OF FIGURES

Figure 1.1: Oil-immersed distribution transformer with liquid insulation volume versus rated power (EWT transformer sdn bhd)	2
Figure 2.1: Comparison chart of natural ester and other types of transformer oil (Oommen, 2002)	10
Figure 2.2: Pour point improvement of several types of vegetable oil (Ab Ghani et al., 2018)	15
Figure 2.3: Flowchart of esterification and trans-esterification process (Abdelmalik, 2014)	16
Figure 2.4: Number of scientific publication on the subject “nanofluids as power transformer application” (Primo et al., 2018)	18
Figure 2.5: Two-step method process to produce nanofluid.....	21
Figure 2.6: Schematic diagram of high-pressure homogenizer for producing nanofluid (Y. Hwang et al., 2008)	22
Figure 2.7: The surfactant structure of (a) CTAB and (b) SDBS	23
Figure 2.8: TEM images of TiO ₂ -based nanofluid; (a) without surfactant (b) small (c) medium (d) large surfactant concentration (Atiya et al., 2015)	26
Figure 2.9: Current-voltage (I-V) characteristics of nitrobenzene (Brière & Gaspard, 1968)	37
Figure 2.10: Typical PD pulses in dielectric liquid (Pompili & Bartnikas, 2012).....	39
Figure 2.11: 2D-PRPD pattern with temperatures variation on a dielectric material (Hazlee Azil Illias, 2011)	41
Figure 2.12: Streamer structure in semi-uniform and divergent electric field (Top, Massala, & Lesaint, 2002)	44
Figure 2.13: Potential well distribution along spherical nanoparticles at different conductivities (Wenxia Sima et al., 2015)	46
Figure 2.14: Conductive path due to micro-bridging formation (Peppas et al., 2016) ...	48
Figure 2.15: Illustration of nanoparticle with interfacial layer in nanofluid suspension (Kotia, Borkakoti, Deval, & Ghosh, 2017)	49
Figure 3.1: Flow chart of the methodology.....	51

Figure 3.2: Refined, bleached, deodorized, palm oil (RBDPO)	52
Figure 3.3: Titanium dioxide and iron (II,III) oxide nanoparticles.....	53
Figure 3.4: A thermal vacuum oven.....	54
Figure 3.5: Ultrasonic bath to produce homogenous dispersion.....	55
Figure 3.6: Time-dependent aggregation and sedimentation of nanoparticles	56
Figure 3.7: A Zeiss EVO® MA10 scanning electron microscope.....	57
Figure 3.8: A Malvern Zetasizer instrument for DLS measurement	58
Figure 3.9: The Metrohm potentiostat for FDS and I-V measurements	59
Figure 3.10: Test chamber for dielectric properties measurements	59
Figure 3.11: Apparatus for PD measurement.....	61
Figure 3.12: Schematic diagram for PD experiment setup	62
Figure 3.13: PD test chamber.....	63
Figure 3.14: PD calibrated waveforms.....	63
Figure 3.15: A typical bipolar PRPD pattern from Omicron®	64
Figure 3.16: MEGGER automated breakdown test kit	66
Figure 3.17: Practical of hemisphere electrodes	67
Figure 3.18: Axial symmetric two-dimensional model geometry (nm).....	69
Figure 3.19: Boundary lines for model geometry	70
Figure 3.20: Model geometry presented in mesh elements.....	71
Figure 4.1: XRD spectra of Fe ₃ O ₄ and TiO ₂ nanoparticles.....	74
Figure 4.2: Sedimentation analysis of palm oil-based nanofluid.....	76
Figure 4.3: Scanning electron microscope (SEM) micrograph; (a) at the beginning and (b) after heat treatment	77
Figure 4.4: Nanoparticle distributions size relative on; (a) numbers and (b) volume.....	78

Figure 4.5: Real permittivity of palm oil with (a) conductive (b) semiconductive nanoparticles	81
Figure 4.6: Imaginary permittivity of palm oil with (a) conductive (b) semiconductive nanoparticles	83
Figure 4.7: Conduction curves of palm oil with; (a) conductive and (b) semiconductive nanoparticles	85
Figure 4.8: Dielectric conduction regime for base oil and nanofluid samples	88
Figure 4.9: Weibull distribution of PDIV average values for base oil and nanofluid samples.....	90
Figure 4.10: PD measurement results at 26 kVrms in 1500 cycles; (a) PD events, (b) total charge, (c) mean charge, and (d) maximum charge magnitude	93
Figure 4.11: PD phase distribution as a function of nanoparticle type.	94
Figure 4.12: PD activities as a function of the applied voltage amplitude in 1500 cycles; (a) PD events, (b) total charge, (c) mean charge, and (d) maximum charge magnitude.....	96
Figure 4.13: PRPD patterns for nanofluid samples with conductive and semiconductive nanoparticles at 26 kVrms applied voltage in 1500 cycles	98
Figure 4.14: The schematic of electron movement for nanofluids between two electrodes; (a) at inception state (b) steady state condition	100
Figure 4.15: Cumulative probability plots of base insulating oil (palm oil), with conductive (Fe_3O_4), and semiconductive (TiO_2) nanoparticles	102
Figure 4.16: Cumulative probability plots of palm oil with conductive nanoparticles (Fe_3O_4)	103
Figure 4.17: Cumulative probability plots of palm oil with semiconductive nanoparticles (TiO_2)	104
Figure 4.18: Weibull plots comparing breakdown strength of palm oil containing treated and untreated nanoparticles (a) Fe_3O_4 (b) TiO_2	106
Figure 4.19: Electric field (V/m) distribution and electric equipotential lines for (a) base oil, (b) with Fe_3O_4 and (c) TiO_2 nanoparticle	111
Figure 4.20: Cross section plot of the electric field magnitude from the FEA model in Figure 4.19.	112

LIST OF TABLES

Table 2.1: Companies of natural ester-based insulation, brand names, and regions	11
Table 2.2: Typical fatty acid composition of some vegetable oils (Asano Jr. & Page, 2014; N. Mohamad et al., 2018).....	12
Table 2.3: Nanoparticles and its base fluid formulation for nanofluid insulation preparation.....	19
Table 2.4: Relationship between zeta potential and nanofluid stability (Ghadimi et al., 2011)	27
Table 2.5: Experimental and numerical investigations on the dielectric and electrical performance of nanofluids	29
Table 3.1: Fatty acid compositions of palm oil.....	52
Table 3.2: General properties of nanoparticles used in this project.....	53
Table 3.3: Palm oil-based nanofluid samples	54
Table 3.4: Material parameters in the geometry model (Muhammad Rafiq, Lv, & Li, 2016)	68
Table 3.5: Boundary conditions and its electric expressions	71
Table 4.1: Average of crystallite size of Fe_3O_4 and TiO_2 nanoparticles.....	74
Table 4.2: Weibull parameters of the average partial discharge inception voltage.	90
Table 4.3: Weibull parameter of base insulating oil (palm oil), with conductive (Fe_3O_4), and semiconductive (TiO_2) nanoparticles	102
Table 4.4: Weibull parameter of palm oil-based nanofluid containing with conductive nanoparticles (Fe_3O_4)	103
Table 4.5: Weibull parameter of palm oil-based nanofluid containing with semiconductive nanoparticle (TiO_2)	105
Table 4.6: Weibull parameters for breakdown strength of palm oil containing treated and untreated nanoparticles (a) Fe_3O_4 (b) TiO_2	107

LIST OF SYMBOLS AND ABBREVIATIONS

Symbols:

A	:	Area (mm ²)
α	:	Scale parameter (kVmm ⁻¹)
β	:	Shape parameter
C	:	Capacitance (F)
d	:	Sample thickness (mm)
E	:	Electric field (kVmm ⁻¹)
exp	:	Exponential
f	:	Frequency (Hz)
I	:	Current (A)
J	:	Current density (Am ⁻²)
L	:	Spacing between electrodes (mm)
λ	:	Wavelength (m)
S	:	Electrode's effective area (mm ²)
ϵ_o	:	Permittivity of free space (Fm ⁻¹)
ϵ'	:	Real permittivity
ϵ''	:	Imaginary permittivity
σ	:	Conductivity (Sm ⁻¹)
π	:	Pi
t	:	Time (s)
θ	:	Angle (°)
V	:	Voltage (V)
V_a	:	Acceleration voltage (kV)
V_{bd}	:	Breakdown voltage (kV)

ω	:	Angular frequency (rads^{-1})
Z	:	Impedance (Ω)
Z'	:	Real part of the impedance
Z''	:	Imaginary part of the impedance

Abbreviations:

AC	:	Alternating current
CNF	:	Nanofluid with conductive nanoparticles
DC	:	Direct current
DLS	:	Dynamic light scattering
FDS	:	Frequency domain spectroscopy
FEA	:	Finite element analysis
Fe_3O_4	:	Iron (II,III) oxide
HV	:	High voltage
PC	:	Personal computer
PD	:	Partial discharge
PO	:	Palm oil
PRPD	:	Phase-resolved partial discharge
RBDPO	:	Refined bleached deodorized palm oil
RMS	:	Root mean square
SEM	:	Scanning electron microscopy
SNF	:	Nanofluid with semiconductive nanoparticles
TEM	:	Transmission electron microscopy
TiO_2	:	Titanium dioxide
XRD	:	X-ray diffractometer

CHAPTER 1: INTRODUCTION

1.1 Background of the study

Since the early of 1900s, liquid has been used as insulation material in power system equipment including transformers, switchgears and cables. Liquid insulation is a vital component in large or medium ranges of high voltage equipment. It plays an important role to ensure the reliability of an equipment towards the sustainability of power delivery in a long period. In fact, failures due to insulation in a power system equipment may cause long interruption and downcast financial revenue due to replacement or maintenance work. It has been statistically reported that highly proportion of shut down time is linked to the failure of the insulation system (M. Wang, Vandermaar, & Srivastava, 2002). The ability of the liquid to adapt with complex geometries of an equipment and self-healing property results in higher practicality as inner-insulator compared to solid material. In addition, liquid insulation always has higher dielectric strength and cooling efficiency than gas (Berger, 2000). Therefore, liquid insulation, mainly mineral oil, which is derived from petroleum-based oil, becomes the 'de facto' for high voltage insulation for most decades. Mineral oil is a mixture of three types of hydrocarbon molecules with specific concentrations. As such, paraffinic (alkanes), naphthenic (cycloalkanes) and aromatic types of hydrocarbon molecules greatly affect the physical and chemical behaviour of mineral oil.

Throughout the years, mineral oil has dominated the standard liquid insulation for high voltage equipment and power apparatus cooling system. For instance, the basic insulation level (BIL) requirement for volume of insulation liquid is proportional to the rated power of the high voltage transformer as shown in Figure 1.1. More liquid insulation is needed when rated power of the transformer is greater. Hence, it is estimated that nearly several billion litres of mineral oil are consumed in power transformers worldwide. Despite of that, mineral oils are flammable, toxic and also non-biodegradable. For instance, in the

event of an accident, oil leaks may cause significant environmental pollution, resulting in a financial cost in a clean-up process. It can also result fires and explosions with potentially death risk due to flammable property (Oommen, 2002). In the last years, there has been an increasing interest in finding sustainable materials with green and environmental friendly to replace the mineral oil. Many research works have focused on natural ester liquids such as canola, soybean, sun-flower, palm oil, and also synthetic ester, which are highly biodegradable materials (Fernández, Ortiz, Delgado, Renedo, & Pérez, 2013; McShane, Corkran, Rapp, & Luksich, 2006).

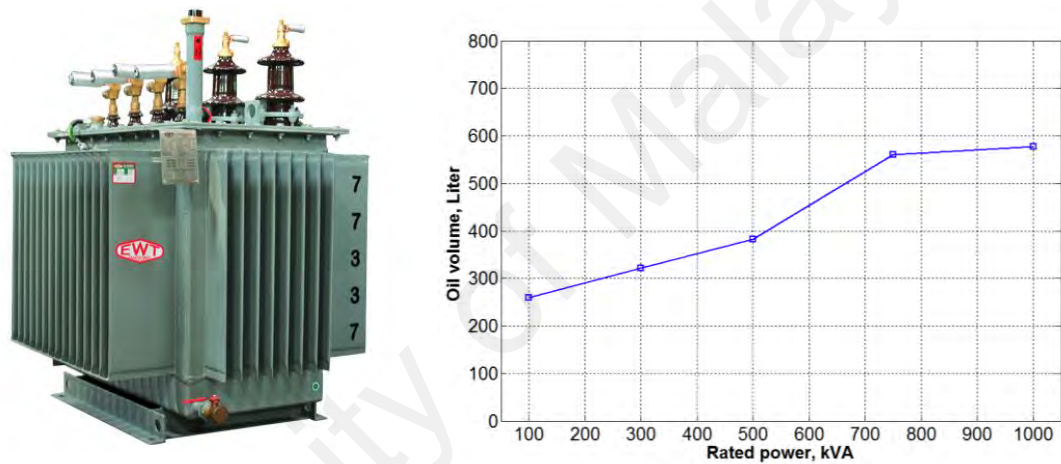


Figure 1.1: Oil-immersed distribution transformer with liquid insulation volume versus rated power (EWT transformer sdn bhd)

Ester liquids have shown inferior characteristics to be qualified as an insulation material at extremely high voltages condition (Mehta, Kundu, Chowdhury, Lakhiani, & Jhala, 2016). This is not a surprise because ester liquids have a different chemical composition than mineral oil. For instance, the breakdown mechanism in liquid insulation, which is initiated by streamer propagation, is a key difference between ester and mineral oil. For example, the experimental result from Duy et al. shows the acceleration voltage, V_a is almost equal to the breakdown voltage, V_{bd} in natural ester. Consequently, when $V_{bd} \approx V_a$, the streamer easily converts to fast streamer and thereby leads to breakdown (Duy, Lesaint, Denat, & Bonifaci, 2009). In order to apply the natural

ester as liquid insulation for high voltage application, the breakdown strength has to be increased up to breakdown voltage level and streamer is initiated at higher voltage.

Recent developments in the field of nanotechnology have led to a remarkable material prospect in order to overcome these challenges. The innovative concept of natural ester based-nanofluid has been developed. In early application of nanofluid, enhancement on the thermal conductivity was focussed on when Choi and Eastman introduced this novel concept in 1995 (S. U. S. Choi & Eastman, 1995). Segal et al. (Vladimir Segal, Hjortsberg, Rabinovich, Natrass, & Raj, 1998) then added the mark with possibility of nanofluid to be used as insulating material when dispersing Fe_2O_3 nanoparticles into transformer oil. From the experimental results, they discovered that the dielectric strength of the base oil is increased. This breakthrough point brought about a wave of studies in this area, predominantly applying experimental investigation on the enormous potential of nanofluid and efforts to realize the natural ester as high voltage insulation material.

1.2 Problem statement

Although the addition of nanoparticles can enhance the insulating property of base oil, where in this study is natural ester, a high voltage stress can cause inevitable insulation degradation. Majority of these nanofluid insulations are not yet commercially available due to certain problematic factors that require further investigation (Primo, Garcia, & Albarracin, 2018). For instance, the stability of nanoparticles when being dispersed into a base fluid, interaction with the magnetic field in a transformer and the effect of high electric field on the performance of nanofluids over time. Along with this phenomenon, it will contribute to dielectric deterioration process such as increasing tangent delta, growing partial discharge (PD) activity and consequently it can lead to insulation breakdown. The previous interpretation of PD activities and their mechanism, which leads to breakdown in a nanofluid is not sufficient enough. Thus, there is a circumstance

of improvement of the current understanding. Since natural ester has become the key of interest in power industries, it is important to investigate the influence of metal-oxides nanoparticle in order to apply the natural ester-based nanofluid as high voltage insulating material. This research work aims to investigate the dielectric and electrical characteristics of natural ester with the incorporation of conductive and semiconductive nanoparticles. PD analysis is used as diagnostic indicator to compare the performance of insulation under high voltage stress before the breakdown occurs. By understanding the dielectric properties, PD phenomenon and breakdown characteristics in nanofluids under electrical field stress, it provides an essential path to pursue for further research works regarding to application of natural ester based-nanofluid as electrical insulating materials.

Therefore, this work is motivated for obtaining dielectric properties, PD behaviours and breakdown distributions from various palm oil-based nanofluid formulations with different nanoparticle conductivities. In order to investigate the influence of metal-oxides nanoparticle, the samples were also prepared by logarithmic order from a very low to higher concentration, representing the possibility of agglomeration condition of static or flowing nanofluid in an electrical equipment. Data from dielectric properties and PD activities such as dielectric constant, losses, conductivity, PD events, PD charge magnitude and PD phase occurrences were recorded and compared between each sample. The Weibull probabilities of breakdown voltage was also analysed to calculate the dielectric withstand voltages of each sample. Since dielectric response measurement is not accurate without adequate nanofluid sample stability, a variety of stability assessment methods were used in this work in the preparation of nanofluid samples including visual analysis, aggregation size and particle size distribution.

1.3 Aim and objectives

Since nanoparticles have shown to improve insulating characteristics, the subject of nanofluids has become increasingly important. At the same time, the usage of natural ester as a liquid base is also beneficial to the environment. Therefore, the main objective of this study is to investigate the influence of different nanoparticles types (conductive and semiconductive) on dielectric and electrical characteristics of palm oil-based nanofluids insulation system. In this study, two types of nanoparticles, iron (II,III) oxide (Fe_3O_4) and titanium dioxide (TiO_2) were selected and used to prepare nanofluids samples based on palm oil as natural ester insulating liquids.

The objectives of this research are:

1. To investigate the influence of nanoparticle types and amount of concentrations on dispersion characteristics of palm oil-based nanofluid
2. To compare the dielectric properties of palm oil-based nanofluid between conductive and semiconductive nanoparticles
3. To determine the influence of applied voltage amplitudes, conductivity of nanoparticles and weight fraction of nanofluid insulation on partial discharge activities
4. To identify the breakdown voltage characteristics of palm oil-based nanofluid with conductive and semiconductive nanoparticles

1.4 Contributions of the research

In this work, iron (II,III) oxide and titanium dioxide have been used as addition particles to produce an enhanced insulation feature of a green insulating liquid, palm oil. By applying dielectric and electrical characterization techniques, the roles of nanoparticle electrical properties and its weight fraction in the suspension had been examined. Therefore, in the future, both conductive and semiconductive types of nanoparticles can

be utilized efficiently in high voltage engineering applications. Nevertheless, the dispersion stability of palm oil-based nanofluid is also one of the key factor that determines the resistance of nanofluids to partial discharge activity and breakdown voltage. Hence, the results of this study have contributed to the feasibility of the applications of palm oil as insulation material.

1.5 Research scope

This study integrates the palm oil, refined bleached deodorized palm oil (RBDPO) as biodegradable insulating liquid with iron (II,III) oxide, Fe_3O_4 and titanium dioxide, TiO_2 as conductive and semiconductive nanoparticles. The purpose is to develop an enhanced dielectric and electrical performance of a nanofluid insulating material. The dielectric properties of the prepared nanofluids with different types of nanoparticles are investigated under the frequency domain spectroscopy (FDS) and current-voltage (I-V) curves. Also, partial discharge (PD) and breakdown voltage (BDV) tests were conducted in order to compare the electrical performance of the nanofluid with conductive and semiconductive nanoparticles. Besides, the prepared nanofluid samples were characterized in terms of dispersion, morphological and stability. The morphological properties of the developed nanofluids were investigated using scanning electron microscopy (SEM). The dynamic light scattering (DLS) method were employed for dispersion analysis. The stability performances of the nanofluid were evaluated by the visual analysis along with sedimentation over period of time.

1.6 Thesis outline

The thesis is organized as follows:

Chapter 1 consists of introduction, which introduces the background, problem statement, research objectives, contributions and thesis outline.

Chapter 2 reviews the advantages of natural ester towards the conventional mineral oil as application in power transformers. This chapter also provides the definition and general concept of insulation-based nanofluid, synthesis and characterization methods. Dielectric response measurements in term of dielectric properties, conductivity, partial discharge (PD) and breakdown voltages were also reviewed. Experimental results of the selected studies were evaluated in view of the parameters such as particle properties, amount of concentration and proposed enhancement mechanisms.

Chapter 3 explains the methodology to achieve the objectives of this study. This includes the sample preparation, characterization technique and the experimental method.

Chapter 4 presents the characterization results of the dispersion stability of palm oil-based nanofluids. The influence of nanoparticles in terms of dielectric and electrical characteristics of nanofluid is systematically presented and discussed in this chapter.

Chapter 5 summarizes the key findings of this research and put forward the recommendation for future work.

CHAPTER 2: LITERATURE REVIEW

2.1 Introduction

This chapter describes high voltage insulation materials using conventional mineral oil and vegetable oil as an alternative. The descriptions include insulation-based nanofluids and their synthesis and characterization, dielectric and electrical measurements of nanofluids and enhancement of the characteristics as high voltage insulation material.

2.2 High voltage insulation material

High voltage (HV) insulation material is often classified into two types; solid and liquid. Solid insulation is usually used to insulate power cables, outdoor insulator, spacer and is the most common insulation material founded in any HV sites. Liquid insulation is mainly invisible due to immersed or filled into the HV apparatus such as power transformers, circuit breakers and switchgears. For instance, in oil-immersed power transformers, the combination of solid and liquid insulation, such as mineral oil derived from petroleum-based products, is frequently used due to its outstanding dielectric performance. However, in the last three decades, natural ester, derived from bio-based feedstock, is used to accommodate health and new environmental laws because conventional mineral oil has hazardous risks, toxicity and is non-biodegradable (Asano Jr. & Page, 2014; Mahanta & Laskar, 2017).

2.2.1 Conventional mineral oil and related hazards

Nowadays, transformer industry is witnessing a shift from petroleum-based mineral oil that is depleting, environmentally unfavourable and proven hazardous to renewable, environmentally friendly and non-hazardous natural esters, such as vegetable oil-based products. For instance, mineral oil has lower fire point ($<160\text{ }^{\circ}\text{C}$) compared to natural

ester (Oommen, 2002). The fire points are measure of minimum temperature at which a liquid ignites and continues to burn for a specified time after a small flame has been applied to its surface under standardized conditions. The amount of energy produced by the complete combustion of mineral oil is also higher. Thus, it will produce more risky catastrophic condition once ignited. Mineral oil-immersed transformer explosions and fires can cause severe collateral damage when it is located within populated areas or shopping centres, which are potentially dangerous from safety point of view.

In some cases, the leakage or spillage from a transformer containing mineral oil may generate toxic chemicals (substances) due to oxidative instability. Additives present in conventional mineral oil, such as polychlorinated biphenyls (PCBs), are banned in many countries (Shin & Kim, 2006). This is due to PCBs are carcinogenic and burning of PCBs can produce high toxicity products such as chlorinated dibenzofurans and chlorinated dioxins. Therefore, the prospective hazard of mineral oil has been recognised by many regulatory bodies. For instance, the Michigan Department of Environmental Quality stated that the usage of mineral oil in liquid form cannot be disposed by any of the following means (Aluyor & Ori-jesu, 2009):

- Dumping in drains, sewers or into surface or ground water
- Disposing in land fills
- Burning in municipal solid waste
- Using as a dust control or weed control

2.2.2 Natural ester-based liquid insulation

Natural ester, such as animal fat and vegetable oil, is well-known as biodegradable material (Figure 2.1) and exhibits very low or completely no toxicity compared to mineral oil. It has become a subject of interest as an alternative to replace mineral oil in high

voltage apparatus mainly for power transformers. Transformer manufacturers have begun using natural ester liquid due to its eco-friendly material while the world is facing the issue of sustainability resources and pollutions. On the other hand, natural ester fluid greatly reduces the risk of fire explosion when being applied as high voltage transformer insulation for indoor or outdoor application (Asano Jr. & Page, 2014). This is mainly due to its high fire points, which is approximately 300 °C compared to 160-180 °C for mineral oil. Natural ester is also naturally hydrophilic where it has moisture tolerance of five to eight times higher compared to mineral oil. In fact, tests have shown that even in the moisture content of 500 ppm in the oil, the dielectric breakdown strength of natural ester remains within the standard limit. Hence, less moisture is held in cellulose insulation material and thereby improving their life and ageing performance (Frimpong, Oommen, & Asano, 2011).

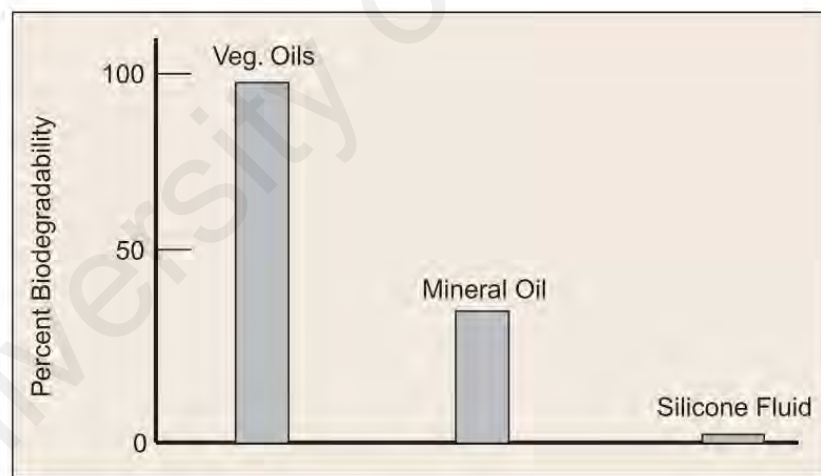


Figure 2.1: Comparison chart of natural ester and other types of transformer oil (Oommen, 2002)

Many efforts have been made to initiate an available commercial product from natural ester-based oil for insulating material application mainly for power transformers. Table 2.1 shows the companies of commercial natural ester, brand names and their regions. The first commercial product is BIOTEMP®, which is highly biodegradable and has high temperature stability (Oommen, Claiborne, & Mullen, 2002). For instance, the first

development of BIOTEMP® has low pour point of -25 °C, which may not posed a problem when a transformer is operating under an extreme cold weather condition. The second generation of BIOTEMP® was produced from high oleic oil with over 80 percent oleic content. The oil was produced mostly from seeds that were developed by selective breeding but more recently, gene manipulation techniques were used. Partial hydrogenation was added as an enhancement technique to minimize the very unstable tri-unsaturated products. A high mono-unsaturated oil is in demand in the food and lubrication industries.

The second generation of BIOTEMP® fluid is currently used in some distribution and network transformers in critical areas, especially in high relative humidity surrounding. Meanwhile, Lion Corporation (Japan) produced a commercial insulating liquid known as PASTELL NEO®, which properties are comparable with mineral oil (Kiyoshi Wakimoto, 2015). The PASTELL NEO® was produced through a molecular design technique and two-stage trans-esterification. In the first stage, fatty acid methyl ester (FAME) was produced through condensation of palm oil with the addition of methanol. In the second stage, trans-esterification was conducted by reacting the FAME with other alkyl alcohols in order to enhance the pour point, dielectric strength and the physiochemical properties of the oil.

Table 2.1: Companies of natural ester-based insulation, brand names, and regions

Company	Brand name	Region	Application
ABB	BIOTEMP®	USA	Compact substation, distribution transformer
Cargill	Envirotemp FR3®	USA, Brazil	Power transformer, distribution transformer
M&I Materials	Midel®	UK, Europe, India	Power transformer (up to 400kV), distribution transformer, Retro-filling

Lion Corp.	PASTELL NEO®	Japan, Southeast Asia	Insulating liquid, oil- immersed transformer
------------	-----------------	--------------------------	---

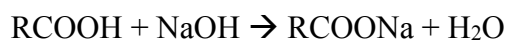
2.2.3 Vegetable oils

Vegetable oil has been used as insulating liquid since the invention of oil-immersed transformer in the late 1880s. Crude vegetable oil extracted from oil seeds contains solid constituents such as proteins and fibres and liquid, e.g. fats and oil. Both fats and oil are triglyceride esters of fatty acids, which appear as saturated and single, double and triple of unsaturated fatty acid. Saturated fatty acids are chemically stable but it will solidify below room temperature. Unsaturated fatty acids usually remains as liquid at -15°C to -30°C (Asano Jr. & Page, 2014). The lower degree of unsaturation from single to triple of fatty acids indicates more stable for vegetable oil to heat and oxidation. Table 2.2 lists typical fatty acid composition of some vegetable oils.

Table 2.2: Typical fatty acid composition of some vegetable oils (Asano Jr. & Page, 2014; N. Mohamad et al., 2018)

Vegetable oil	Saturated fatty acids, %	Unsaturated fatty acids, %		
		Single	Double	Triple
Palm oil	43.0	42.3	12.4	0.3
Coconut oil	81.3	6.0	1.1	-
Sunflower oil	10.5	19.6	65.7	-
Corn oil	12.7	24.2	58.0	0.7
Olive oil	13.2	73.3	7.9	0.6
Soybean oil	14.2	22.5	51.0	6.8
Canola oil	7.9	55.9	22.1	11.1

The basic step to produce a vegetable oil-based insulation material is by treating the crude oil to obtain refined, bleached, deodorized (RBD) oil. The first step in eliminating free fatty acids in vegetable oil is alkaline refinement. The equation of neutralization can be expressed as:



Bleaching is the second step in removing materials for colouring. In this step, clay filter presses are normally used to further purify the oil. Lastly, deodorization is performed, which is a process of high-temperature and high-vacuum steam-distillation to remove volatile and odorous materials. Furthermore, a wintering process can also be used to easily remove frozen saturated fats from the oil. As result, RBD oil has improved insulation properties compared to their crude oil (Abeyesundara, Weerakoon, Lucas, Gunatunga, & Obadage, 2001; Azis, Jasni, Ab Kadir, & Mohtar, 2014).

Palm oil has the potential to be used as insulating liquid while addressing the situation of Malaysia as one of the main contributors of palm oil in the world. Globally, palm oil share is around 36% of the total world oil production, followed by soybean and rapeseed oil at 29% and 15% respectively. According to Rudnick (2013), a major criteria to use a feedstock food-grade oil such as palm oil to other industrial applications are; (1) vegetable oil resources for oil production should be enough in quantity, (2) the selected vegetable oil should have more single-unsaturated fatty acid than triple-polyunsaturated fatty acids and (3) the respective vegetable oil should have a stable trading price.

2.2.4 Methods to improve the vegetable oil as insulation oil

In view of numerous properties to be considered in selection of vegetable oil as new green insulation material, researchers soon recognized that vegetable oil needs further improvement to be used in power equipment for many years. The presence of metallic part such as cooper in a power transformer, enhances tendency for oxidation of vegetable oil (Oommen, 2002). The degree of unsaturation is also an indicator of thermal instability and can constitute to low resistance of lightning impulse (LI) flashover (Unge et al., 2013). Therefore, promoting the use of vegetable oil in power transformers is a challenge. One of the strategies that can be implemented to overcome this barrier is to

enhance its properties so that they are superior or at least comparable to conventional mineral oil.

A few methods are used to overcome the disadvantages of vegetable oil and improve their workability in power transformers. The following methods are listed as follows:

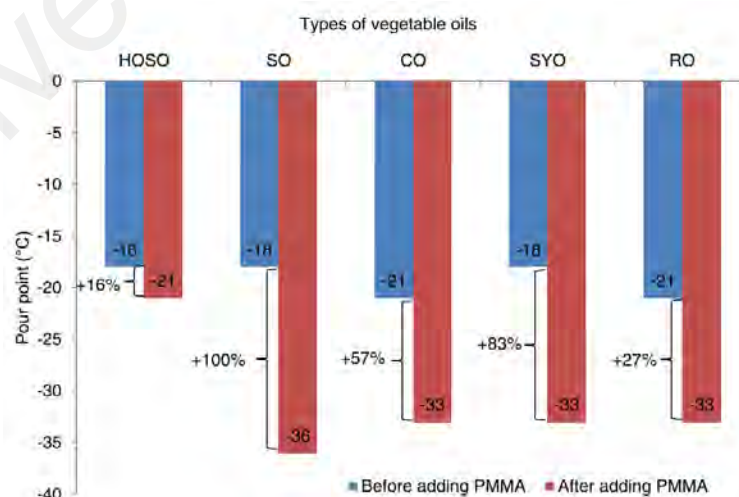
2.2.4.1 Antioxidant

One of the challenges to apply vegetable oil as dielectric insulation in power transformers is low oxidation stability. Thus, the easiest way to improve the oxidation stability of vegetable oil is by adding the antioxidants. Butylated hydroxytoluene (BHT) or commonly known as 2,6-di-*tert*-butyl-*p*-cresol (DBPC) has been widely used as a radical scavenger additive that prevents the material from free radicals and oxidation. For instance, Wilhelm et. al. used DBPC at 0.3 wt. % as an antioxidant agent to inhibit a corn oil-based natural ester insulating fluid from oxidation process (Wilhelm, Feitosa, Silva, Cabrino, & Ramos, 2015).

Several researchers have suggested a combination of various antioxidants can also be applied to improve the stability of base oil. For example, combination of two types of antioxidant, DBPC as synthetic agent and citric acid as natural agent can be used to improve the physical and electrical performance of vegetable oil (Raymon, Pakianathan, Rajamani, & Karthik, 2013). It is noteworthy that, even though antioxidants can improve the oxidation stability of the oil and reduce the degradation progress along time, addition of the antioxidant above the recommended limit will likely decrease the electrical resistivity of the oil (Hao, Yu, Qi, Qin, & Zhang, 2019).

2.2.4.2 Chemical additive

Apart of antioxidant, there are several chemical additives employed with vegetable oil to improve its characteristics. As vegetable oil has low performance towards lightning impulse breakdown compared to mineral oil, low ionization potential additives, such as dimethylaniline (DMA) and azobenzenes, added to vegetable oil can improve the level of impulse breakdown voltage (Unge et al., 2013). From the result, the addition of DMA causes a significant improvement in the level of acceleration voltage, V_a , which is defined as the voltage where the velocity of the streamer increases rapidly from 1 to 10 km/s. Hence, the breakdown is initiated at higher voltage level. Other than impulse breakdown, vegetable oil also has poor pour point limit. According to IEC, the pour point is defined as the minimum temperature at which a liquid will continue to flow when it is cooled under standardized conditions. This is very crucial especially when the vegetable oil is intended for use in a cold region. The breakdown voltage of natural ester oil decreases as the temperature drops from 0 to -21 °C (S.-H. Choi & Huh, 2013). The addition of 1 wt. % of poly-methyl-methacrylate (PMMA) enhances the pour point of vegetable oil as can be seen in Figure 2.2 (Quinchia, Delgado, Franco, Spikes, & Gallegos, 2012).



high oleic sunflower oil: HOSO, sunflower oil: SO, castor oil: CO, soybean oil:
SO, rapeseed oil: RO

Figure 2.2: Pour point improvement of several types of vegetable oil (Ab Ghani et al., 2018)

2.2.4.3 Esterification and trans-esterification

Esterification is a chemical reaction where vegetable oil (glycerol) or any fatty acid (carboxylic acids) undergo hydrolysis process in the presence of catalysis to produce ester (triglycerides). Meanwhile, trans-esterification is a process of functionalization of esters in the presence of alcohol as a catalyst. Both of the process will alter the physiochemical properties of the vegetable oil and the electrical characteristics of the base oil. Abdelmalik (2014) developed different types of palm kernel oil-based esters from esterification and trans-esterification process using different types of catalysts as demonstrated in Figure 2.3. The esters only improved its dielectric strength and cooling ability compared to mineral oil after second stage of trans-esterification and reduce at third and fourth stage. Hence, determining suitable alcohol, reagent or catalyst is proved to be a big challenge in the esterification and trans-esterification processes in producing better insulating oil.

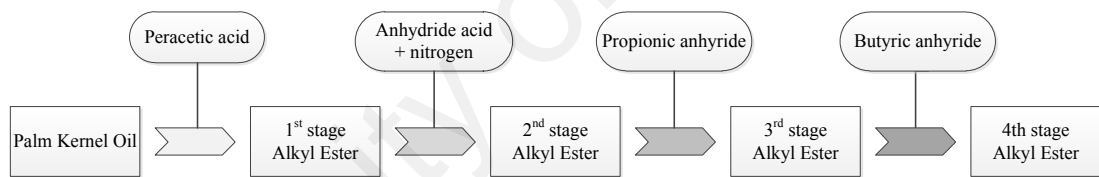


Figure 2.3: Flowchart of esterification and trans-esterification process
(Abdelmalik, 2014)

2.2.4.4 Addition of nanoparticles

Adding nanoparticles to a base oil to improve its dielectric strength is considered as a new breakthrough and has become popular among researchers. Since the discovery by Segal et. al. (1998) on the nanofluid-based insulating oil concept, which enhanced the breakdown voltage of mineral oil after dispersing the iron oxide nanoparticles, the tendency to improve a base insulating liquid using nanoparticle has become more prominent among researchers. The state of the art of nanoparticles when added to base oil is not only improving the electrical properties of insulating oil but most importantly, enhanced the physiochemical of the base oil (Yu & Xie, 2012). For instance, Jian Li et.

al. (2012) conducted an experiment with vegetable oil and found that the addition of Fe_3O_4 at 0.05 wt. % increased the breakdown voltage and impulse breakdown of the base oil. Further discussion about nanofluid-based insulation material concept and mechanism is presented in details in the next subtopic.

2.3 Nanofluid as high voltage insulation material

One of the most critical aspects in the power industry is insulation material, which is applied in many stages, including generation, transmission and distribution systems. Nowadays, energy demands on national grid system are driving increased electric loads, requiring advances in insulation materials (M., Salamah, Iqtiyani, & Hang, 2016). Conventional insulation system increases the space or volume available to use insulating material for spacing conductors and consequently enhances the dielectric strength. However, this approach is limited by the size and weight of electrical apparatus especially for ultra-high voltage application. Therefore, there is an essential need for new and novel insulation material with improved characteristics. The prospect of nanofluids, dielectric fluid dispersed with nanoparticles, has been proposed as insulating liquid for coming future. As shown in Figure 2.4, the number of scientific publications has increased rapidly over the last 10 years. In other words, insulation-based nanofluid is a colloidal suspension containing two phase systems with solid phase, or nanomaterial and liquid phase, or insulating liquid base, which possess enhanced dielectric characteristics and thermophysical properties.

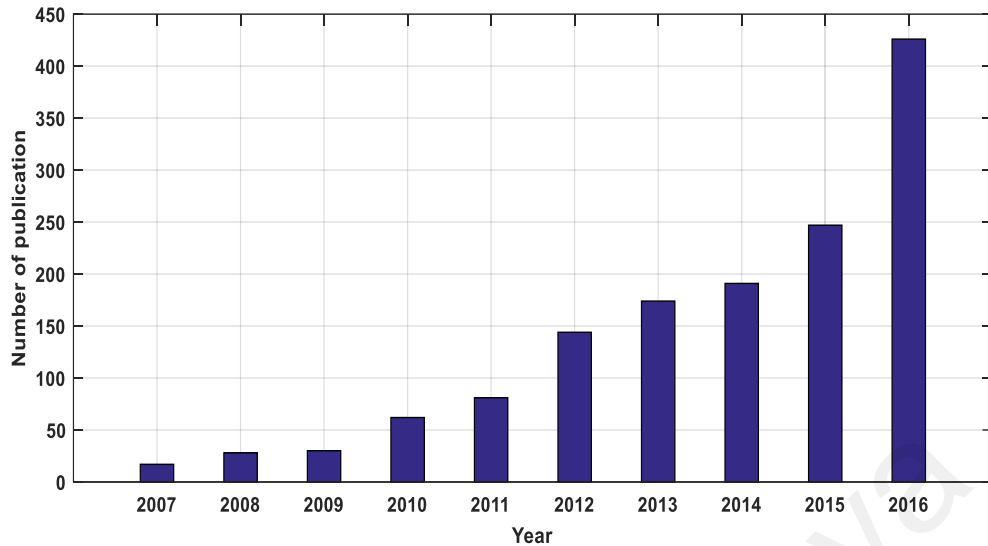


Figure 2.4: Number of scientific publication on the subject “nanofluids as power transformer application” (Primo et al., 2018)

2.3.1 Synthesis and nanofluid characterization

Nanofluid insulation is a colloidal suspension containing nano-meter size particles (1~100 nm) dispersed in insulation liquid such as natural ester, mineral oil, synthetic oil and silicone oil. Various combinations of nanoparticles and base insulating liquid reported in literature are tabulated in Table 2.3. In recent years, natural ester insulating oil has gain much interest amongst researchers as base insulation for nanofluid production due to their biodegradability and sustainable resources. To date, natural esters are used by several power provider in Australia, Brazil, United Kingdom, Sri Lanka and Germany as insulating oil in electrical transformers (Martin, Krause, & McPherson, 2016; Martins, 2010; Matharage, Fernando, Bandara, Jayantha, & Kalpage, 2013). Apart from natural ester, palm oil is another type of natural insulating oil that potentially can be used as dielectric insulation material (Azis et al., 2014). Palm oil has long composition of fatty acids, which include a wide carbon chains accounting to good oxidation stability (Kano et al., 2008), AC breakdown voltage (Sinan et al., 2014) and partial discharge resistance (Rajab et al., 2011).

Table 2.3: Nanoparticles and its base fluid formulation for nanofluid insulation preparation

Nanoparticles	Base fluid	References
Cu	Mineral oil	(Mergos, Athanassopoulou, Argyropoulos, & Dervos, 2012)
CuO	Mineral oil	(Mergos et al., 2012)
Fe ₂ O ₃	Transformer oil	(Sartoratto, Neto, Lima, Rodrigues de Sá, & Morais, 2005)
Fe ₃ O ₄	Mineral oil, Natural ester	(J. Li et al., 2012)
ZnO	Mineral oil, Natural ester	(Miao et al., 2013)(Saengkhumwong & Suksri, 2015)
TiO ₂	Mineral oil, Natural ester	(Atiya, Mansour, Khattab, & Azmy, 2015; Nor et al., 2017)
SiO ₂	Mineral oil, Natural ester	(Karthik, Negri, & Cavallini, 2016)(Mentlik, Trnka, Hornak, & Totzauer, 2018)
SiC	Mineral oil, Polyalphaolefin	(Chiesa & Das, 2009)
Al ₂ O ₃	Mineral oil, Natural ester	(Q. Wang, Rafiq, Lv, Li, & Yi, 2016)
Graphene	Mineral oil	(Cavallini, Karthik, & Negri, 2015)
Silver	Mineral oil	(D. Li, Hong, Fang, Guo, & Lin, 2010)
Diamond	Mineral oil	(Fontes, Ribatski, & Bandarra Filho, 2015)
CNTs	Mineral oil	(Dhar, Katiyar, Maganti, Pattamatta, & Das, 2016)

Nanofluids can be synthesised by two methods; one-step method and two-step method.

The descriptions are as follows:

2.3.1.1 One-step synthesis method

One-step method is a process that produces nanoparticles at the synthesis of nanofluid simultaneously. Traditionally, nanoparticles are directly produced by the solidification from the gaseous phase when running inside the base fluid, known as Vacuum Evaporation onto a Running Oil Substrate (VEROS) technique (Akoh, Tsukasaki, Yatsuya, & Tasaki, 1978). Direct Evaporation Condensation (DEC) method developed by Choi et. al. (S. U. S. Choi, Yu, Hull, Zhang, & Lockwood, 2001) provides more

excellent control on the nanoparticles dispersion, resulting in stable nanofluid without surfactant treatment. This method skips drying, storage and transportation process of solid nanoparticles so that the agglomeration of nanoparticles can be minimized and produce stable nanofluids (Ghadimi, Saidur, & Metselaar, 2011). The cost of drying and dispersion can also be avoided by one-step method. However, the mass production of nanofluid is the limit of this method. Lo et. al. (Lo, Tsung, & Chen, 2005) introduced a novel system to synthesis nanofluid using Submerged Arc Nanoparticle Synthesis System (SANSS), which was improved later by Chang and Kao (Chang et al., 2005; Jwo, Chang, Kao, & Lin, 2007). This method helped to boost the quantity of nanofluid production and improved the quality of nanoparticles.

2.3.1.2 Two-step synthesis method

Two-step method is the most widely used method for the synthesis of nanofluid. The general schematic of two step method is shown in Figure 2.5. In the first step, base fluid and nanomaterials such as nanoparticles, nanofibers, nanopowder, or nanotubes are prepared in dry form. During second step, the prepared nanomaterials are directly dispersed to the base oil with the assistance of dispersing device such as magnetic stirrer, homogenizer, sonicator or the combination of them (Babita, Sharma, & Gupta, 2016; Y. Z. Lv, Zhou, Li, Wang, & Qi, 2014). This method works very well for oxide nanoparticles rather than metallic nanoparticles (Murshed, Leong, & Yang, 2005). However, its disadvantage due to aggregation and sedimentation are unavoidable and will quickly appear. Thus, producing a homogeneous dispersion with high stability nanofluid remains a challenge. Furthermore, there are some successful techniques to minimize this problem by applying the physical and chemical treatment, which is discussed in the next section.

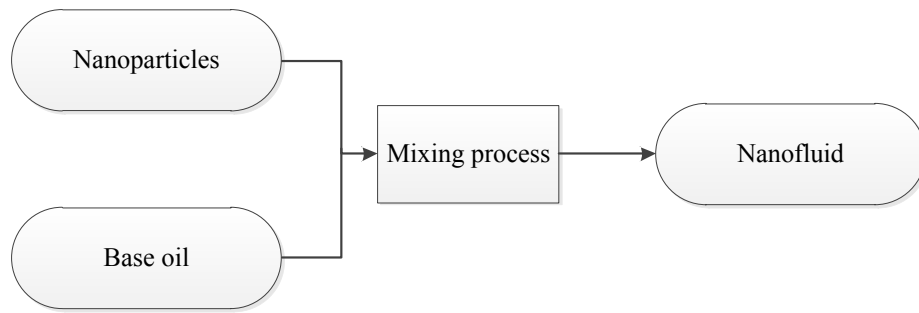


Figure 2.5: Two-step method process to produce nanofluid

2.3.2 Stability treatment techniques

Long stability of nanofluids is one of the basic characteristics for its better application as liquid insulation. Agglomeration can appear quickly in two-step method production of nanofluid due to high surface energy of nanoparticles. Agglomeration means that the particles start to aggregate within significant rate of time, which is mainly driven by the frequency of collision and the probability of cohesion during collision. Derjaguin, Verwey, Landau and Overbeek (DVLO) theory stated that the stability of a nanoparticle in base oil is determined by the summation of van der Waals attractive force and electrical double layer repulsion force when two identical particles are close to each other due to Brownian motion (Missana & Adell, 2000). Under high voltage operation, the nanofluid insulation is exposed to external high electric field and leads to mitigation and faster aggregation of nanoparticles. This will lead to a localized electric field and consequently stimulate the breakdown process (Lee, Lee, Lee, & Lee, 2012). Therefore, treatment was applied to reduce the aggregation and coagulation process of nanoparticles to enhance the nanofluid stability. Treatments on agglomeration are described in the following section.

2.3.2.1 Physical treatment

Ultrasonication is the most widely used physical treatment for agglomeration hindrances. During sonication process, thousands of bubbles were formed and collapsed

into the solution and creates cycles of pressure known as cavitation. This causes effective wave of vibrations that produce an energy force in the cavitation field, which disrupts sub-atomic connections such as interaction between molecules, particles separation and thereby facilitates mixing process. Yuzhen et. al (Yu-zhen Lv et al., 2016) found that ultrasonic bath with combination of stirring method exhibits better dispersion efficiency than the ultrasonic probe.

The ultrasonication method by using probe can obstruct the functional group on the surface of nanoparticles due to the localization of the high intensity sonication energy around the probe tip. This affects the stability of nanofluid and leads to the reduction of its dielectric strength. On the other hand, longer period of sonication may cause defects and deteriorate the optimal size of nanoparticles (Mahbubul et al., 2014). Meanwhile, homogenization is quite different from the ultrasonication where high mechanical shear and pressure are applied during dispersion settlement as depicted in Figure 2.6. Fedele et. al. (Fedele, Colla, Bobbo, Barison, & Agresti, 2011) concluded that high pressure homogenization is more effective than ultrasonication during preparation of metal-oxides nanoparticle-based water nanofluid.

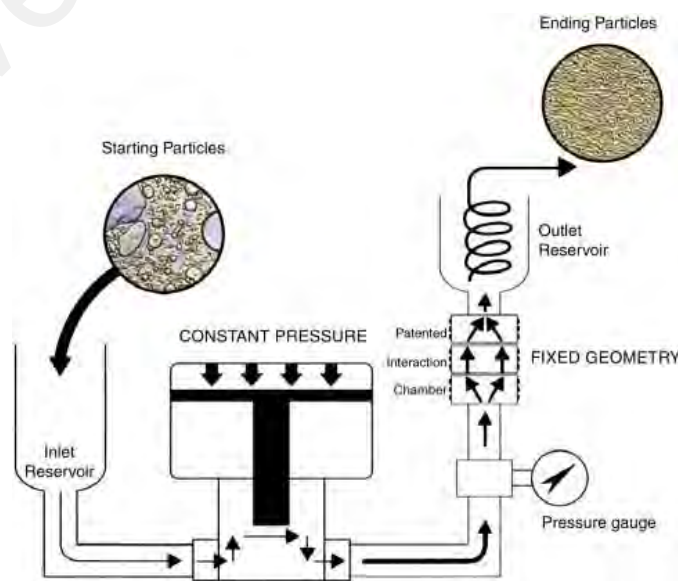


Figure 2.6: Schematic diagram of high-pressure homogenizer for producing nanofluid (Y. Hwang et al., 2008)

2.3.2.2 Chemical treatment

Generally, nanoparticles can be hydrophilic or hydrophobic and base oil can be attributed as polar or non-polar liquid. Hydrophilic nanoparticles will be easily dispersed to the polar base fluid such as water while hydrophobic nanoparticles will be more dispersible into non-polar liquid such as oil. However, when there is a requirement to disperse inversely between hydrophilic nanoparticles into non-polar and hydrophobic into polar molecules, the third component is required, where in this case known as surfactant. Surfactants are categorized according to their head charge group. For instance, anionic or negative charge such as sodium dodecylbenzene sulphonate (SDBS), cetyl trimethyl ammonium bromide (CTAB) and non-ionic Gum Arabic (GA). An example of the structure of anionic and cationic surfactants is shown in Figure 2.7. For instance, when Al_2O_3 nanoparticles are dispersed into mineral oil, the hydroxyl group absorbed on the surface of particle is H^+ . Therefore, anionic surfactant such as SDBS is more suitable to be used and performed $\text{H}^+ - \text{SO}_3^-$ interfaces bonding, leaving NaOH behind (Mansour, Elsaeed, & Izzularab, 2016).

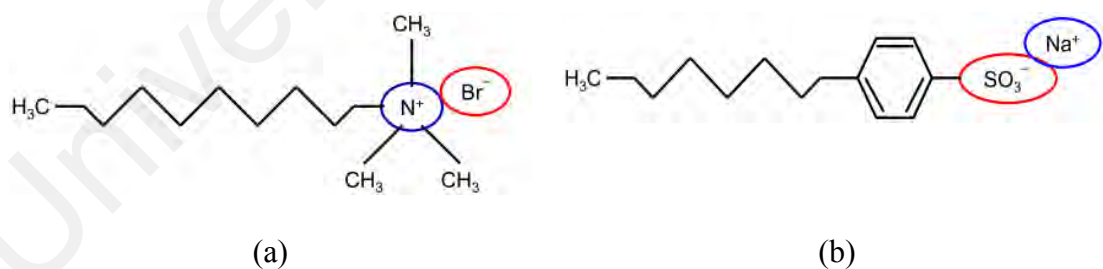


Figure 2.7: The surfactant structure of (a) CTAB and (b) SDBS

Surfactant technique is an effective way to improve the nanofluid stability. However, the presence of excessive surfactant, which dissolves in base fluid coherently, reduces the dielectric breakdown (Yuzhen Lv, Rafiq, Li, & Shan, 2017), producing foam during thermal heating (Darton & Sun, 1999) and increases the viscosity of base oil. In order to

overcome the problem, surface modification technique is proposed by modifying the surface functionalization of nanoparticles. This technique is known as surfactant-free method and it enhances the base oil without any contamination effect. Jian Li et. al. (J. Li et al., 2012) prepared vegetable oil-based surface modified Fe_2O_3 nanoparticles by using oleic acid. Under particle size analyser, the distribution size of nanoparticles before and after surface modification technique was analysed. It was found that the agglomerated nanoparticles in the range 0.2 to 2 μm were abolished. However, the average size of nanoparticles was increased by several nano-meter due to coating effect on their surface. Jian Li et. al. (Jian Li, Du, Wang, Yao, & Yao, 2016) also revealed that the surface functionalization on nanoparticles can also be polarized and can affect the trapping depth of nanofluid. The trapping depth determines the dielectric strength of nanofluid under the presence of high electric field.

2.3.3 Stability characterization method

Nanofluid stability can be characterized using several methods such as physical method, morphology analysis, dynamic light scattering and zeta potential.

2.3.3.1 Sedimentation analysis

Sedimentation is a versatile and inexpensive method compared to other techniques. The variation of weight fraction of dispersion particle with sedimentation time is an indication of the nanofluid stability where the suspension is considered to be a stable when the concentration or precipitation is kept constant (Yu & Xie, 2012). One of the usual methods for sedimentation analysis is by using camera photograph of nanofluid in test tubes over a period of time (X. Li, Zhu, & Wang, 2007). Apart of that, tray submerged method is a method where a tray of sedimentation balance is immersed in a fresh suspension (Palm, 2013). The weight of sediment nanoparticles after a certain period was

measured. However, long period of observation time in sedimentation analysis required another alternative known as centrifugation method. Singh and Raykar (Singh & Raykar, 2008) investigated the stability of silver nanofluids by comparing two methods, sedimentation in stationary condition and centrifugation method. It was found that the obtained nanofluids are stable for 10 hour under centrifugation at 3000 rpm and 1 month in a stationary condition. The results indicated that the centrifugation method has shortened the effective observation time for sedimentation analysis by 1:72 ratio.

2.3.3.2 Electron microscopy

Scanning electron microscopy (SEM) and transmission electron microscope (TEM) are widely used as tools to distinguish the shape, size and distribution of nanoparticles. However, they are not able to demonstrate the real condition of nanoparticles in the suspension due to dried samples are required (Ghadimi et al., 2011). The suspension fluid is poured on a SEM/TEM specimen holder and leave to dry at room temperature or in a vacuum oven until it solidify (M. S. Liu, Lin, Tsai, & Wang, 2006). The solid particles then undergo SEM/TEM vacuum chamber for micrograph distribution analysis. For instance, Herchl et. al. measured the hydrodynamic average diameter of magnetite particles dispersed in transformer oil by using TEM (Herchl et al., 2008). The normal distribution of particle size obtained from the measurement can be plotted by applying the Chantrell et. al. method (Chantrell, Popplewell, & Charles, 1978). Atiya et. al. (Atiya et al., 2015) investigated the effect of excessive surfactant on the agglomeration of TiO₂-based transformer oil using TEM. It was found that agglomeration of nanoparticles is noticed with the formation of bulk-sized particles as shown in Figure 2.8 and negatively affects the dispersion.

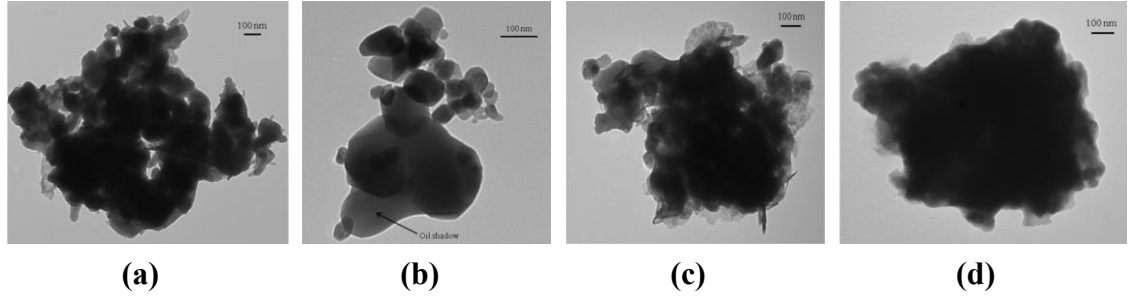


Figure 2.8: TEM images of TiO₂-based nanofluid; (a) without surfactant (b) small (c) medium (d) large surfactant concentration (Atiya et al., 2015)

2.3.3.3 Light scattering

Dispersed particle-size in a nanofluid can also be measured based on the light scattering or Dynamic Light Scattering (DLS) technique. The measurement concept is based on the Brownian motion due to particle random collisions, causing the particles to diffuse through the medium. According to Stokes-Einstein equation (Edward, 1970), the diffusion coefficient D_e is inversely proportional to the particle size as follows:

$$D_e = \frac{k_B T}{3\pi\eta_0 d} \quad (2.1)$$

where k_B is the Boltzmann's constant, T is the absolute temperature, η_0 is the viscosity and d is the hydrodynamic diameter. Zhang et. al. (J. Zhang, Wang, Li, Ran, & Huang, 2017) studied the distribution of copper particles in transformer oil using DLS technique and determined the median size, which denotes the diameter at which the cumulative size distribution achieves 50%. The impact of aging in transformer oil dispersed with nanoparticles can be observed under DLS while the increment of particle diameter distribution along the aging process shows poorer performance on the suspension stability (Emara, Mansour, & Azmy, 2017). Hence, the suitability of DLS technique in order to quantify and analyse the nanofluid stability is widely accepted.

2.3.3.4 Zeta potential

Zeta potential is an electrical potential measured in the interfacial double layer, either positive or negative, from the position of slipping layer towards away from the interface, between a solid particle surface and its liquid medium. The potential in this region decays with increasing distance from the surface until at sufficient distance, where it reaches the bulk solution value and conventionally taken to be zero potential. The importance of zeta potential is its value that is related to the stability of nanofluid suspension. Dispersions, which attain high zeta potential, are electrically stable while colloidal with low zeta potential tends to coagulate or precipitate (Yu & Xie, 2012). Ghadimi et. al. (Ghadimi et al., 2011) summarised the obtained values from zeta measurement with the stability of nanofluids as shown in Table 2.4.

Table 2.4: Relationship between zeta potential and nanofluid stability (Ghadimi et al., 2011)

Zeta potential (mV)	Nanofluid stability
0	Very little or no stability
15	Little stability with settling
30	Moderate stability with sedimentation
45	Good stability with possible settling
60	Excellent stability, little settling

However, there are some restrictions in the analysis of zeta potential due to dependability on the pH of the suspension. A repulsion force between interparticle caused by zeta potential increases with the increase of surface charge of the dispersion particles (Y. Hwang et al., 2007). The surface charge of particles is also influenced by pH value of the suspension. For instance, Zawrah et. al. investigated the stability on the pH dissolution of water-based Al_2O_3 nanofluids (Zawrah, Khattab, Girgis, El Daidamony, & Abdel Aziz, 2016). The pH value of Al_2O_3 -based nanofluids was adjusted to be alkaline (NaOH solution) or acidic (HCl solution). They found that higher pH value creates strong negative surface charges on the nanoparticles measured by zeta potential and improved

the nanofluid stability. On the other hand, this mechanism will lead to reduction of insulation property of the suspension.

2.4 Dielectric and electrical performance of nanofluid insulation

Nanofluids are potentially new generation of liquid insulation material in electrical apparatus, which have been investigated conscientiously in recent years. Nanoparticles dispersed into the base fluid have significant influence on their dielectric and electrical characteristics. Some experimental and numerical investigations on the electrical performance of nanofluids are summarized in Table 2.5.

Table 2.5: Experimental and numerical investigations on the dielectric and electrical performance of nanofluids

Researcher	Particle	Liquid base	Amount of concentration	Surfactant	Method of production	Dielectric enhancement/reduction of nanofluid as insulation	Possibly mechanism
(Vladimir Segal et al., 1998)	Fe ₃ O ₄	Mineral oil	No information	No information	No information	Increase impulse breakdown by, <ul style="list-style-type: none"> • 0% (<5 ppm water content) • 9.3% (10-20 ppm water content) • 18.9% (20-30 ppm water content) • 42.9% (>30 ppm water content) 	Electron trapping by nanoparticles
(V Segal, Natrass, Raj, & Leonard, 1999)	Fe ₃ O ₄	Mineral oil	No information	No information	Dilution	Increase breakdown by, <ul style="list-style-type: none"> • 25.8% (AC breakdown after 12 weeks thermal aging, 185 °C) • 36.2% (Positive after 12 weeks thermal aging, 185 °C) • -8.4% (Negative impulse after 12 weeks thermal aging, 185 °C) 	Suspension stability and thermal aging resistance
(Herchl et al., 2008)	Fe ₃ O ₄	Transformer oil ITO 100	0.0019, 0.0024, 0.019, 0.032	Oleic acid	Magnetic stirrer	Increasing permittivity and losses with increasing of amount of nanoparticle concentration and applied electric field PD resistance enhanced at concentration = 0.0024 at all electrode distance.	Cluster and space charge formation at liquid-electrode interface

(Ganguly, Sikdar, & Basu, 2009)	Al ₂ O ₃	Water	0.005, 0.01, 0.015, 0.02, 0.025 and 0.03	No information	Ultrasonication and stirrer	Effective electrical conductivity increased with the increasing of particle volume fractions	Electric double layer (EDL) and ionic concentrations
(Z. Zhang, Li, Zou, & Grzybowski, 2010)	Fe ₃ O ₄	Natural ester	No information	No information	Ultrasonication	<p>Enhancement in AC breakdown voltage by 16.56%</p> <p>Enhancement in lightning impulse breakdown voltage by 10.83%</p> <p>Volume resistivity improved in the frequency range 0.4-50 Hz</p> <p>Relative permittivity increased by 9.23% and 7.94% approximately</p> <p>Dissipation factor decreased in the lower frequency region</p>	Particle surface modification
(Y. Du et al., 2011)	TiO ₂	Transformer oil (Karamay)	No information	No information	No information	AC and positive impulse breakdown voltages of nanofluid are increased by 19% and 24% respectively	Electron trap density at shallow traps
(Yuefan Du et al., 2012)	TiO ₂	Mineral oil	0.075	No information	No information	<p>Permittivity increased by 42%</p> <p>DC resistivity decreased around 21%</p> <ul style="list-style-type: none"> -0.5% (10% relative humidity) 	Electron trap density at shallow traps

						<ul style="list-style-type: none"> • 25.5% (20% relative humidity) • 63.2% (40% relative humidity) • 59.9% (60% relative humidity) • 55% (80% relative humidity) 	
(Yuzhen Lv et al., 2013)	TiO ₂	Mineral oil	0.075	Oleic acid	Stirrer (5 min), heating 24h (150 °C) and Ultrasonication 36 days	54.8% (AC breakdown after 36 days thermal aging, 130 °C) 25.1% (Impulse breakdown after 36 days thermal aging, 130 °C)	Space charge and electron trap density at shallow traps
(H. Jin et al., 2014)	SiO ₂	Mineral oil	0.005 0.01 0.02 0.18	No information	Stirrer (15min) and sonication (2h)	Breakdown voltages increased by <ul style="list-style-type: none"> • 16% (0.01 g/L concentration and 25 ppm humidity) • 21.5% (0.02 g/L concentration and 25 ppm humidity) • 10.5% ((0.01 g/L concentration and 15 ppm humidity) • 14.6% (0.02 g/L concentration and 25 ppm humidity) 	Moisture reduction due to hydrophilic surface of untreated silica nanoparticles
(Cavallini et al., 2015)	Fe ₃ O ₄ GO SiO ₂	Mineral oil	0.1, 0.2, 0.4 and 0.5	No information	Ultrasonication and drying process	Breakdown voltages increased by <ul style="list-style-type: none"> • 27.41% (NF based Fe₃O₄) • 22.3% (NF based GO) • 21.15% (NF based SiO₂) Partial discharges activities compared to base oil,	Improvement from electrophoretic and electrohydrodynamic forces

						<ul style="list-style-type: none"> • Under negative DC voltage, all NF perform better PD resistance • For positive DC voltage, NF based SiO₂ is the best PD resistance • Under AC voltage, NF based SiO₂ perform better than NF based GO. Meanwhile, NF based Fe₃O₄ shows worse performance to PD resistance 	
(Mansour et al., 2016)	Al ₂ O ₃ (cationic surface), TiO ₂ (anionic surface)	Transformer oil	0.01, 0.04, 0.07 and 0.1	Sodium Dodecyl Benzene Sulfonate (SDBS), Cetyl Trimethyl Ammonium Bromide (CTAB)	Magnetic stirrer (15 min.) Sonication (2 hours)	<ul style="list-style-type: none"> • The dielectric constant increases with increasing weight fraction of Al₂O₃ and TiO₂ without surfactant • Dielectric constant decreases for Al₂O₃ and TiO₂ with surfactant • Weight fraction influences the particle dispersion ability in a base oil (in this study, 0.1 g/L). 	Interfacial zone consists of two layers; the aligned (rigid structure) and affected layer (oil chains).
(Nor et al., 2017)	TiO ₂	Natural ester	0.001 to 0.05	Cetyl Trimethyl Ammonium Bromide (CTAB)	Stirrer (15 min.), Sonication (1 hour), Drying (85 °C, 48 hours)	<ul style="list-style-type: none"> • The AC breakdown voltages of natural esters slightly increase with the introduction of TiO₂. • The presence of CTAB could cause reduction on the breakdown voltages of natural esters at certain concentration of TiO₂ 	The role of surfactant

						<ul style="list-style-type: none"> Dielectric dissipation factors and resistivity of nanofluids are significantly affected by the presence of CTAB. Relative permittivity of nanofluids less influenced by the presence of TiO₂, with and without CTAB. 	
(Mauricio Aljure, Becerra, & Karlsson, 2018)	ZnO, SiO ₂ , Al ₂ O ₃ , TiO ₂ , C ₆₀	Mineral oil	0, 0.002, 0.005, and 0.01	No information	Sonication (30 min.)	<ul style="list-style-type: none"> SiO₂, TiO₂, and Al₂O₃ improve the 50% probability inception voltage (V_{50%}) of positive streamers Surface modified ZnO and C₆₀ improve V_{50%} under both polarities SiO₂, TiO₂, and Al₂O₃ as hydrophilic nanoparticle types can absorb water 	Water adsorption of hydrophilic nanoparticles. Electron attachments through the relaxation time constant.
(Kurimský et al., 2019)	Fe ₃ O ₄	Transformer oil	0 to 0.0004	Oleic acid	No information	<ul style="list-style-type: none"> The presence of Fe₃O₄ results in the significant reduction in the PDIV and pulse repetition rate The reduced PD activity was also observed visually 	Electric field modification and charge trapping

2.4.1 Measurement of dielectric permittivity and losses

The fundamental theories behind dielectric measurements for high voltage application are well discussed in (Zaengl, 2003). In general, dielectric spectroscopy measurement consists of time and frequency domain, where the complex permittivity in frequency domain can be used to characterize the insulation quality (Bouaicha et al., 2009). It is expressed in a real part as relative permittivity, which represents the energy stored in the electric field within the material and an imaginary part is called dielectric losses. Relative permittivity, also known as dielectric constant, indicates how easily a material can be polarized by imposition of an electric field. Relative permittivity is equivalent to the absolute permittivity of the material relative to the permittivity of free space. Since the breakdown characteristics of an insulating material depend on its behaviour against electrical potential and electric field (Lau, Piah, & Ching, 2017), the measurement of permittivity within the insulating material is also important in order to understand their breakdown mechanism.

One of the common techniques to determine the relative permittivity of any material is by using capacitance method. In the case of two-parallel conductor plates, the relationship between the capacitance C and relative permittivity ϵ_r can be expressed by

$$C = \epsilon_0 \epsilon_r \frac{A}{d} \quad (2.2)$$

$$\epsilon_r = \epsilon' + j\epsilon'' \quad (2.3)$$

where ϵ_0 is the free space permittivity ($8.854 \times 10^{-12} \text{ Fm}^{-1}$), A is the surface area between the electrodes and the material at thickness d .

The addition of nanoparticles causes major changes in the dielectric permittivity of base insulation liquid due to polarization effect from the nanoparticle dispersed within

the fluid (J. Li et al., 2012; J. Liu et al., 2012; Tagmouti, Bouzit, Costa, Graça, & Outzourhit, 2015). Permittivity usually increases due to the nanoparticles have higher permittivity by nature than base insulating liquid. The apparent polarization in the nanofluid is the summation of the polarization of the base oil, inner polarization of nanoparticles and orientation polarization of charged nanoparticles as polar molecules (Miao et al., 2013). However, the permittivity is also found to decrease as reported by several researches. It is fair to state that the decrement of permittivity after addition of nanoparticles is due to nano-structuration process and interfaces between filler-base materials takes place properly. For instance, Mansour et. al. carried out dielectric spectroscopy measurement on TiO_2 and Al_2O_3 based transformer oil with and without surfactant (Mansour et al., 2016). They concluded that the permittivity of nanofluids decreases at the presence of surfactant and increases or no change at nanofluid samples without surfactant.

The reduction in permittivity can be described by the restriction of ions mobility by nanoparticle interfaces chain mechanism (Dong et al., 2017). Hanai et. al. (Hanai, Hosomi, Kojima, Hayakawa, & Okubo, 2013) presented a model that is correlated between nanoparticles-based oil and permittivity characteristics of the nanofluid. The measurement result of relative permittivity with TiO_2 -based mineral oil increases with increasing particle concentration and agreed with the calculation result from the random model. On the other hand, the experimental results for ZnO -based mineral oil and TiO_2 -based synthetic oil are slightly different from the predicted model. This is possibly due to interfaces mechanism, which has been mentioned previously. Generally, the weight fraction of base oil contains microscopic interfaces between molecules but new types of interface is developed between the molecules of base oil and nanoparticle surface in the nanofluid electro-hydrodynamic system. This type of interface creates an interfacial

layers similar to the nanodielectrics and therefore taking a dominant role for the nanofluid properties.

2.4.2 Measurement of electrical conductivity

Electrical conductivity measurement is one of the simplest methods to investigate the insulation performance. Usually, the conduction mechanism in the fluid is due to physical and chemical factors. In polar liquid, electrolytes become the main substances that can ionize and lead to conduction process even though in a low electric field. For non-polar liquid such as insulating oil, the molecules are formed by covalent bonds and hardly generate free ions. However, due to addition of a specific substances, it can produce ionic pairs and the dissociation of ionic pairs can produce free ions (Castellanos, 1998). During charge injection, charge carriers are created at the interfaces between conductor and the liquid. Then, they are extracted by the electric force as charge transport where the injection current is proportional to the ion concentration at thermodynamic equilibrium (Alj, Denat, Gosse, Gosse, & Nakamura, 1985). Hence, previous studies have indicated that the conduction mechanism of insulating liquid increases with increasing electric field. As can be seen from the Briere and Gaspard results for nitrobenzene in Figure 2.9, the first region (1) is a low field region where the current density is proportional to the electric field. The second region (2) is a medium region where the current density is almost saturated. The third region (3) is a high field region, which the total density of charge carriers increases gradually with the electric field and can easily lead to breakdown (Brière & Gaspard, 1968).

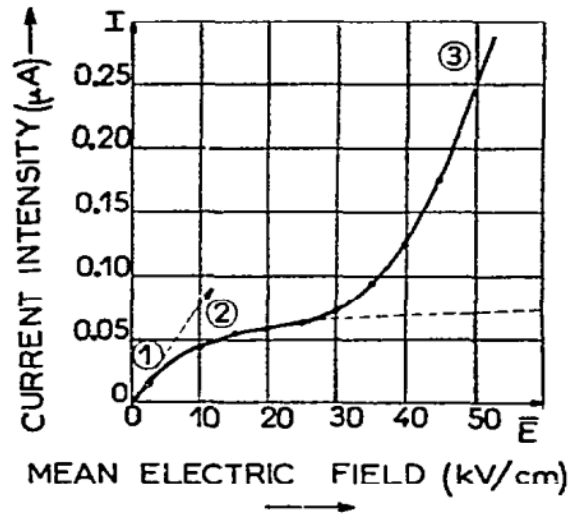


Figure 2.9: Current-voltage (I-V) characteristics of nitrobenzene (Brière & Gaspard, 1968)

The conductivities under DC and AC field are two important parameters to evaluate the dielectric properties of insulating material. In AC field measurement, the charge carriers move back and forth between the two measuring electrodes. At higher frequency, most of the charge carriers do not have sufficient time to travel between two electrodes and form a charge layer in the vicinity of the electrode. At lower frequency, mobile charge carriers in insulating liquid can form charge layers at the electrodes and thereby increases the real part of complex permittivity. At last, there is an accumulation of charge at an interface between two materials or between two regions within a material. This effect is known as the space charge polarization (Bartnikas, 1997).

In DC field measurement, atomic and dipole polarization occurs in several micro second and therefore, the measurement must be conducted at the very beginning when a voltage is applied. The measured current drops instantaneously and becomes steady-state condition due to constant charge carrier generation, injection and recombination (Sha, Zhou, Nie, Wu, & Deng, 2014). Furthermore, high field conduction in nanofluids can also be treated by the Thermally Stimulated Current (TSC) method where the current is injected from a pre-electro stressed dielectric as a result of heating (Donglin Liu, Zhou,

Yang, Zhang, & Jin, 2016). Hence, the curve plotting from the TSC dependent on temperature is used to calculate the trap energy level and electron trap density. These two parameters are related to the enhancement of nanofluids conductivity as insulation material.

In nanofluid, electrical conductivity is defined as the ability of charged particles in the suspension to carry the charges towards respective electrodes when an electrical potential is applied. When nanoparticles are dispersed into base oil, an electric double layer (EDL) is formed around the particle surface and can move oppositely to the charged electrode under electric field. This mechanism is known as electrophoretic mobility and determines the electrical conductivity of a nanofluid. All of the processes are mainly affected by surface charge, size and amount of nanoparticles concentration in nanofluids (Sarojini, Manoj, Singh, Pradeep, & Das, 2013). For instance, Ganguly et. al showed in their study that electrical conductivity is more dependent on nanoparticles concentration than temperature in the Al_2O_3 -based nanofluid (Ganguly et al., 2009). For the insulating material purpose, the conductivity needs to be reduced in order to increase the resistivity of the base fluid. However, the electrophoretic mobility of nanoparticle due to DC electric field associated with high conductivity value on a particle surface will drive the conduction current in nanofluid and lead to aggregation process (Negri & Cavallini, 2017). In order to avoid the impact, long chain non-polar molecules are used as base oil and surfactants are adapted as spacer between particle interfaces.

2.4.3 Measurement of partial discharge activities

Partial discharge (PD) is defined as a localized electrical discharge that partially bridges the insulation between conductors. The occurrence of PDs associated with high electric field within a dielectric material consequently leads to electrical ageing and material breakdown. The time period of a single PD pulse is normally less than 1 μs as

depicted in Figure 2.10. In case of liquid insulation, PD activities play a major role in the acceleration of thermal ageing and degradation of the oil (Junhao Li, Si, Yao, & Li, 2009). Early theoretical studies suggested that the existence of gaseous cavities and bubbles in dielectric liquid under electrical stress implies the occurrence of PD. The current flow between the conductor-dielectric-conductor interfaces could cause local heating and thereby vaporizing the liquid and increases the bubble formation (Pompili & Bartnikas, 2012).

At electron injection condition, the collision energies from the electrons, which enters the oil can break the carbon-hydrogen bonding and carbon-carbon atoms of dielectric material. In many conditions, energy from the electrons is transferred to the oil near to the injection electrode, resulting in heating and prolonging to a vapour formation phase commonly known as streamer. The streamer formation can be elongated and can develop the propagation of breakdown streamers in liquid dielectric (Z Liu, 2016).

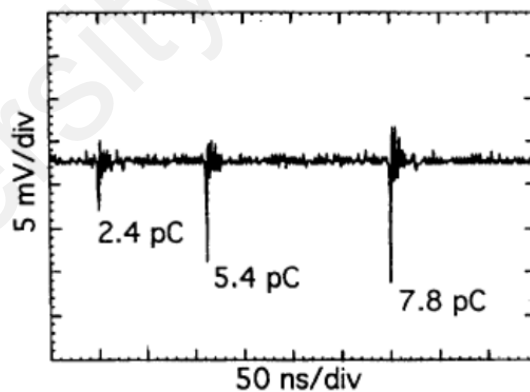


Figure 2.10: Typical PD pulses in dielectric liquid (Pompili & Bartnikas, 2012)

The main objective of PD measurement on liquid insulation is to assess the early formation of streamer and evaluating the new proposed oil insulation performance (Jaroszewski & Rakowiecki, 2017). A needle-to-plane electrode system in conjunction with a narrow band detector adapted from the IEC Standard (IEC-60294) is mainly used

for PD measurement technique on liquid insulation material. Data from the PD measurements are presented in several features to provide useful information about the current state of material insulation. One of them is pulse sequence analysis (PSA), which is analysing two consecutive discharges and comparing the differences between the voltage magnitude or time (Hoof & Patsch, 1994).

Another common pattern is phase resolved partial discharge (PRPD) pattern, which relies on 2-dimensional (2D) distribution of phase, charge and numbers ($\phi-q-n$) of PD pulses (H. Illias, Chen, & Lewin, 2011; Okamoto & Tanaka, 1986). A typical feature of 2D-PRPD pattern is shown in Figure 2.11. Based on the respective features, it is indicated by previous works that PSA has greater suitability as diagnostic approach for characterization and interprets the degradation stage of dielectric material due to PD activities (Patsch & Berton, 2002). Parameters from PSA employ monotonicity, prognosability and trendability as the three criteria of PD measurement to predict the breakdown time (Aziz, Catterson, Rowland, & Bahadoorsingh, 2017).

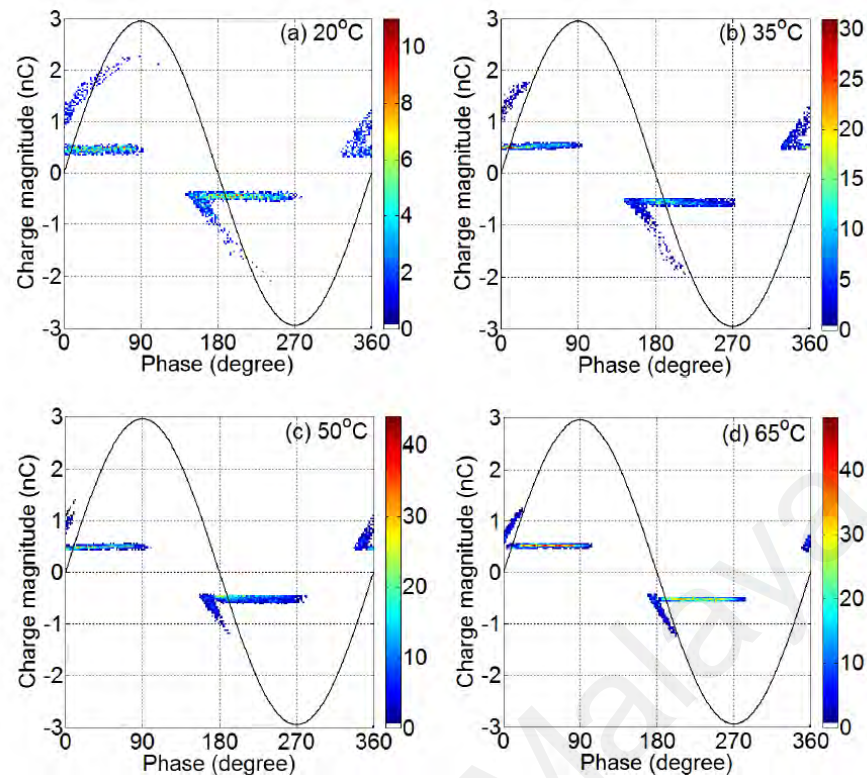


Figure 2.11: 2D-PRPD pattern with temperatures variation on a dielectric material (Hazlee Azil Illias, 2011)

It was found that in nanofluid material, resistance to PD is enhanced by addition of certain amount of nanoparticle into the base insulating oil. Herchl et. al. reported an experimental study on the PD behaviour of magnetite (Fe_3O_4) nanoparticle-based transformer oil (ITO 100) coated with oleic acid (Herchl et al., 2008). The nanofluid exhibits an effective resistance to PD at low concentration of magnetite nanoparticles in all electrode distances. This result shows agreement with the previous hypothesis, which states that oil-based magnetic nanofluid has better insulating properties compared to base oil if the concentration of magnetite does not exceed 0.01 g/L (Kopčanský et al., 2005). Du et. al. investigated the effect of semiconductive nanoparticles (TiO_2)-based transformer oil (Karamay #25) on PD inception voltage (PDIV) under needle-plane electrode configuration (Yuefan Du et al., 2012). The measured PDIV shows an anomalous increase of mean value by 8.2 % from base oil. It is proposed that electron trapping and de-trapping in the shallow trap density created by TiO_2 nanoparticles could convert fast electrons to slow electrons and thereby increases the resistance to PD. Similar

trends were also revealed when semiconductive nanoparticles were dispersed into natural ester base oil where PDIV increased about 7.4 % from the pure ester (Zhong et al., 2013).

In order to study the influence of electrical properties of nanoparticles on the PD activities in a nanofluid, Jin et. al. synthesized nanofluids using two different conductivities of nanoparticles with transformer oil (Shell Diala) (Huifei Jin, Morshuis, Mor, & Andritsch, 2014). The two types of nanoparticles are silica as dielectric and fullerene as conductive nanoparticle respectively. The study shows a significant PD resistance for both types of nanofluids where the silica nanoparticle has higher resistance to PD compared to fullerene. This observation demonstrates a contradiction with previous literature that suggested conductive nanoparticles are expected to increase the insulation property due to reducing the speed of positive streamer propagation by trapping the electron on their surface (J. G. Hwang et al., 2008). The possible explanation behind this contradiction is due to interfaces between nanoparticles and base oil.

Since the surface of fullerene is hydrophobic and the silica is hydrophilic, hydrophilic tends to adsorb moisture or impurities and leaves a larger dynamic impact on the resistance to PD of base oil (Huifei Jin, Morshuis, Mor, Smit, & Andritsch, 2015). In the experimental investigation of Cavallini et. al. (Cavallini et al., 2015), three different conductivities of nanofluids were prepared by dispersing magnetite, graphene, and silica into mineral oil. PDIV was measured for both AC and DC systems from the initial applied voltage of 2 kV and raised within a step of 1 kV. PDIV data shows that magnetite does not enhance significantly the base oil except for AC applied voltage at 0.1 g/L concentration.

2.4.4 Measurement of breakdown strength

Breakdown voltage in AC system, also described as voltage at which electric breakdown occurs under prescribed test conditions, is generally used as one of the quality

assessment and acceptance test for transformer insulation liquid before operation or under routine maintenance. The mean breakdown voltage is commonly reported to evaluate the ability of a transformer oil to withstand the electrical stress. The breakdown mechanism of insulating liquid is usually divided into three categories:

- Ionization theory
- Weakest link theory
- Streamer theory

Ionization theory considers that electrons can be accelerated to ionization energy under high electrical field stress. The earlier assumption is accumulative ionization-collision process will lead to final breakdown (Jian Li et al., 2017). The weakest link theory states that the breakdown voltage in liquid dielectrics starts with a local instability due to the presence of impurities or inhomogeneities in the bulk liquid or irregularities on the electrode geometry surface (Kao, 1976). Streamer theory, in conjunction with the development of high speed imaging devices, becomes prominent to explain the breakdown process of an insulating liquid associated with three stages, which are streamer initiation, streamer propagation and final breakdown.

Although there are different theories on the breakdown mechanism of liquid insulation, all of them can be related to each other. For instance, breakdown process in uniform electric field, where the measurement in industrial applications is in the range of 0.1 MV/cm up to 1 MV/cm, allows the breakdown process to be dominated by streamer initiation and the weakest link theory can also be adopted. On the other hand, in diverging electric field, ionization theory is stated as influencing factor for streamer propagation until reaching the opposite electrode to form a final breakdown stage (Smalo, Astrand, & Ingebrigtsen, 2010). A typical streamer structure at the same breakdown voltage in the semi-uniform and divergent field is shown in Figure 2.9. The streamer structure in the

semi-uniform field under impulse breakdown voltage illustrates more branches compared to the structure in diverging field.

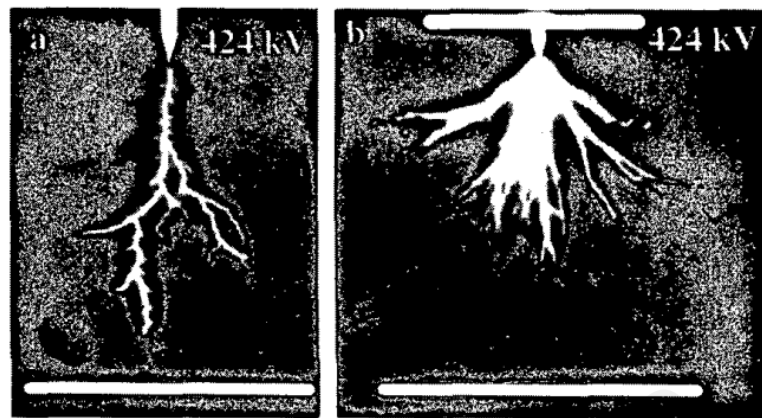


Figure 2.12: Streamer structure in semi-uniform and divergent electric field
(Top, Massala, & Lesaint, 2002)

Most of the transformer manufacturers have adopted the standard of ASTM (American Society for Testing and Materials) and IEC (International Electrotechnical Commission) to measure the dielectric breakdown voltage of insulating liquid. For instance, IEC 60296 states that the minimum breakdown voltage of unused mineral oil of power transformer application is $28 \text{ kV} \cdot \text{mm}^{-1}$ [R]. The minimum breakdown voltage of natural ester should be higher than $30 \text{ kV} \cdot \text{mm}^{-1}$ as required by IEEE 57.104 (“IEEE Guide for Acceptance and Maintenance of Natural Ester Fluids in Transformers,” 2008). However, in the case of nanofluid, there is no such specific standard for measuring the dielectric breakdown. Most of nanofluid breakdown measurements are only adopted from the previous technique as per IEC 60156 or ASTM D1816. For instance, the IEC 60156 standard test normally applies the hemisphere electrode system with a gap of 2.5mm at voltage rise of 2.5 kV/s. Furthermore, statistical analysis has been widely used to evaluate the breakdown voltage distribution (Martin & Wang, 2008). The distribution analysis can be used to fit the cumulative breakdown voltage at low possibilities, which is determined as withstand voltage capacity (Q. Liu & Wang, 2013).

Various investigations have been done to investigate the effect of nanoparticles on dielectric breakdown of nanofluids. Initially, it was experimentally done by Segal et. al. when dispersing the magnetite (Fe_3O_4) to the transformer oil and measured the impulse breakdown voltage. It was found that oil-based TiO_2 nanoparticle exhibits almost positive increment in AC short-term breakdown strength up to 1.0 g/L. Many researchers found that conductive nanoparticles mainly magnetite tend to decrease the breakdown at higher concentration (Kopčanský et al., 2005; Y. Lv et al., 2016; M. Rafiq, Li, Lv, Yi, & Sun, 2016). Titanium oxide (TiO_2) has three types of crystal habits, which are brookite, anatase and rutile. Only anatase and rutile have stable properties and therefore, they are mainly used in research and industrial applications.

2.5 Effects of nanoparticles on enhancement mechanism of nanofluid insulation

The experimental results in Table 2.5 show that dielectric and electrical characteristics of base oil are enhanced by the addition of nanoparticles. The role of nanoparticles when added to a base oil is affected by several mechanisms such as nanoparticle electrical properties, volume concentration, interfacial layer and existence of moisture and impurities.

2.5.1 Effect of nanoparticle properties

Each nanoparticle type has its basic electrical properties such as conductivity and permittivity. Hwang et. al suggested that the dispersed nanoparticles modify the charge relaxation time in the electrodynamics of insulating oil according to their own conductivity and permittivity values by (J. G. Hwang et al., 2010)

$$\tau_r = \frac{2\varepsilon_1 + \varepsilon_2}{2\sigma_1 + \sigma_2} \quad (2.4)$$

where σ_1 and σ_2 are conductivities of base oil and nanoparticles; ε_1 and ε_2 are the permittivities of base oil and nanoparticles respectively. A small value of charge

relaxation time τ_r means fast retention of electrons on the surface of the nanoparticles. In the case of base oil dispersed with magnetite Fe_3O_4 , the relaxation time constant is 7.47×10^{-14} s, which is shorter compared to streamer breakdown propagation. Thus, the surface of nanoparticles can capture high mobility electrons and are converted to slow negatively charged carriers. However, in some cases, it is not satisfactory to explain the enhanced breakdown strength of base oil modified with longer relaxation time constant such as TiO_2 nanoparticles.

Sima et. al. (Wenxia Sima, Shi, Yang, Huang, & Cao, 2015) deduced that all types of nanoparticles either conductive, semiconductive or dielectric will enhance the breakdown performance of base oil. This is due to the electrical properties of each nanoparticle will create mismatch condition with the surrounding of base oil and thereby, forming a potential well on its surface. The mismatch between nanoparticle surface and base oil induces polarized charge between interfaces and can trap passing electrons to improve the breakdown performance of base oil. Assuming that the electric field and nanoparticle size are uniform, the potential well on the surface of conductive, semiconductive and dielectric nanoparticles can be depicted in Figure 2.13.

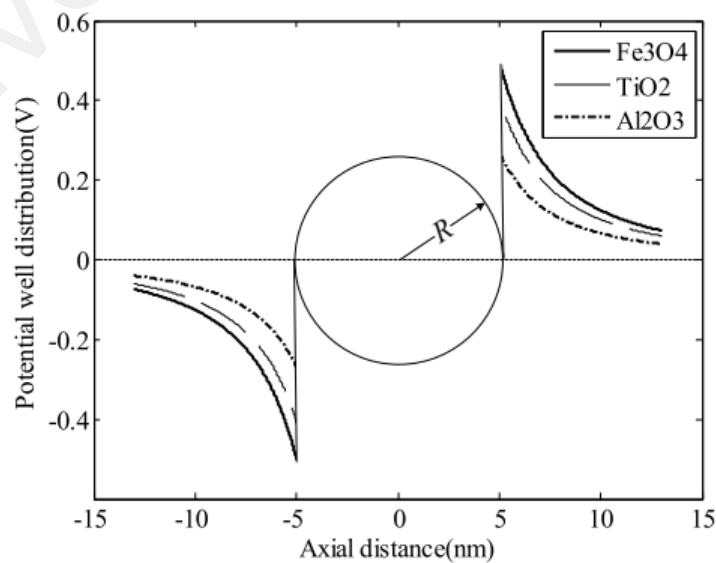


Figure 2.13: Potential well distribution along spherical nanoparticles at different conductivities (Wenxia Sima et al., 2015)

2.5.2 Effect of mass fraction

Volume or mass concentration of nanoparticles also influences the breakdown strength of base oil. Some research works manifested a relationship between the amount of nanoparticle concentration with fluid stability and how it affects the breakdown strength. Electrostatic stabilization by using ultrasonication process is attained through charging the surface of nanoparticles with the same polarity and consequently avoids agglomeration. For instance, Atiya et. al. investigated the effect of TiO_2 nanoparticles on dispersion behaviour and breakdown strength of mineral oil (Atiya et al., 2015). The increasing amount of concentration reduces the nanofluid stability due to surface charge formation on the surface of nanoparticles. This surface charge produces repulsion force that resists the molecular attraction force between nanoparticles and leads to mechanism, which reduces the breakdown strength.

In a DC system, agglomeration will lead to the formation of a conductive micro-bridge across the gap between two electrodes (Kopčanský et al., 2005). The applied electric field on nanofluid also mobilizes the accumulation of nanoparticles on each electrode and contributes to the fast formation of conductive path between electrodes (Ibrahim, Abd-Elhady, & Izzularab, 2016). Therefore, in the case of conductive particles, excessive amount will decrease the breakdown faster compared to nanoparticles with lower conductivity (Nazari, Rasoulifard, & Hosseini, 2016; Sartoratto et al., 2005).



Figure 2.14: Conductive path due to micro-bridging formation (Peppas et al., 2016)

2.5.3 Effect of interfacial layers

Interfacial layer concept in insulation was discussed after Lewis introduced a new solid remarkable material called “nanodielectrics” in 1994 (Smith, Hui, Nelson, & Schadler, 2009). In the case of nanofluid, the specific dielectric properties have been assigned to an interfacial layer surrounding the nanoparticles-base oil interfaces as shown in Figure 2.15. This interfaces resulted in different electrical properties with respect to the base oil and nanoparticles itself (Lewis, 2005). The thickness of the interfacial layer depends not only on the intrinsic properties of base material and a nanoparticle, but also strongly relies on the physical, chemical and electrical conditions (Pourrahipi, Olsson, & Hedenqvist, 2017). With respect to the interfacial layer, previous researchers investigated the interface effects on the formation of electrical double layer introduced by Tanaka et. Al, which plays a major role in enhancing the dielectric strength and the thermal conductivity of base material (Toshikatsu Tanaka, Kozako, Fuse, & Ohki, 2005).

Mansour et. al. suggested that the structure of interfaces formed between Al_2O_3 and TiO_2 nanoparticles with mineral oil depends on their surface species (Mansour et al., 2016). As comparison, Al_2O_3 nanoparticles absorb H^+ and promote positive charges on its surface while TiO_2 absorbs OH^- and is negatively charged. With addition of surfactant

either anionic or cationic, the surfactant head is adsorbed on the opposite polarity of nanoparticle surface and leaves the tail perpendicular towards the base oil. This molecular arrangement keeps the optimal distance between nanoparticles by two stages of interfacial layers; the aligned layer, which is more robust and rigid due to molecular perpendicular arrangement by surfactant addition, and the affected layer, which is less aligned and exists in a nanofluid without addition of surfactant due to incarceration of oil chain in the vicinity of nanoparticles.

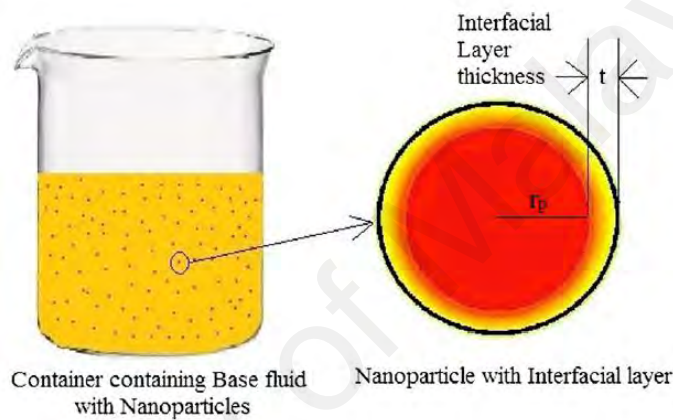


Figure 2.15: Illustration of nanoparticle with interfacial layer in nanofluid suspension (Kotia, Borkakoti, Deval, & Ghosh, 2017)

2.6 Summary

This chapter describes a brief review of high voltage insulation material, the effects of conventional mineral oil and its related hazards. Natural ester, which is mainly extracted from vegetable oil as an alternative for mineral oil, has been discussed. There are several methods implemented in improving the characteristics of vegetable oil as required in power transformer applications. One of the widely used techniques is the addition of nanoparticles.

To understand the basic knowledge of the potentially new nano-modified dielectric liquids or known as nanofluid, a review of synthesis, stability treatment and characterization of nanofluid-based insulation have been presented in Section 2.3. The basic principle of dielectric and electrical measurements of liquid insulation in terms of

dielectric properties, partial discharges activities and breakdown have also been discussed in Section 2.4. This information will help in understanding the breakdown mechanisms in base oil and nanofluid dielectric liquids. The influence of nanoparticles on their enhancement properties as dielectric insulation is also discussed in Section 2.5..

University of Malaya

CHAPTER 3: METHODOLOGY

3.1 Introduction

This chapter describes the methodology that has been applied in this work. A step by step and extensive research methodology has been adopted for effective palm oil-based nanofluid insulation. The material preparation, nanofluid synthesis, stability characterization, experimental setup and various techniques that have been used to conduct the study are described in detail. The general flow chart of methodology of this work is shown in Figure 3.1.

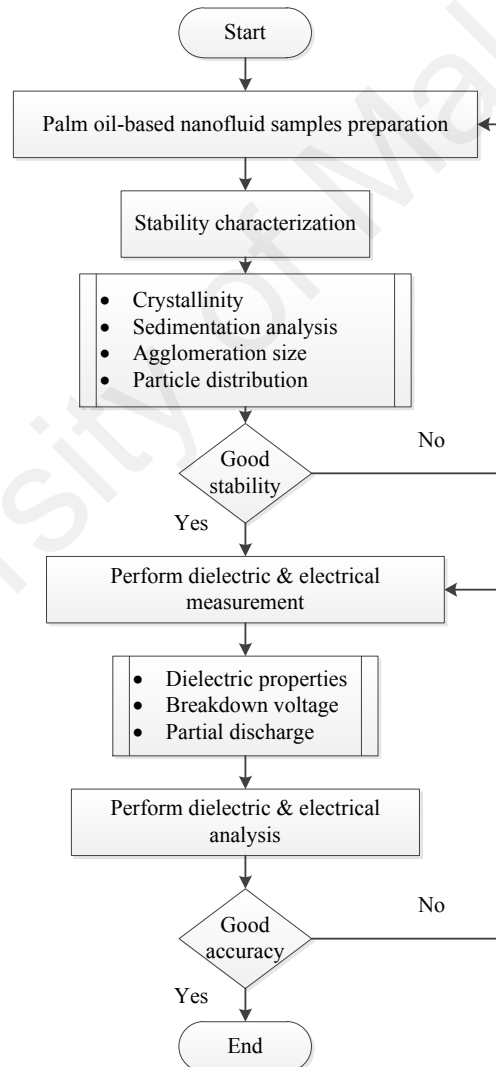


Figure 3.1: Flow chart of the methodology

3.2 Material preparation

3.2.1 Base oil

The natural ester used as the base insulation oil in this study is from the grade of highly-refined, bleached, deodorized palm oil (RBDPO). The palm oil has a deep yellow colour as shown in Figure 3.2. This liquid possess a high dielectric strength as reported in the previous study (A. N. Mohamad et al., 2018). The fatty acid compositions of the palm oil used as the base oil in this study are tabulated in the Table 3.1.



Figure 3.2: Refined, bleached, deodorized, palm oil (RBDPO)

Table 3.1: Fatty acid compositions of palm oil

Type of fats	Total per 100 g
Saturated	43 g
Mono-saturated	45 g
Poly-saturated	12 g

3.2.2 Nanoparticles

Conductive and semi-conductive nanoparticles used are iron (II,III) oxide, $\text{Fe}_3\text{O}_4 \geq 97\%$ and titanium dioxide, $\text{TiO}_2 \geq 99.5\%$ of purity, which are purchased from Sigma Aldrich in nanopowder form (Figure 3.3). The particle size ranges have been quoted

averagely at 50 nm. The general properties of both nanoparticles obtained from the supplier are tabulated in Table 3.2.

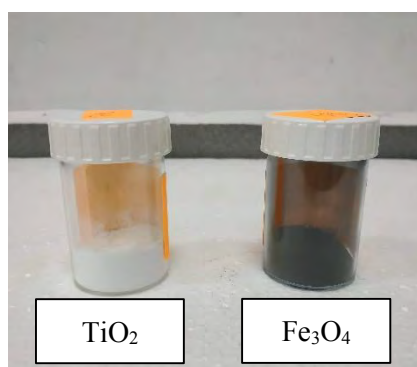


Figure 3.3: Titanium dioxide and iron (II,III) oxide nanoparticles

To remove moisture and impurities, the nanoparticles are subjected to the drying process as described in section 3.2.3.

Table 3.2: General properties of nanoparticles used in this project

Properties	Iron (II,III) oxide, Fe_3O_4	Titanium dioxide, TiO_2
General form	Nanopowder (spherical)	Nanopowder (anatase)
Color	black	white
Particle size (nm)	50 - 100	21 (primary)
Melting point ($^{\circ}\text{C}$)	1538	1850
Density at 25 $^{\circ}\text{C}$ (g/mL)	4.8 - 5.1	4.26
Surface area (m^2/g)	> 60	35 - 65

3.2.3 Drying process

All materials were treated by drying process at a temperature of 80°C for base oil and 300°C for nanoparticles in thermal vacuum at 90 kPa chamber for at least 48 hours, as shown in Figure 3.4. After drying, all materials were cooled down at ambient temperature.



Figure 3.4: A thermal vacuum oven

3.3 Synthesis of nanofluid

3.3.1 Amount of nanoparticles

The palm oil-based nanofluid insulation was synthesized using the two-step method. Nanoparticles were added into 500 ml of base oil with specific ratios as tabulated in Table 3.3 and were stirred for 15 minutes. The concentration of the nanofluids can also be presented in percentage of volume fraction by Eq. (3.1).

Table 3.3: Palm oil-based nanofluid samples

Sample abbreviation	Amount of nanoparticles (g/L)	
	Iron Oxide	Titanium Dioxide
NE	-	-
CNF1	0.01	-
CNF2	0.1	-
CNF3	1.0	-
SNF1	-	0.01
SNF2	-	0.1
SNF3	-	1.0

$$\phi = \frac{\frac{m_p}{\rho_p}}{\frac{m_p}{\rho_p} + \frac{m_f}{\rho_f}} \times 100\% \quad (3.1)$$

where:

ϕ	: particle volume fraction
m_p	: mass of nanoparticles
ρ_p	: density of nanoparticles
m_f	: mass of base fluid
ρ_f	: density of base fluid

3.3.2 Ultrasonication

For long stationary application such as in power transformers, stable nanofluid is required to maintain its effectiveness as insulating material. To improve the dispersion stability, ultrasonication treatment was applied in order to ensure the homogeneity of nanoparticles in the suspension. Sonication treatment was performed for 30 minutes for each of nanofluid samples using an ultrasonic bath at room temperature, as shown in Figure 3.5 (output power = 120 W, applied frequency = 40 kHz).



Figure 3.5: Ultrasonic bath to produce homogenous dispersion

3.4 Dispersion characterization techniques

The stability characterization techniques applied in this work are as follows: crystallinity test, sedimentation analysis, agglomeration size, and particle distribution analysis.

3.4.1 Crystallinity test

The XRD analysis of nanoparticles phase and structure were evaluated using PANalytical X'Pert³ Powder with CuK α radiation at 1.54056 Å. The investigations were carried out using scanning method at angle of 2θ within the range of 10° to 70° with a step size 0.1972° . The average crystalline size of particle was determined from the XRD line broadening using Scherrer's equation:

$$d_{XRD} = \frac{0.9\lambda}{\beta_{FWHM} \cos\theta} \quad (3.2)$$

where, λ is wavelength of X-Ray, β is FWHM (full wave at half maximum) θ is diffraction angle, and d_{XRD} is calculated crystallite size.

3.4.2 Sedimentation analysis

Sedimentation analysis is a technique for evaluating the tendency of nanofluids to aggregate and eventually boost the sedimentation process with time. After the palm oil-based nanofluid samples were prepared, each sample was poured into a cylindrical glass tube. The samples were left for 24 h without shaking to observe any changes of the condition due to natural ambience before measurements were performed. Figure 3.6 illustrates the evolution of nanofluid aggregation and sedimentation progress within a period of time.

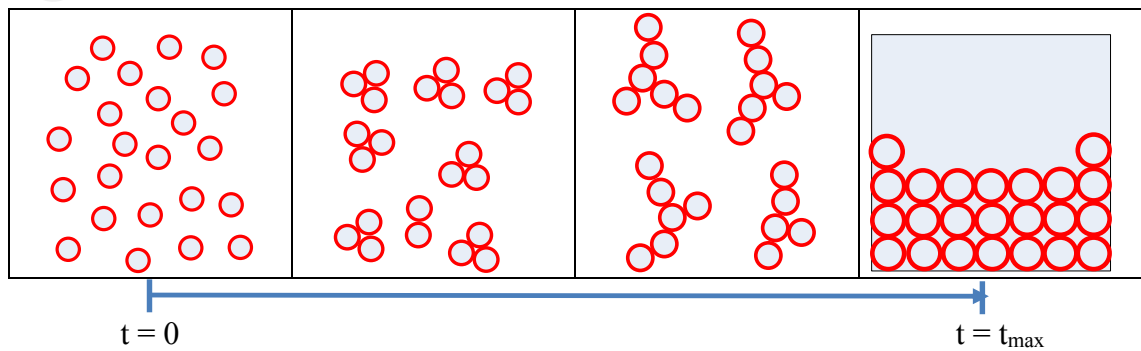


Figure 3.6: Time-dependent aggregation and sedimentation of nanoparticles

3.4.3 Agglomeration size

The morphology analysis was conducted using a scanning electron microscope (SEM) (Zeiss EVO® MA10, Figure 3.7). SEM provides qualitative information about topography, morphology and general appearance of the specimen. The nanofluid sample was deposited on a sticky tape of the SEM specimen holder and was dried until solid particles were obtained. The edge of high-quality filter paper was used to remove the excessive nanofluid from the tape. Different magnification scales were used in order to achieve the best aggregation image. The agglomeration size was measured as an arbitrary distance by SEM.

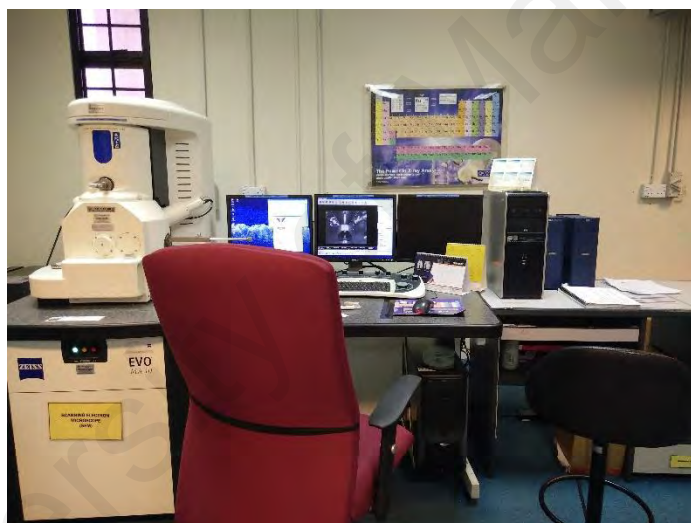


Figure 3.7: A Zeiss EVO® MA10 scanning electron microscope

3.4.4 Particle distribution

The dynamic light scattering (DLS) method was applied to compare the average particle size of the nanoparticles (Fe_3O_4 and TiO_2) at 0.01 g/L. Measurements were performed at 25 °C using a Malvern Zetasizer (Figure 3.8), within 24 hours after nanofluid preparation. The average size of the nanoparticles were investigated using a laser analyser. Therefore, the particle size distribution can be determined in a uniform

stable suspension. The particle distribution measurement was conducted without diluting the concentration and without adjusting the pH of the suspension.



Figure 3.8: A Malvern Zetasizer instrument for DLS measurement

3.5 Dielectric and electrical measurements

Dielectric and electrical characteristics of palm oil-based nanofluids were measured at different experimental setup under various amounts of concentration and nanoparticle types. The measurement procedures are discussed in the following section.

3.5.1 Dielectric properties

3.5.1.1 Experiment setup

The Metrohm® potentiostat as shown in Figure 3.9 was used to measure dielectric properties of nanofluid under frequency domain spectroscopy (FDS) response and current-voltage (I-V) characteristic method. For FDS measurement, a sinusoidal AC voltage of 0.5 V_{rms} was applied to the test cell at room temperature with various frequencies, ranging between 0.1 Hz and 0.1 MHz. The impedance results from the measurement were plotted in terms of real permittivity, ϵ' and imaginary permittivity, ϵ'' . For I-V characteristic measurements, the parameters were adjusted using linear sweep

voltammetry (LSV) with a scan rate of 0.05 V/s and a step potential of 0.20 V. The applied DC voltage was within a range of 1 to 10 V.



Figure 3.9: The Metrohm potentiostat for FDS and I-V measurements

3.5.1.2 Test chamber

In this study, about 100 ml of nanofluid was poured carefully into a test chamber. The setup consists of two cylindrical copper plates with a diameter of 25 mm and 100 μm gap distance. Both electrodes were fully immersed with liquid under test (LUT) to overcome the fringing capacitance as shown in Figure 3.10.

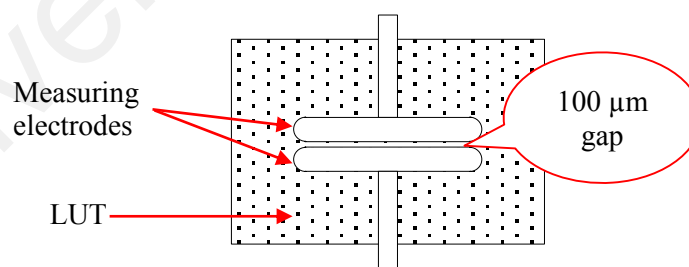


Figure 3.10: Test chamber for dielectric properties measurements

3.5.1.3 Dielectric constant and losses

The real permittivity ϵ' and the imaginary permittivity ϵ'' of the LUT were calculated according to:

$$\varepsilon' = \frac{Z''}{2\pi f C_o Z^2} \quad (3.3)$$

$$\varepsilon'' = \frac{Z'}{2\pi f C_o Z^2} \quad (3.4)$$

where Z' and Z'' are the real and imaginary components of the complex impedance Z , f is the frequency of the applied AC voltage and C_o is the capacitance of test fixture without LUT and is given by:

$$C_o = \frac{\varepsilon_o A}{d} \quad (3.5)$$

where ε_o is the permittivity of the free space, $\varepsilon_o \approx 8.854 \times 10^{-12}$ (Fm⁻¹), A and d is the area and a gap distance between two copper plates respectively.

3.5.1.4 Current-voltage (I-V)

For I-V characteristic measurements, the parameters were adjusted using linear sweep voltammetry (LSV) with a scan rate of 0.05 V/s and a step potential of 0.20 V. The applied DC voltage was within a range of 1 to 10 V. For DC conductivity (σ_{DC}), the electrical conductivity of the nanofluid sample can be calculated by using

$$\sigma_{DC} = \frac{I}{V} \cdot \frac{L}{S} \quad (3.6)$$

where V is the applied voltage, I is the measured current, L is the spacing between the electrodes and S is the effective area of the measuring electrodes.

3.5.2 Partial discharge

3.5.2.1 Experiment setup

The Mtronix® MPD 600 setup manufactured by Omicron (Germany) was used for PD measurement in conjunction with high voltage generation kit (TERCO, Sweden). The list of apparatus used in PD experiment setup is shown in Figure 3.11. The PD signals measured by MPD 600 were in current pulses across nanofluid sample between the needle and plane electrodes. When electrical discharges occur, the coupling capacitor transfers equivalent charges to the test object to preserve the voltage drop across the electrodes. By the time of PD events, the short duration of voltage pulses in the nanosecond range are detected by coupling device and the PD detector, which are transferred through fibre optic to the personal computer (PC) as represented in Figure 3.12.

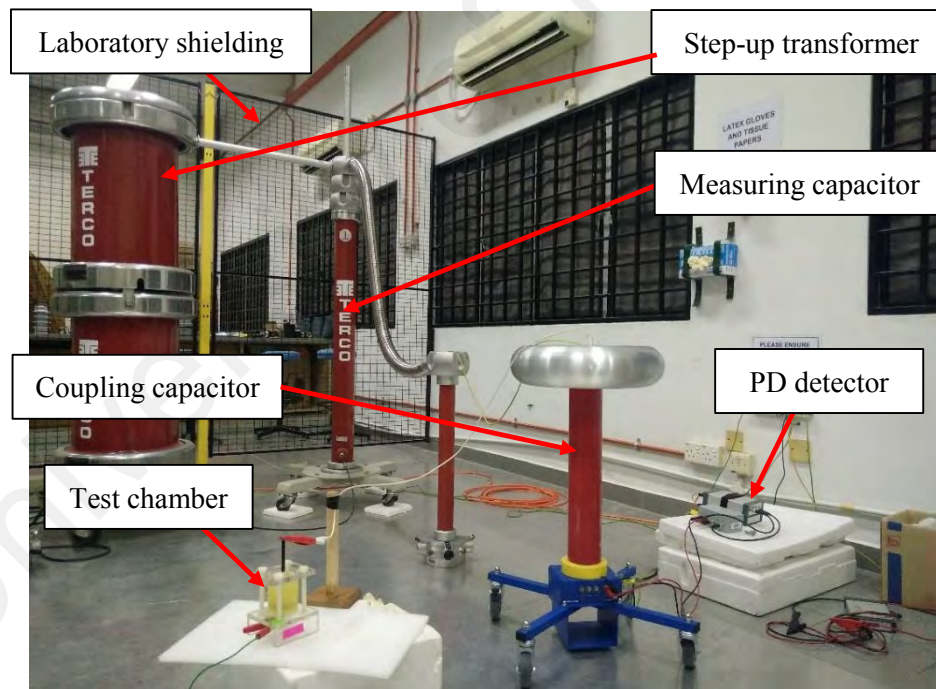


Figure 3.11: Apparatus for PD measurement

The experimental condition consists of two stages:

- Inception condition: Measurement was taken immediately after the first PD occurrence. The applied voltage U_{app} was ramped-up from 0 to 25 kV.

- Steady-state condition: Measurement was taken after 30 min of the applied voltage. The applied voltage U_{app} was fixed at 26, 28, and 30 kV

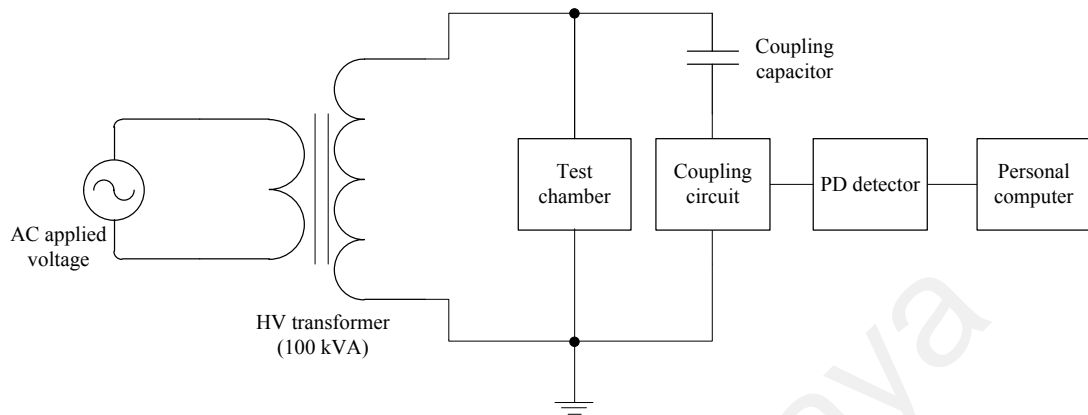


Figure 3.12: Schematic diagram for PD experiment setup

3.5.2.2 PD test chamber

Figure 3.13 shows a schematic diagram of the test chamber used for PD measurement in a nanofluid sample. The self-fabricated chamber was adopted from IEC 60343 configuration, which consists of two conductors; high voltage and ground stainless steel electrodes. The rod electrode has a 1 mm curvature radius and 10 mm gap distance to the plane electrode. The edges of the test chambers were sealed with silicone glue to prevent the fluid under test from spilling out. This setup allows PDs to occur without causing any breakdown. The nanofluid samples of 400 mL volume in test chamber were stressed by being subjected to 50 Hz sinusoidal applied voltage. The voltage was controlled at a rate of rise of 1 kV/s.

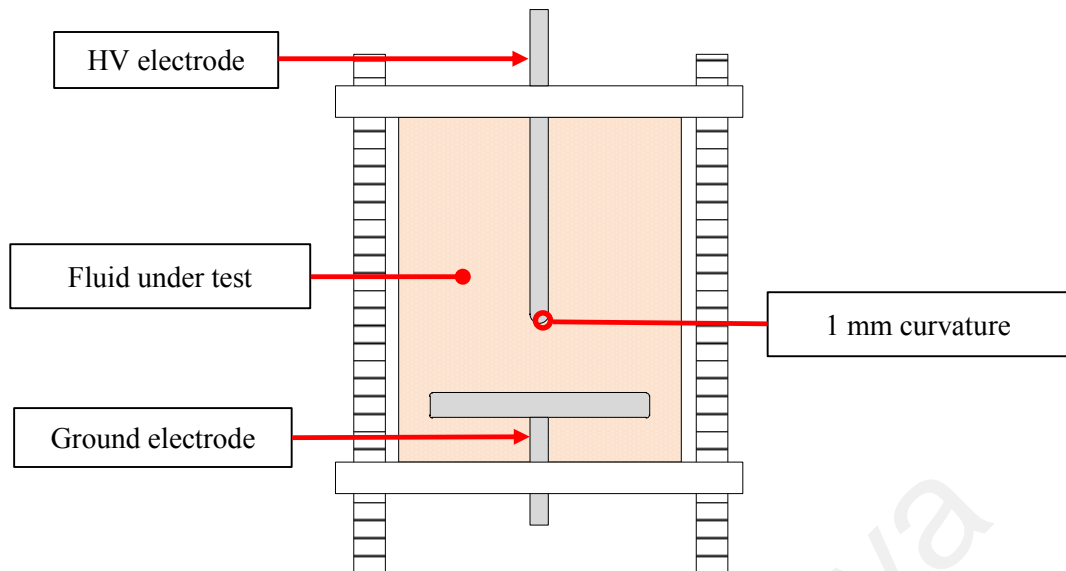


Figure 3.13: PD test chamber

3.5.2.3 Charge calibration

Calibration was required each time the measurement was started. Calibration of PD waveform was performed by using a charge calibrator unit, which has a charge range of 1 to 100 pC as shown in Figure 3.14.

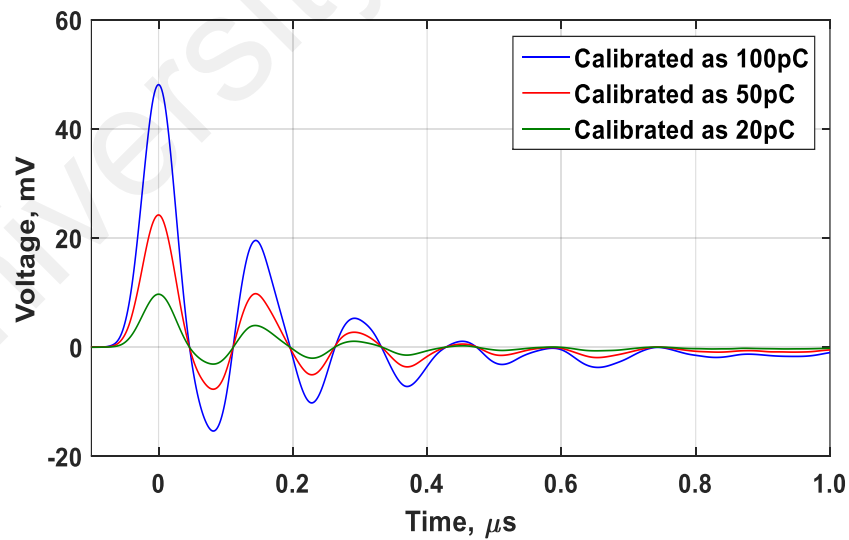


Figure 3.14: PD calibrated waveforms

3.5.2.4 Partial discharge inception voltage (PDIV)

According to IEC 61294, partial discharge inception voltage (PDIV) is the minimum applied voltage that is needed for PD with 100 pC value to occur at 1 kV/s of increasing rate. In this work, the PDIV was recorded for each type of nanofluid sample. The test designed with the objective to identify the ability of insulating oil to prevent the electrical discharges especially for PDs when they are subjected to high electrical stress. Due to non-destructive type test of PDIV, most transformer manufacturers accepted and regularly implemented the PDIV test. In this study, all the measurement results of PDIV were plotted using statistical functions.

3.5.2.5 Phase resolved partial discharge (PRPD) pattern

The PD measurement analysis technique that is generally used is phase resolved partial discharge (PRPD) pattern. The PRPD pattern, also known as ϕ - q - n plot is obtained by sorting and counting each number of charge magnitude q , repetition n at phase of the applied voltage ϕ and is displayed into a single voltage cycle within a range of 0° to 360° . The colour intensity represents the number of events, where the higher colour intensity is the larger number of PD occurrences. Figure 3.15 shows an example of PRPD pattern obtained from the measurement work. In order to compare each PRPD pattern from each nanofluid, a comparison graph is used to visualize all of the nanofluid data.

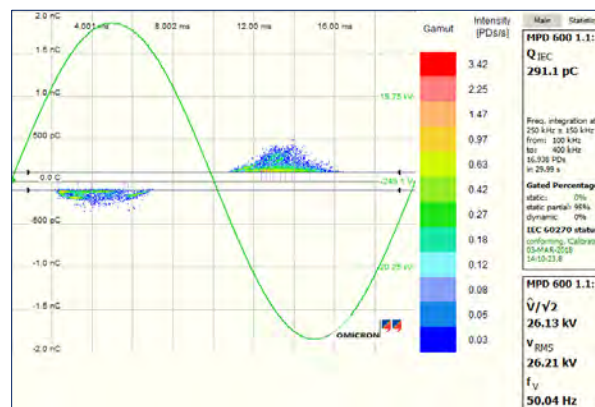


Figure 3.15: A typical bipolar PRPD pattern from Omicron®

The graphical user interface (GUI) of the Omicron software has an option to export PD measurement data to MATLAB software. Thus, by using a MATLAB code, the data can be processed further for other meaningful analysis, such as evaluating the PD sequences, PD phase and charge magnitude distribution.

The commonly used PD phase distributions are:

$H_n^+(\phi)$ and $H_n^-(\phi)$ – Positive and negative number of PDs per cycle against phase distribution respectively, where

$$H_n^\pm(\phi_i) = \frac{1}{N} \sum_{j=1} n(\phi_i, q_j^\pm) \quad (3.7)$$

$H_{qs}^+(\phi)$ and $H_{qs}^-(\phi)$ – Positive and negative total apparent charge magnitude per cycle against phase distribution respectively, where

$$H_{qs}^\pm(\phi_i) = \frac{1}{N} \sum_{j=1} q_j^\pm n(\phi_i, q_j^\pm) \quad (3.8)$$

$H_{qn}^+(\phi)$ and $H_{qn}^-(\phi)$ – Positive and negative mean charge magnitude per cycle against phase distribution respectively, where

$$H_{qn}^\pm(\phi_i) = \frac{H_{qs}^\pm(\phi_i)}{H_n^\pm(\phi_i)} \quad (3.9)$$

$H_{qm}^+(\phi)$ and $H_{qm}^-(\phi)$ – Positive and negative maximum charge magnitude per cycle against phase distribution respectively, where

$$H_{qm}^\pm(\phi_i) = \max |q_j^\pm(\phi_i)| \quad (3.10)$$

Each phase distribution indicates the behaviour of PD activity in nanofluid in terms of phase of discharge event. The $H_n(\phi)$ distribution reveals how frequent discharges occur

at each phase of applied voltage per cycle. The $H_{qs}(\phi)$ distribution indicates the total apparent charge per cycle at each phase of applied voltage. The $H_{qn}(\phi)$ distribution is the mean discharge events at each phase and $H_{qm}(\phi)$ distribution shows the trend of maximum charge magnitude with respect to each phase of applied voltage.

3.5.3 Breakdown voltage

3.5.3.1 Experiment setup

The dielectric breakdown voltage (BDV) of each sample was measured using an AC automated test kit with a maximum applied voltage of 60 kV, as shown in Figure 3.16. The setup and procedure for each breakdown of samples were in accordance with the ASTM D1816 standard.



Figure 3.16: MEGGER automated breakdown test kit

3.5.3.2 BDV test chamber

The gap distance of the hemisphere electrodes was set to 1.0 mm and the practical of breakdown test chamber is shown in Figure 3.17. The measured breakdown voltage of each sample was compared with the average breakdown voltage and Weibull distribution. The dielectric breakdown strength, E of the nanofluid samples can be determined through the following equation:

$$E = V_{bd}/d \quad (3.11)$$

where V_{bd} is the breakdown voltage and d is the gap distance. Due to the voltage limitation of the automated test kit, nanofluid with 2 mm gap distance was unable to break down. Hence, the gap distance was adjusted to 1 mm. During the test, the hemisphere electrodes were washed with ethanol after every 10 breakdown tests.

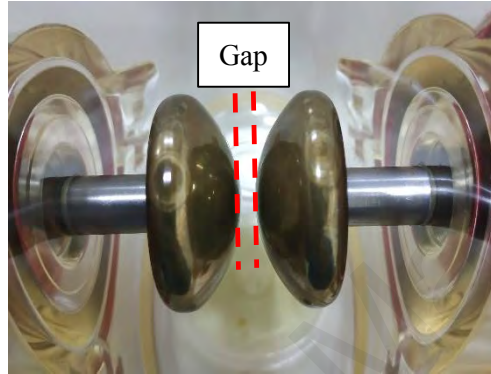


Figure 3.17: Practical of hemisphere electrodes

3.5.3.3 Weibull distribution

The cumulative distribution function of Weibull distribution for any random variable x is defined as

$$f(x) = 1 - \exp(-x/\alpha)^\beta \quad (3.12)$$

where α is the scale parameter corresponding to a probability of 63.2% and β is the shape parameter that is related to the scattering of the data and failure rate. To estimate the probability of x as a function of breakdown voltage and PDIV, the Weibull cumulative distribution function can be transformed into a straight line form as given by

$$\ln \left[\ln \frac{1}{1 - f(x)} \right] = \beta \ln(x) - \beta \ln(\alpha) \quad (3.13)$$

Hence, β is directly represented by the slope of the line and α is evaluated from the y data that intercepts with it. The withstand voltage calculated by using 99% of upper and lower limit of which the breakdown voltages will occur.

3.6 Electric field simulation

In order to study the level of electric field intensity and its distribution associated with the addition of a nanoparticle (in this study, Fe_3O_4 and TiO_2), the electric field distribution and displacement were modelled and calculated by Finite Element Method (FEA) using COMSOL Multiphysics software.

3.6.1 Model geometry and parameters

Figure 3.18 shows the two-dimensional axial symmetric model geometry, which consists of high voltage and zero potentials electrode surrounded by base oil and a spherical nanoparticle with permittivity and conductivity values as shown in Table 3.4. This model was built according to Ibrahim's work (Ibrahim et al., 2016), which is analysing the electric field distribution around nanoparticle surface when an electric potential applied.

Table 3.4: Material parameters in the geometry model (Muhammad Rafiq, Lv, & Li, 2016)

Domain (Figure 3.15)	Description	Material	Relative permittivity, ϵ_r	Conductivity, σ (S/m)
1	High voltage electrode	Stainless steel	1	4.03×10^6
2	Ground electrode	Stainless steel	1	4.03×10^6
3	Nanoparticle surface	Fe_3O_4	80	1×10^5
3	Nanoparticle surface	TiO_2	100	1×10^{-11}

4	Base oil	Natural ester	2.44	2.02×10^{-11}
---	----------	---------------	------	------------------------

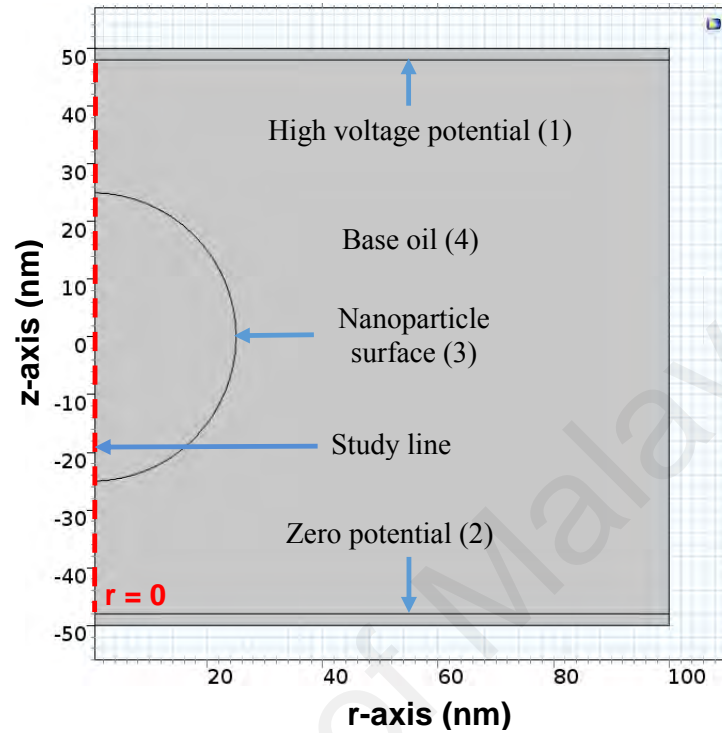


Figure 3.18: Axial symmetric two-dimensional model geometry (nm)

3.6.2 Boundary condition

In Figure 3.19, the electric displacement boundary condition of the geometry is governed by

$$D = \epsilon_0 \epsilon_r E \quad (3.14)$$

The high voltage (HV) side of the hemisphere electrode boundary was specified as a terminal source of time-dependent AC voltage by

$$V(t) = V_{peak} \sin(2\pi ft) \quad (3.15)$$

To evaluate the electric field, a single sinusoidal voltage of 10 kV peak magnitude, 50 Hz frequency was applied on the HV electrode and the ground boundary condition equals

to zero electric potential. The interface condition of the remaining geometry boundaries were set to continuity by

$$n_2 \cdot (J_1 - J_2) = 0 \quad (3.16)$$

Since the geometry was enclosed in a rectangular insulated domain, where J is defined as current density. The outermost boundary condition was assigned to

$$n \cdot J = 0 \quad (3.17)$$

Finally, the electric potential distributions in the geometry were solved according to the following partial differential equation (PDE),

$$-\nabla \cdot (\sigma \nabla V) - \nabla \cdot \left(\epsilon \frac{\partial \nabla V}{\partial t} \right) = 0 \quad (3.18)$$

where $\epsilon = \epsilon_0 \epsilon_r$ is the permittivity, V is the electric potential and σ is the conductivity. Figure 3.19 and Table 3.5 are present the boundary conditions and electric current expressions of the model respectively.

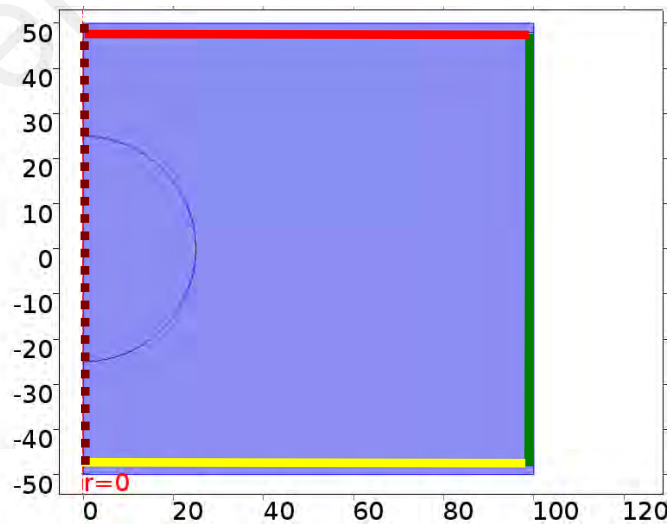


Figure 3.19: Boundary lines for model geometry

Table 3.5: Boundary conditions and its electric expressions

Boundary lines	Boundary condition	Expressions
Red	Applied potential	$V(t) = V_{peak} \sin(2\pi ft)$
Green	Insulation	$n \cdot J = 0$
Yellow	Ground potential	$r = 0$
Brown	Axial-symmetry	$V = 0$
All interior boundaries	Continuity	$n_2 \cdot (J_1 - J_2) = 0$

3.6.3 Meshing

After the parameters and boundaries of the model were appointed, the geometry model is fractioned into smaller elements for effective computation, which is called mesh. Elementary shape functions such as tetrahedral, triangular, edge and vertex elements were used to estimate the solution for FEA model. In this study, the geometry model was meshed by employing 27514 triangular elements as presented in Figure 3.20. The mesh area was also solved by the finest mesh elements in order to ensure the precision and accuracy of the electric field distribution.

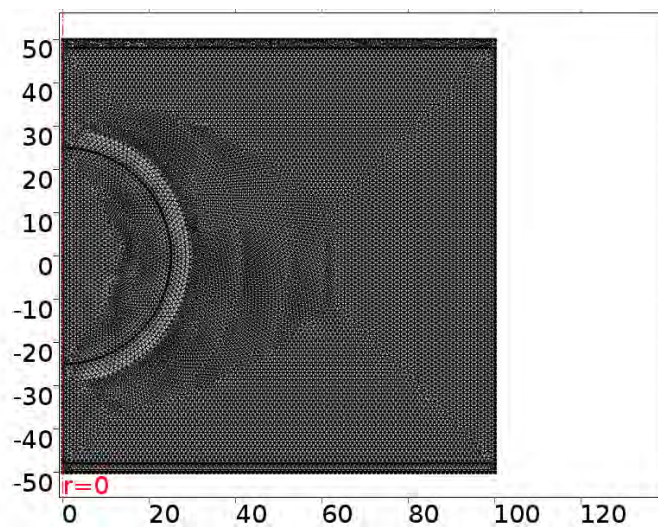


Figure 3.20: Model geometry presented in mesh elements

3.7 Summary

In this chapter, the research methodology used in this work is described in detail. The endeavour was begun by the preparation of nanofluid samples, followed by their stability characterization. Ultrasonication technique was adopted to produce homogenous and stable suspensions. Sedimentation, agglomeration size and particle distribution analysis were carried out to analyse the dispersion stability of the nanofluid samples. Dielectric and electrical characteristics were investigated by experimental works in the laboratory-controlled conditions. In the phase of experimentation, frequency domain spectroscopy (FDS) response and current-voltage (I-V) were employed to calculate the dielectric constant, losses and conductivity. Partial discharge (PD) measurements were performed to study the resistance of nanofluid towards the electrical discharges. Finally, AC breakdown voltages were measured in order to study the dielectric strength of the samples.

CHAPTER 4: RESULTS AND DISCUSSION

4.1 Introduction

This chapter describes the results that have been successfully obtained from the assessment and measurement in this work. In the first stage, dispersion characteristics of palm oil-based nanofluid is reported and discussed. It is followed by the investigation on dielectric properties for all samples under the frequency and I-V analysis. After that, the PD behaviour of palm oil-based nanofluids is discussed. In the next phase, the results of dielectric breakdowns strength with the effect of nanoparticles are stated. Also, the electric field distribution when a nanoparticle dispersed into the base oil is shown in this chapter. As a remark, palm oil, palm oil with conductive nanoparticles and palm oil with semiconductive nanoparticles sample are referred to as PO, CNF and SNF according to Table 3.1 from this point onwards.

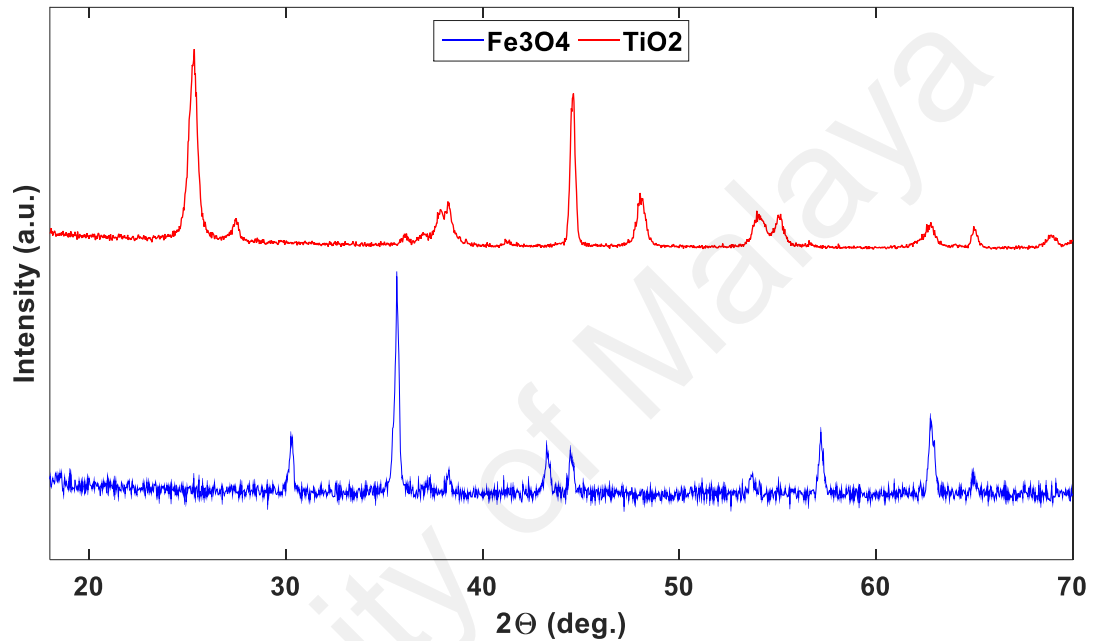
4.2 Dispersion characteristics of palm oil-based nanofluid insulation

4.2.1 Crystalline size of dispersed nanoparticles

Figure 4.1 shows XRD spectra of the nanoparticles powder, which has been used in this study. The strong peak for the Fe_3O_4 nanoparticles especially at 35.6° demonstrates the crystalline phase of the particle. Meanwhile, strong diffraction peaks at 25.3° and 48° of TiO_2 spectra also indicate the anatase phase and the drying temperature during sample preparation can affect the phase transforming to the rutile form (B. Li, Wang, Yan, & Li, 2003). The higher intensity of XRD peaks reflect that the nanoparticles structure is in crystalline form and broad diffraction peaks indicate very small size crystallite. According to the XRD pattern, the average crystalline size can be estimated by using Scherer's equation (Eq. 3.2), where the results are enumerated in Table 4.1. The value of FWHM (full width at half maximum) is determined by a profile fitting software, OriginPro®.

Table 4.1: Average of crystallite size of Fe₃O₄ and TiO₂ nanoparticles

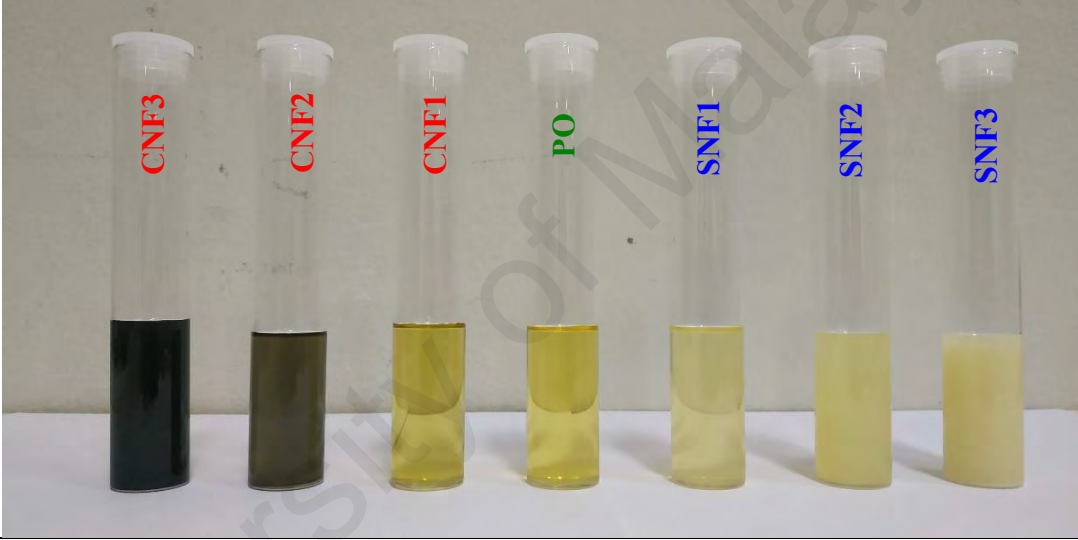
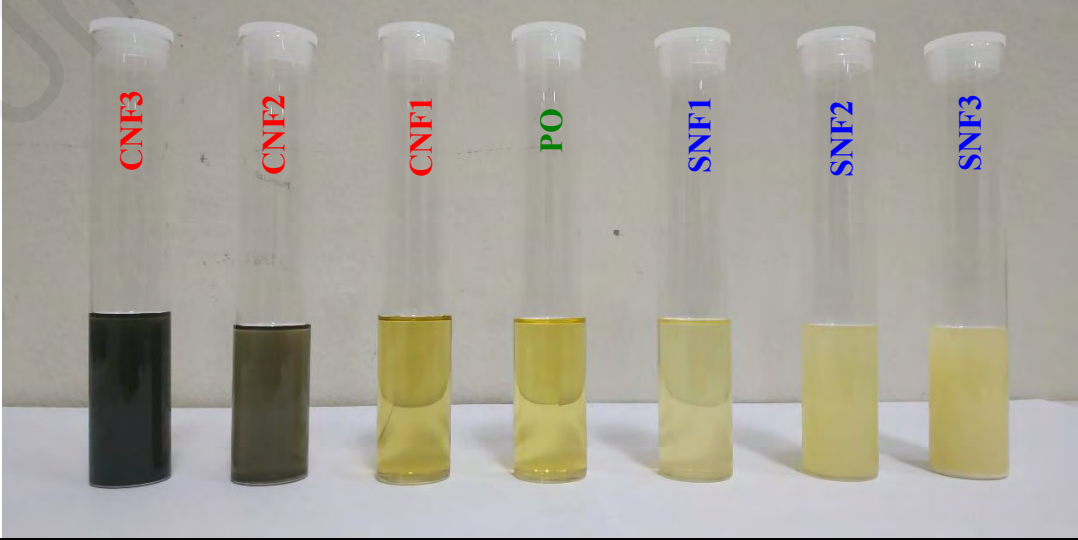
Nanoparticles	Average of crystallite size (nm)
Iron (II,III) oxide, Fe ₃ O ₄	31.6
Titanium dioxide, TiO ₂	110.9

**Figure 4.1: XRD spectra of Fe₃O₄ and TiO₂ nanoparticles**

4.2.2 Sedimentation analysis with elapsed time

After nanoparticle powder was dispersed into the base oil accordance to the formulation ratio and went through the sonication process, the visual inspection method, a qualitative tool, was used to analyse the sedimentation time of nanofluid samples. Figure 4.2 shows the PO, CNFs and SNFs samples, which were suspended with different amount of Fe₃O₄ and TiO₂ nanoparticles at different stage of elapsed time. The stability period can be defined as the elapsed time after the preparation of nanofluids, at which the traces of sedimentation are visible (Choudhary, Khurana, Kumar, & Subudhi, 2017). Initially, at higher nanoparticle concentration, the CNF samples became dark colour while the SNF

samples turned into milky. Visual inspection was made at the base of the glass tube to observe any sedimentation occurrence. In this work, no sedimentation sign occurred in 24 hours, indicating that the dispersion of nanoparticles within the sample was stable and the measurement of dielectric and electrical characteristics should be made within 24 hours after the sample preparation. For an industrial application, it can be concluded that the only suitable concentration for nanoparticles dispersed into a base oil is below 0.1 g/L.

Elapsed time = 0 hour						
						
Observation: <ul style="list-style-type: none"> • Highest concentration of Fe_3O_4 displays more dark colour • Highest concentration of TiO_2 represents a more milky colour 						
Elapsed time = 24 hour						
						
Observation:						

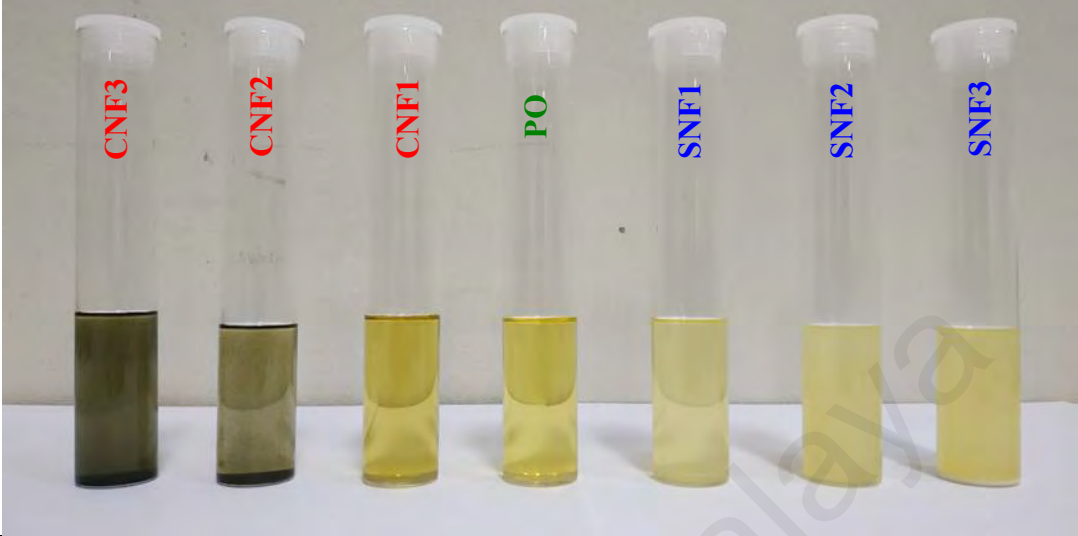
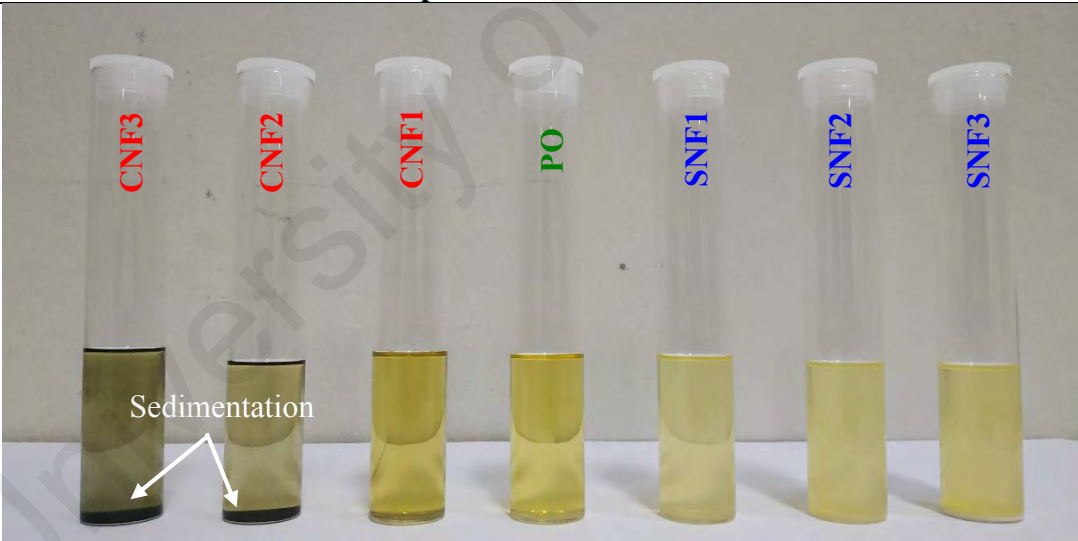
<ul style="list-style-type: none"> • There is no discoloration appeared in the samples • Samples are considered as stable within 24 hours
<p style="text-align: center;">Elapsed time = 72 hour</p>

<p>Observation:</p> <ul style="list-style-type: none"> • The colour deterioration appeared on the CNF2, CNF3 and SNF3 sample • The colour for CNF1 and SNF1 remained unchanged
<p style="text-align: center;">Elapsed time = 132 hour</p>

<p>Observation:</p> <ul style="list-style-type: none"> • Sedimentation clearly occurred on CNF2 and CNF3 sample • The milky colour for SNF2 and SNF3 degraded

Figure 4.2: Sedimentation analysis of palm oil-based nanofluid

4.2.3 Agglomeration size observation under SEM

Figure 4.3 shows the morphology of the formed particles, which were deposited from the nanofluid samples. In Figure 4.3 (a), high agglomeration of nanoparticles was

observed. The microstructure shows the particle aggregation size in the larger range of over 2 μm , which the nanoparticles are found in strong clustering among the particles. Therefore, it could be predicted that nanoparticles will easily agglomerate in base oil along the suspended time. After the nanoparticles were treated with 300 $^{\circ}\text{C}$ in thermal vacuum chamber, they were suspended into base oil and the microstructure of aggregation size was analyzed by SEM again. The SEM image after suspension to base oil by sonication is shown in Figure 4.3 (b). It is clear that the nanoparticles were properly dispersed and only small aggregation was found. The aggregation only occurred when the nanoparticles were dried after being deposited on the specimen holder for SEM measurement..

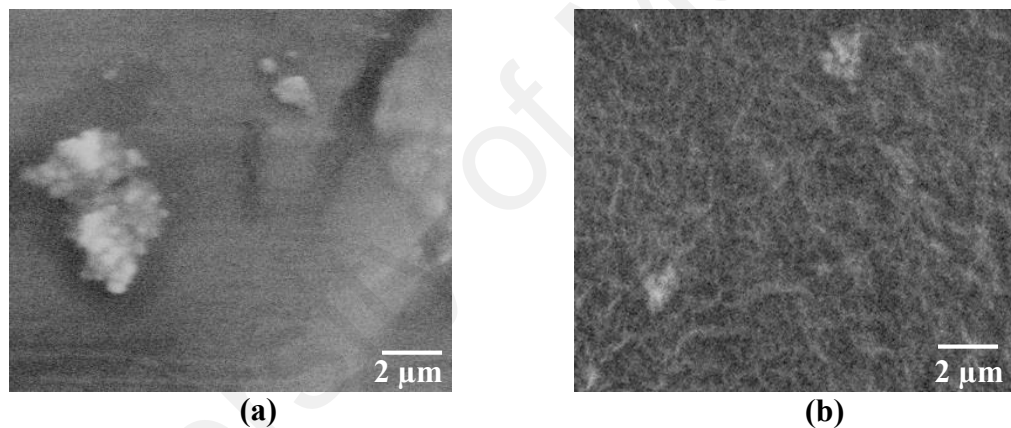


Figure 4.3: Scanning electron microscope (SEM) micrograph; (a) at the beginning and (b) after heat treatment

4.2.4 Particles distribution assessment using Zetasizer

The size distributions of dispersed nanoparticles were measured using dynamic light scattering (DLS) method in order to investigate the dependence of size in the base insulating oil. Figure 4.4 shows the distribution of the particles' cross-sectional diameter and the volume of the diversely-sized particle constituted. The Brownian motion caused by the movement of particles in the suspension occurred in the nanofluid. It can be seen that Fe_3O_4 particles occupied a higher distribution of per numbers and volume compared

to TiO_2 . The average particle size of Fe_3O_4 and TiO_2 nanoparticles in the suspension are 47 nm and 60 nm respectively. This hydrodynamic diameter results indicate that Fe_3O_4 nanoparticles employed higher diffusion speed in the base insulating oil, in this case is PO. A higher diffusion speed would result in a smaller hydrodynamic diameter and constitute to the stability of the nanofluid sample (Babita et al., 2016). However, TiO_2 nanoparticles still occupies a low amount of number and volume at the same concentration compared to Fe_3O_4 . Therefore, this allows TiO_2 to have the possibility to employ more amount with increased concentration levels in the fluid.

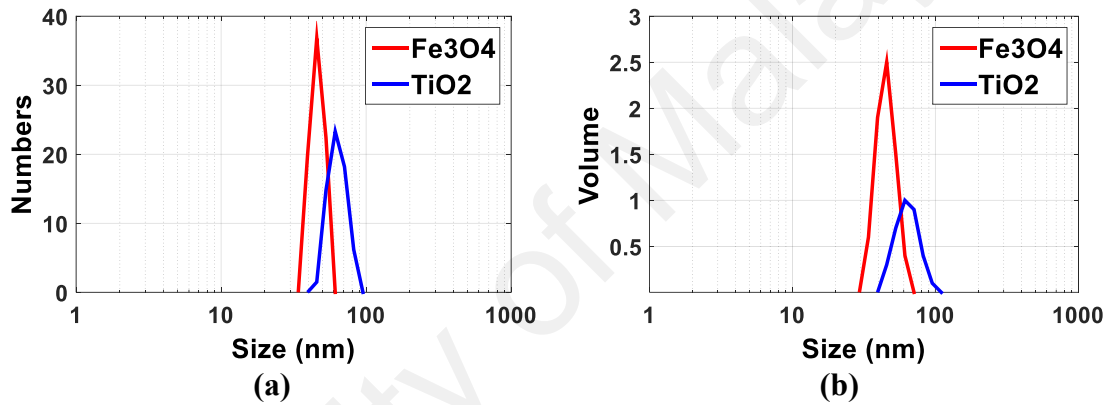


Figure 4.4: Nanoparticle distributions size relative on; (a) numbers and (b) volume

4.2.5 Discussion

In characterising the crystallite size of nanoparticles between Fe_3O_4 and TiO_2 nanopowder, it can be suggested that the larger crystallite size of TiO_2 at 110 nm could be attributed to the lower dispersion rate in the base fluid (Suttiaponparnit et al., 2010). The larger crystallite size of TiO_2 compared to Fe_3O_4 can affect the limitation imposed by the number of particles dispersed into the base oil. When the limit is exceeded, the nanoparticles are unable to disperse well in the base oil and leads to aggregation and sedimentation process. This can be seen from the hydrodynamic size of TiO_2 when dispersed into oil, where it is occupied larger size compared to Fe_3O_4 nanoparticles. The

dispersion property could be improve by increasing the sonication time as reported in Mahbubul et al. (2014).

When metal oxide nanoparticles, such as Fe_3O_4 and TiO_2 , are suspended in a non-polar liquid (in this case, natural ester), the response of base oil and nanoparticles to external electric field such as in sonication, develops electric charges on their surface. A Van Der Waals force from ultrasonication creates a repulsive electrostatic potential between the electric double layers surrounding the particles. In fact, it is much more challenging to generate charge in non-polar liquid compared to water due to low dielectric constant of oil (Kemp, Sanchez, Mutch, & Bartlett, 2010). Additionally, studies on the nanofluid stability suggest that adding commercial dispersant could improve the formation of surface charge and the dispersion characteristics of nanofluid (Ab Ghani et al., 2018). However, in this study, no surfactant was added into the dispersion to avoid its direct influences on the measurement of dielectric and electrical characteristics of nanofluid. Therefore, the stability mechanism applied in palm oil-based nanofluid mainly depends on electrostatic stabilization, where the surface charges are developed through accumulation or depletion of electrons at the surface and physical adsorption of charged species onto the surface of nanoparticles (Yu & Xie, 2012).

Furthermore, stability of dispersion is playing important role on the dielectric strength of nanofluids. The aggregation of nanoparticles into bigger particle clusters will lead to the performance degradation of nanofluids, particularly decreasing the breakdown voltages of the respected material (Lee et al., 2012).

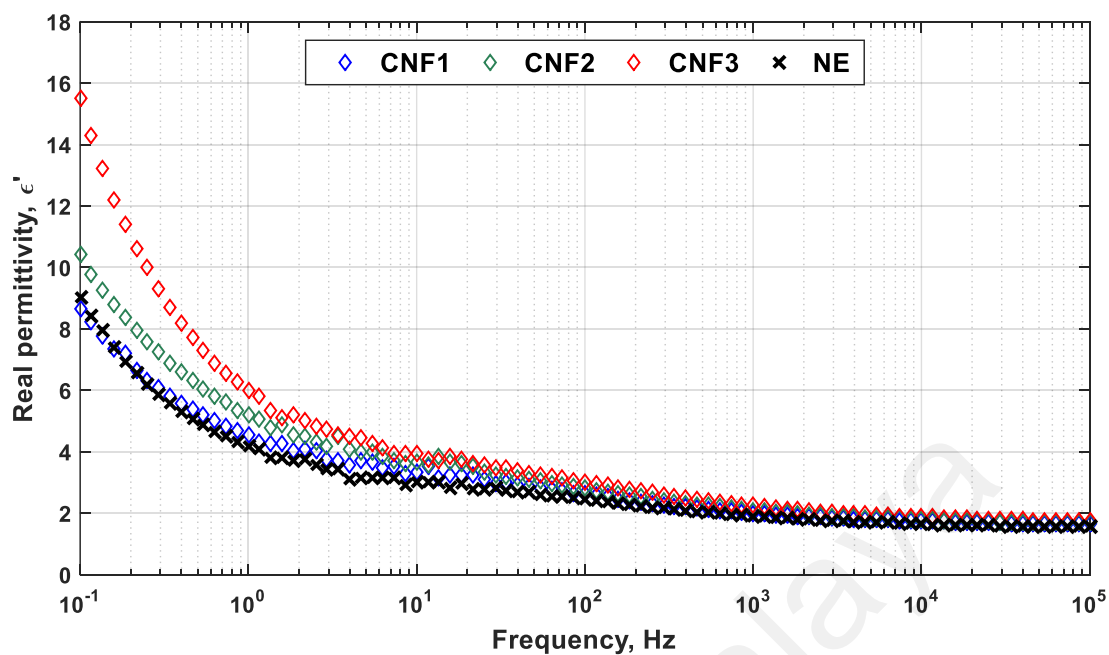
4.3 Dielectric properties of palm oil-based nanofluid insulation

When an electric field is applied on a dielectric material, displacement mechanism will occur within the material, leading to polarisation of the material and probably

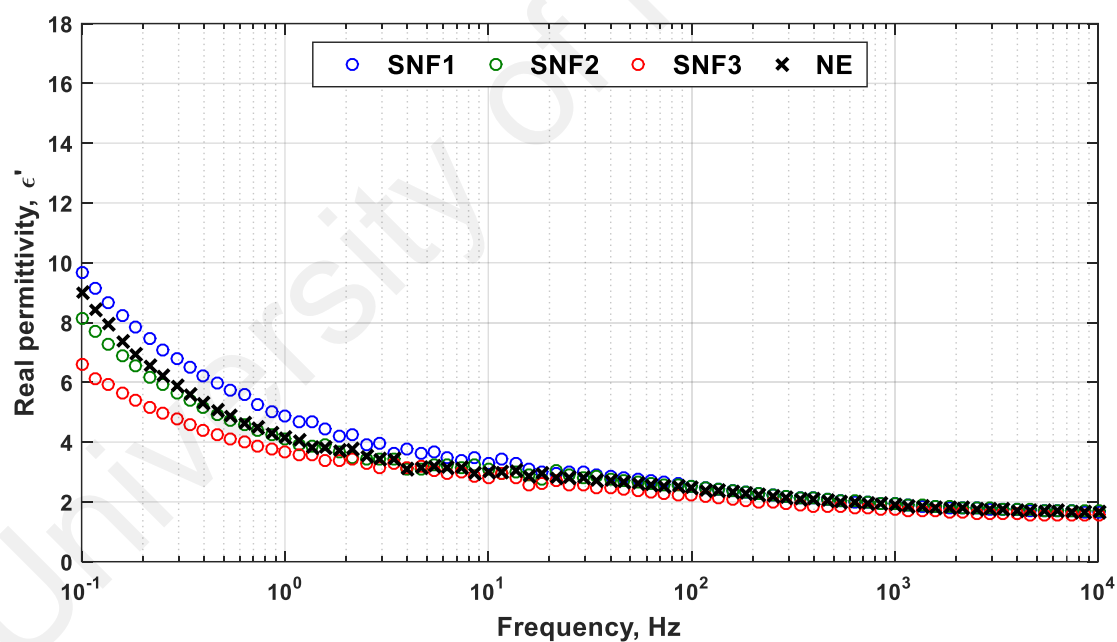
conduction if the electric field is sufficiently high. The measurement of dielectric properties is based on the interaction of the electric dipole moment and ion mobility within the nanofluid.

4.3.1 Effect of nanoparticles on dielectric constant

Figure 4.5 shows the measured real permittivity as a function of frequency for palm oil-based nanofluid samples. By presenting the base oil, which is PO as a reference, it can be seen clearly that the dielectric constant of CNFs and SNFs exhibits slightly stronger frequency-dependence with variation of nanoparticles concentration at 0.01, 0.1 and 1.0 g/L respectively. At lower frequencies (0.1/1.0/10 Hz), higher variation in the dielectric constant measurements can be clearly seen. This is possibly due to Maxwell-Wagner-Sillars (MWS) interfacial polarization, where the frequency-dependent contributes to the formation of the charge build-up at the nanoparticle interfaces and dipole molecules of the base oil (Lau, Vaughan, Chen, Hosier, & Holt, 2013). At higher frequencies (1k/10k/0.1M Hz), it can be seen that the dielectric constant is strongly influenced by the increment of the frequencies, where it drops at 2.0 for all samples.



(a)



(b)

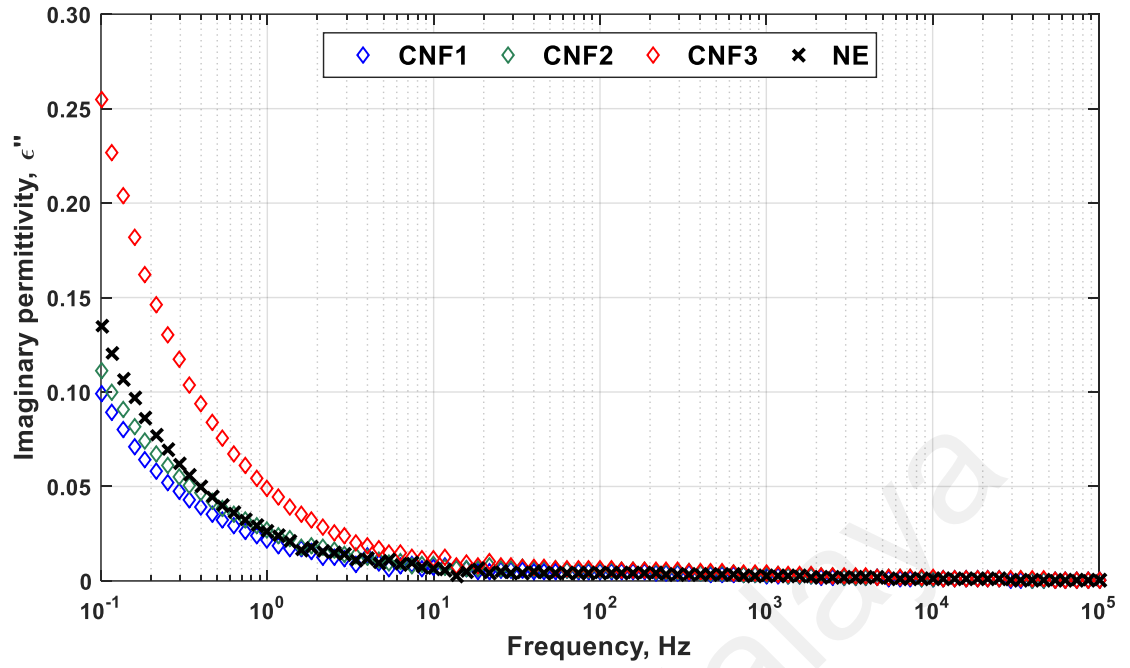
Figure 4.5: Real permittivity of palm oil with (a) conductive (b) semiconductive nanoparticles

For base oil, the increase in dielectric constant is associated with lower frequency due to presence of functional groups, which will respond to the electric field due to their polar

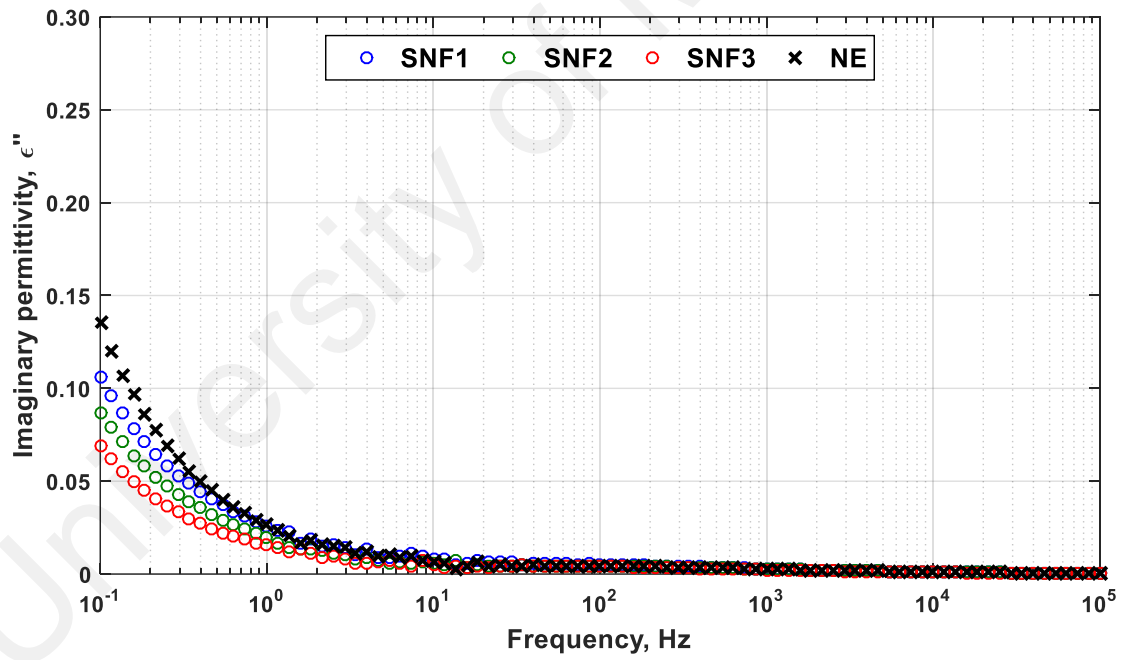
nature. For palm oil-based nanofluids, as the amount of Fe_3O_4 increases, an apparent increase in dielectric constant can be observed. However, the dielectric constant of the SNFs shows quite different trends, especially for the concentration amount of TiO_2 at 0.1 and 1.0 g/L. Therefore, it can be concluded that the apparent polarization in this study is the summation of the polarization of the base oil, inner polarization of nanoparticles and orientation polarization of charged nanoparticles as polar molecules due to Miao et al. (2013). Since the electrical properties of Fe_3O_4 are more conductive than TiO_2 , it can be charged and polarized easier than TiO_2 when being dispersed in palm oil. The mobility of charged particles can also influence the polarization process at low frequencies.

4.3.2 Effect of nanoparticles on dielectric loss

While investigating the influence of nanoparticles in the base oil at lower frequency (0.1/1.0/10 Hz) in Figure 4.6, it is noteworthy that the dielectric loss peak increases with the addition of conductive nanoparticles and decreases with the incorporation of semiconductive nanoparticles. The reduction in dielectric loss responses are associated with the restriction on the mobility imposed by the interaction between nanoparticle electron trapping capabilities and the base oil molecules (Mansour et al., 2016). When considering the effect of nanoparticle concentration, the dielectric loss response of the CNFs appears to be different from that associated with the SNFs. For CNFs, the increasing concentrations up to 1.0 g/L results in a tube-tube conduction mechanism between the particles. This condition is associated with high surface conductivity of Fe_3O_4 and particle concentration. As the volume fraction is increased as shown in Figure 4.6(a), dielectric loss becomes higher due to the increasing interfacial charge conductivity as obtained experimentally.



(a)



(b)

Figure 4.6: Imaginary permittivity of palm oil with (a) conductive (b) semiconductive nanoparticles

More importantly, the presence of high amount of conductive nanoparticles in a base fluid means a greater likelihood of tube–tube conduction than in the case of low

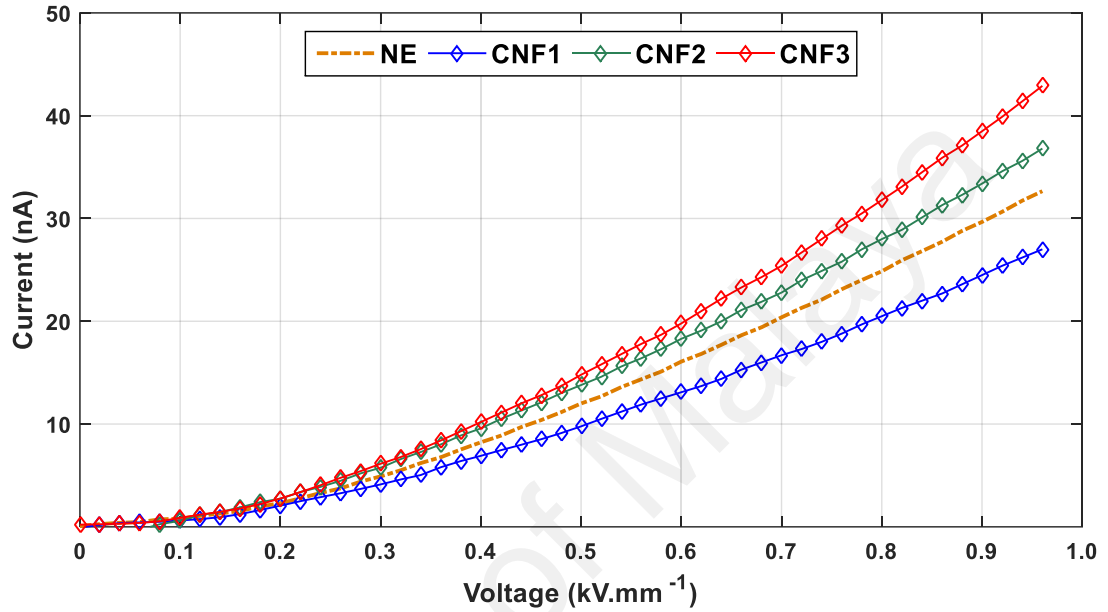
conductive particles, which is referred to TiO_2 in this instance. In the presence of TiO_2 , there is a slight decrement of dielectric loss towards the increment of TiO_2 concentration, such that it still remains less than the base oil, as shown in Figure 4.6(b). This could be due to the reflection of low interfacial charge conductivity upon the increment of TiO_2 concentration, which subsequently affects the dielectric loss responses. When the content of nanoparticles is increased, it is more difficult to achieve good dispersion of nanoparticles throughout the suspension and aggregation can occur. This results in different interphase conductivity regions, which causes the increment or decrement of dielectric loss values with increasing nanoparticle concentration.

It is noteworthy that the addition of Fe_3O_4 or TiO_2 in a certain amount (0.01/0.1/1.0 g/L) to base oil occasionally resulted in a small difference in the losses response of nanofluids, as can be seen in CNF1-CNF2 and SNF2-SNF3. Although this effect could be associated with the introduction of nanoparticle itself as described previously, as with such cases, it can be suggested that the observed responses are due to the presence of the polar species (D. Liu et al., 2016). With an increasing or decreasing number of nanoparticles, more or less surface hydroxyl groups will present at the interfaces, resulting in a direct consequence on the dielectric responses.

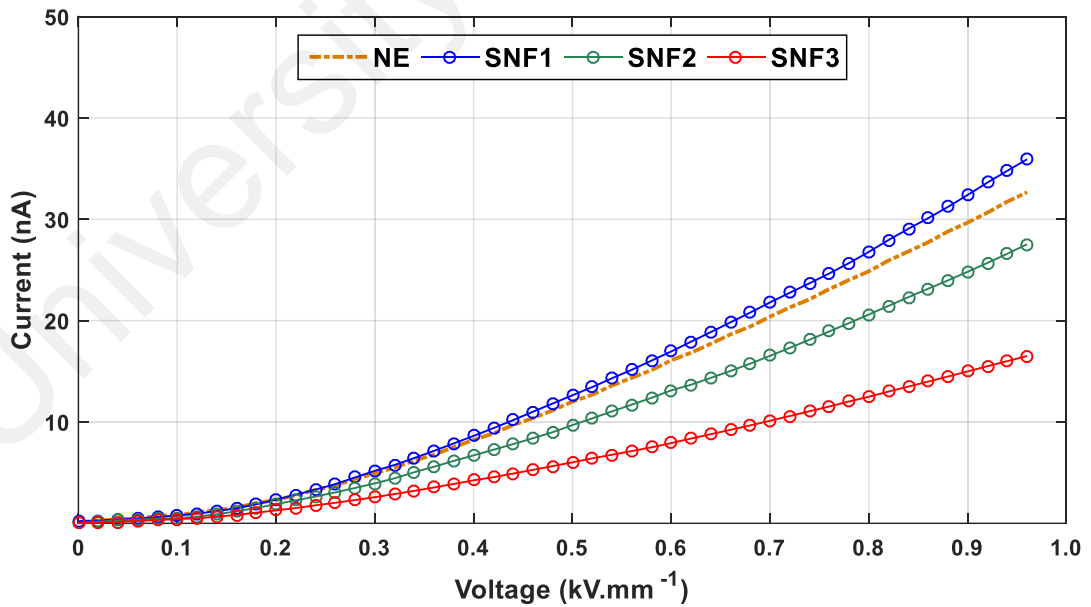
4.3.3 Effect of nanoparticles on dielectric conduction

Figure 4.7 shows the conduction current I vs. voltage V of palm oil-based nanofluids at base oil (PO), with conductive (CNF) and semi-conductive (SNF) samples. It was found that the I vs. V results show that the conduction current increases gradually with the voltage and this verifies that the samples have a resistance mode that is similar to the behaviour of nanofluids (Negri & Cavallini, 2015). Under the applied DC electric field, the number of electrons as charge carriers increases in the channel above the threshold voltage. Thus, the conduction current increases in symmetrical non-linear fashion with

the voltage. At low loading of nanoparticles, both CNF1 and SNF1 samples show a reduction of charge mobility in the DC electric field. At this critical interface distance, it shows a trapping charge ability through a polarization and charge induction mechanism, consequently enhancing the insulation properties (J. G. Hwang et al., 2010).



(a)



(b)

Figure 4.7: Conduction curves of palm oil with; (a) conductive and (b) semiconductive nanoparticles

When the particle loading is increased in the suspension, a higher volume of particles in conjunction with the electric field orientation can deteriorate the critical interface distance between inter-particles. Therefore, it leads to a new condition where the intrinsic properties (particle surface conductivity) are more dominant. It can be seen from the I vs. E curve that the current is reduced for SNFs especially for SNF2 and SNF3. This is due to the larger amount of TiO_2 in natural ester, which could improve the charge trapping and increase the surface resistance. However, for SNF samples (SNF2 and SNF3), the incorporation of conductive nanoparticles in larger amounts has modified the tube–tube contact resistance, which improved the conduction mechanism of the nanofluid. This proposed mechanism can also be attributed as the percolation threshold in nanofluid cases.

4.3.4 Discussion

When an electric field is applied to any dielectric material, charge tends to shift their position according to the external electric field, where positive charges move along the electric field direction and negative charges move towards the opposite direction. This is called as dielectric polarization. The obtained experimental results on palm oil-based nanofluid with conductive and semiconductive nanoparticles reveal that dielectric responses are in qualitative agreement with the electron trapping theory proposed by (J. G. Hwang et al., 2010) and further explained by Wenxia Sima et al. (2015). At the optimum amount of concentration, the existence of conductive and semiconductive nanoparticles perform a potential well caused by induced or polarization charge on nanoparticle interfaces. This potential well traps passing electrons and consequently enhances the dielectric properties of insulating material. Upon excessive amount of concentration, the potential well is no longer effective and therefore, the influence of interfacial (nanoparticle-base oil interface) conductivity takes part.

For CNFs, higher amount of Fe_3O_4 produces higher interfacial polarization at the interface between base oil and conductive nanoparticles. It is known that the effective dielectric constant of the nanofluid is governed by the summation of polarization of base oil, inner polarization of nanoparticles and charged nanoparticles (Miao et al., 2013). With increasing amount of conductive nanoparticles, more conductive particles reside at the interface, resulting in the formation of additional, interfacial charge conductivity. This causes the increment pattern of dielectric constant and loss peaks of CNFs towards the lower frequency region.

For SNFs, since the properties of TiO_2 is more to an insulator, it will not be easily polarized by an electric field compared to Fe_3O_4 nanoparticles. It is therefore reasonable to deduce that in higher concentration, surface conductivity of TiO_2 causes a resistance to low polarisation in the nanofluid interphases. It is suggested that this is mainly attributed to the reduction of dielectric constant and peak loss. Similar observation by Liao et al. (2013) reported that the relative permittivity, dielectric loss and conductivity decrease with increasing amount of TiO_2 nanoparticles.

Meanwhile, the dielectric conduction mechanism of palm oil with and without nanoparticles were examined according to Fowler-Nordheim theory by plotting current, $I^{1/2}$ versus electric field, E as shown in Figure 4.8. Typically there are three regimes in the conduction process prior to the applied electric field strength in a dielectric (Sha et al., 2014). In the first regime (1), the ionic, at low electric field, the current through the base oil and nanofluids is directly proportional with the applied electric field. Dielectric conduction in this stage obeys the Ohm's law and is mainly affected by impurity ions with low mobility. The second regime (2), known as injection, is at the medium electric field, where electrons are injected from the electrode. Unfortunately, in this study, there is limited indication to describe how nanoparticles enhance electron injection within this

regime. This is due to the conduction current versus electric field responses for base oil and nanofluids are almost the same and are stacking each other. Similar observation was found with Aljure et. al. (2016) about the conduction current in transformer oil with and without MgO nanoparticles. Hence, it can be suggested that the injection regime is mainly influenced by the applied electric field rather than the dielectric properties itself. In the third regime (3), the space-charge limited, is where electrons are injected from the high electric field electrode, drifting away and further ionizing via electron impact ionization. Since negative ions are drifting in a lower velocity compared to electrons, they tend to accumulate and build a space charge cloud in front of the electrode. The accumulation of space charge at the electrode acts as a shield and therefore, limiting the injection of new electrons. Consequently, this mechanism leads to the reduction of the ratio between the conduction current and the applied electric field.

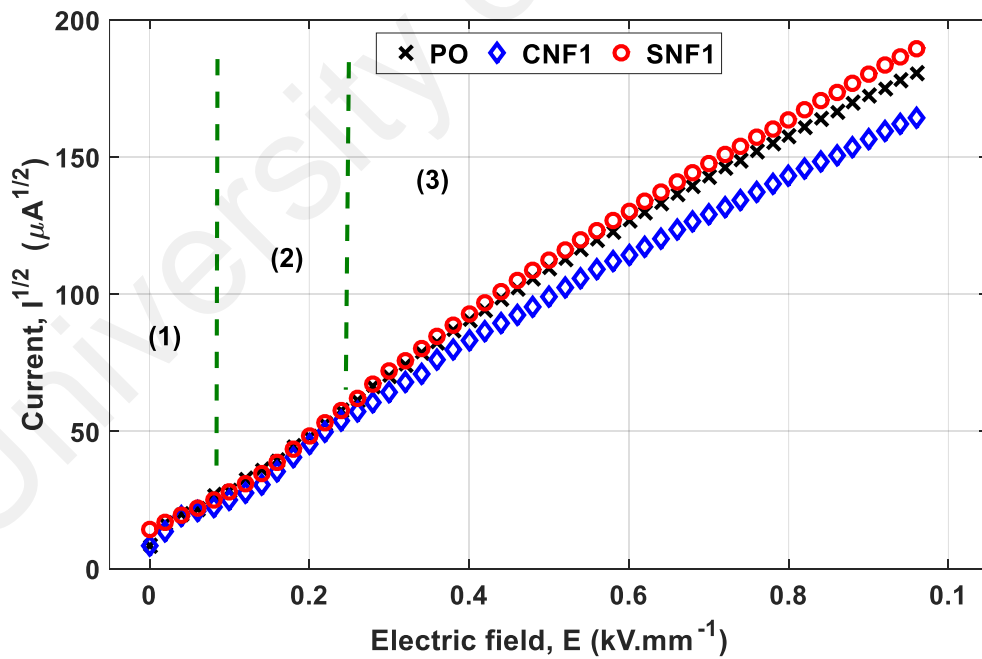


Figure 4.8: Dielectric conduction regime for base oil and nanofluid samples

4.4 Resistance to PD of palm oil-based nanofluid insulation

PD measurement results are presented in this section. PD measurements were performed on different type of nanoparticle addition, concentration and applied voltage amplitudes within 1600 cycles. Results of PD events are summarized through the number of PDs, total charge magnitude, mean charge magnitude, charge distributions and PRPD patterns.

4.4.1 PD activities at inception condition

Partial discharge inception voltage (PDIV) was recorded at the inception condition of the PD measurement when the applied voltage magnitude was increased at 1 kV/s rate until the minimum of 100 pC of PD occurred, based on IEC 61294. An occurrence probability distribution of PDIV average results according to Weibull statistical function, which was plotted for each of sample, is shown in Figure 4.9. Since the lowest inception voltage at which PD occurs is also the main interest for insulation applications, it is important to observe the lower tail of the Weibull distribution slope. Table 4.2 shows the Weibull parameters for each sample, where α or the scale parameter is the PDIV at 60% of cumulative probability, β is the shape parameter, which indicates the range of PDIV values within the distribution, and $U_{1\%}$ is the prediction of PDIV at 1% of probability.

In general, the shape parameter β of all nanofluid samples is higher than the base oil. This indicates that the incorporation of nanoparticles leads to the narrower distribution of PDIV, or in other words, the localization of PD. A very high localization of PD occurrences is exhibited by the sample with the highest conductive nanoparticle concentration, namely CNF3. The cumulative probability α shows that the incremental increase in nanoparticle concentration contributes to a reduction in PDIV for CNF samples, but there is a significant escalation for SNF nanofluids. At the lowest probability of the inception condition $U_{1\%}$, all nanofluid samples, especially SNF3, have a higher PD

tolerance compared to the base oil. This is due to the trapping characteristics of nanoparticles on the charge mobility for both types of nanofluids. Similar observations were also reported by Cavallini et al. in (Cavallini et al., 2015).

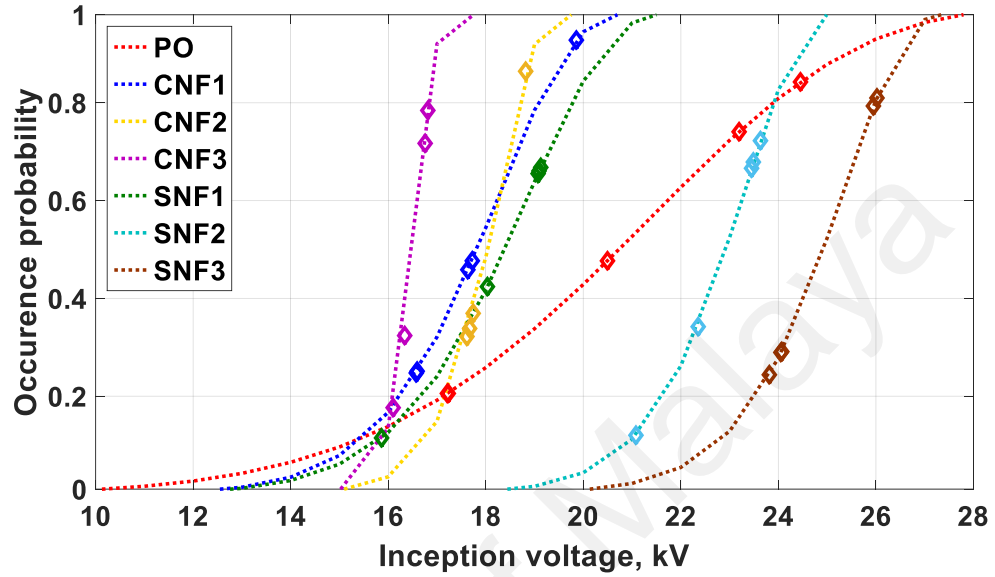


Figure 4.9: Weibull distribution of PDIV average values for base oil and nanofluid samples.

Table 4.2: Weibull parameters of the average partial discharge inception voltage.

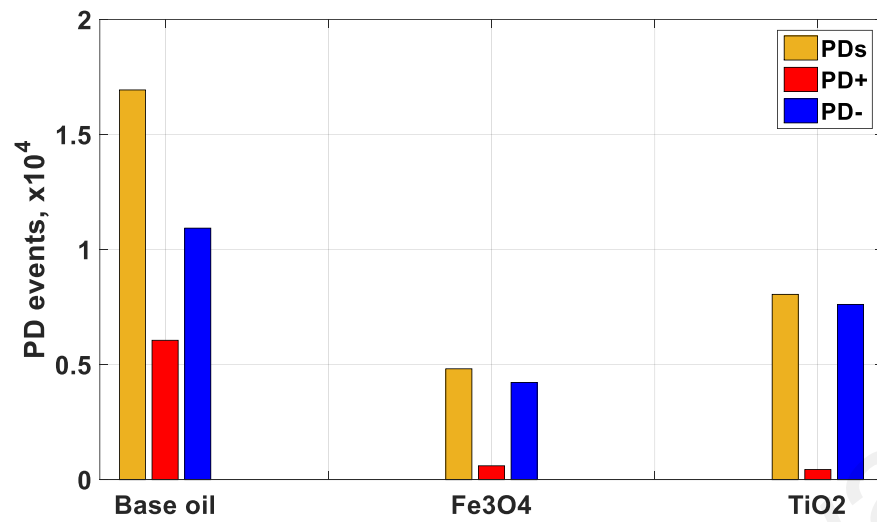
Samples	Shape Parameter, β	PDIV Average Value at 60%, α (kV)	PDIV Withstand Value, $U_{1\%}$ (kV)
PO	5.95	22.05	10.18
CNF1	12.40	18.35	12.66
CNF2	21.49	18.30	15.20
CNF3	47.14	16.67	15.12
SNF1	11.77	18.97	12.83
SNF2	20.15	23.34	18.58
SNF3	20.21	25.37	20.21

4.4.2 PD activities at steady state condition

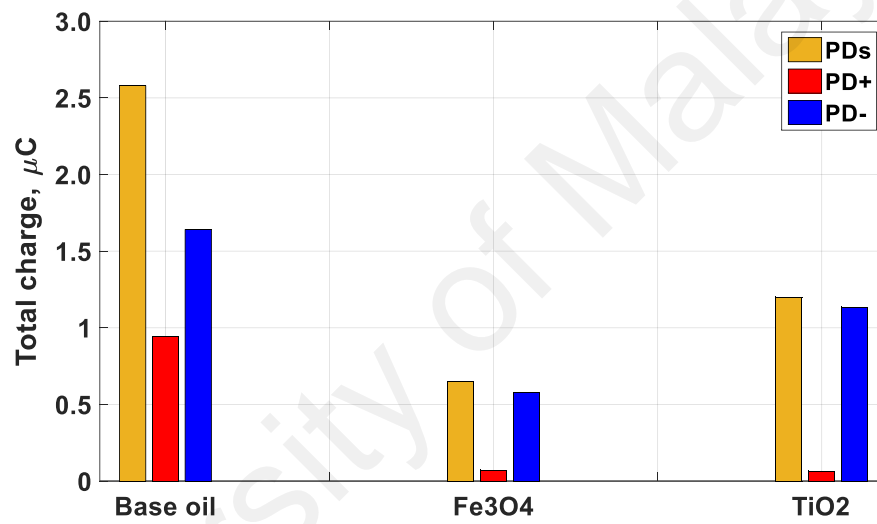
4.4.2.1 Effect of nanoparticle type on PD resistance

The PD measurement results for PO, CNF1, and SNF1 at a steady state of 26 kVrms of applied voltage are shown in Figure 4.10. With the addition of Fe₃O₄ and TiO₂ nanoparticles, the number of PD events, total charge, mean charge, and maximum charge magnitude are lower compared to the base oil. A comparison between conductive and semiconductive-based nanofluids with equal nanoparticle concentration (0.01 g/L), clearly indicates that the addition of small amounts of conductive nanoparticles, such as Fe₃O₄, enhances the PD resistance of nanofluids more effectively than the semiconductive-based TiO₂.

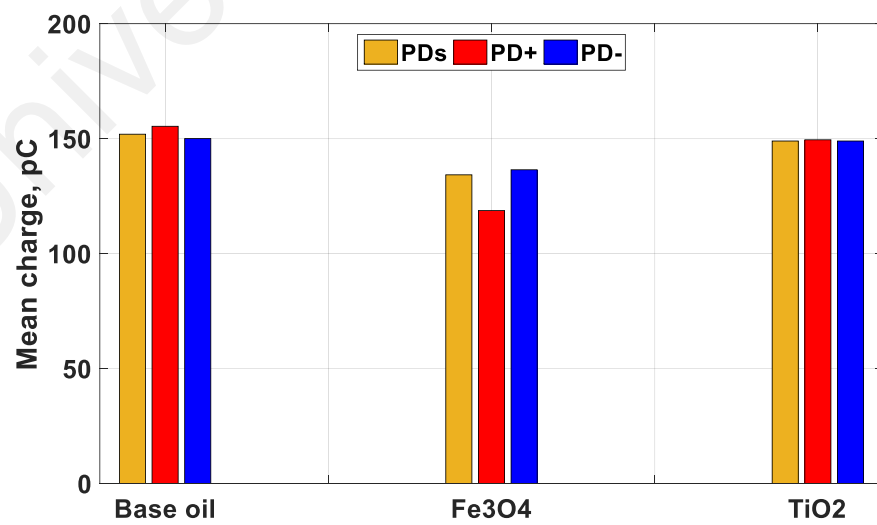
To explain the differences between the two types of nanoparticles, according to Sima et al., under the applied electric field, both are induced and polarized within a very short timescale (Wenxia Sima et al., 2015). The electrons initiated by charge injection move quickly towards the positively-charged nanoparticle surface. This process represents the electron catchment on the nanoparticle surface and reduces the electron movement and PD activities. Upon completion of the charge catchment, spherical nanoparticles are saturated with negative charges, and thereby no longer trap the electron. The value of charge saturation for each type of nanoparticle is determined by the value of their conductivity and permittivity, where Fe₃O₄ nanoparticles can potentially trap higher number of electrons compared to TiO₂.



(a)



(b)



(c)

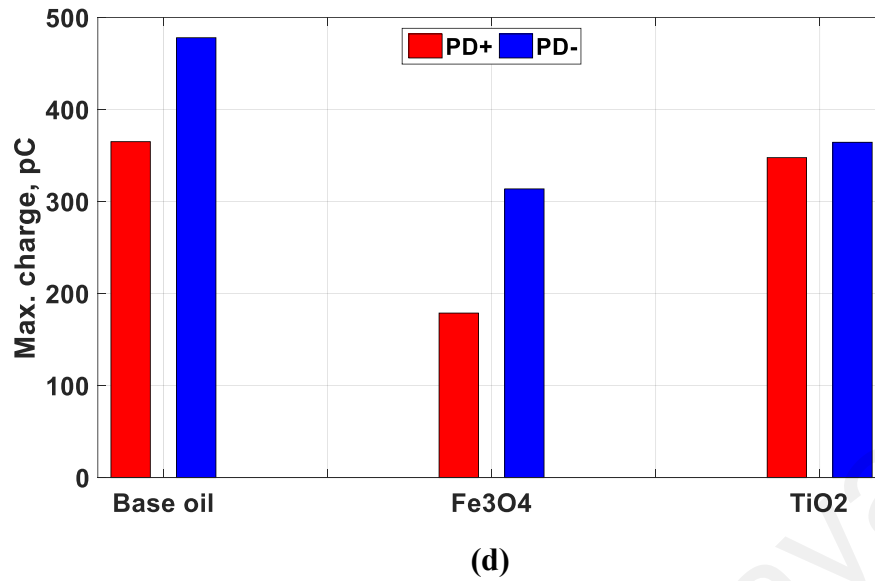


Figure 4.10: PD measurement results at 26 kVrms in 1500 cycles; (a) PD events, (b) total charge, (c) mean charge, and (d) maximum charge magnitude

Figure 4.11 presents the PD phase distributions of PO, CNF1, and SNF1 nanofluids. The PD phase distribution shows that most PDs occur from 45° to 113° and 180° to 270° . The peak of the distribution is slightly higher at 180° to 270° for each sample. This is due to the influence of the larger area of the ground electrode in the ionization process during the charge injection. The molecular ionization, which causes the PD occurrences, is dependent on the electric field and geometry of the electrodes. In this mechanism, a high electric field derives a free electron from a neutral molecule and generates a positive ion. The electrons with high mobility relative to positive ions are swept away from the ionization zone and are absorbed by the positive electrode and initiate PDs (J. G. Hwang et al., 2010). In the case of nanofluids, the charging of nanoparticles takes place, during which many of the mobile free electrons produced by the ionization are trapped before they can reach the electrode.

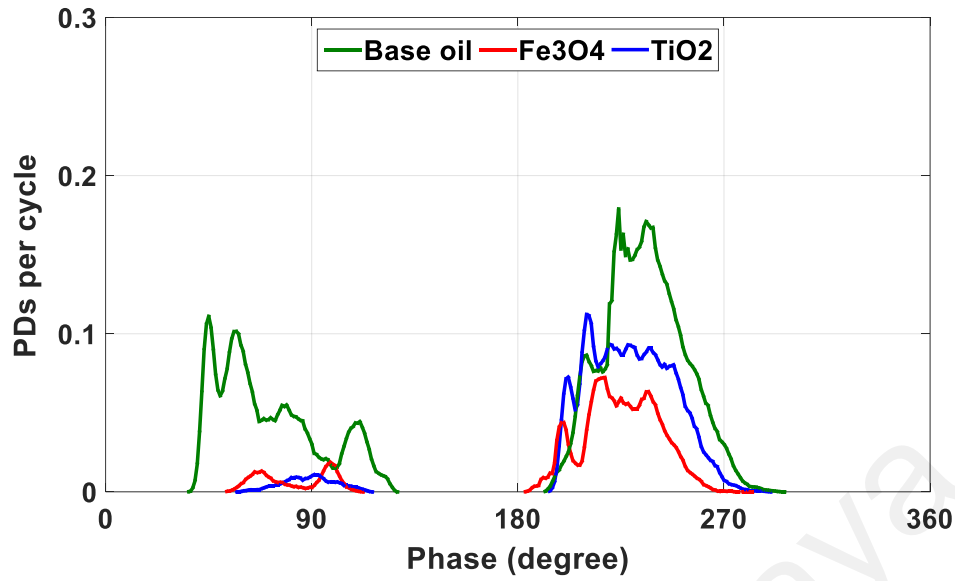
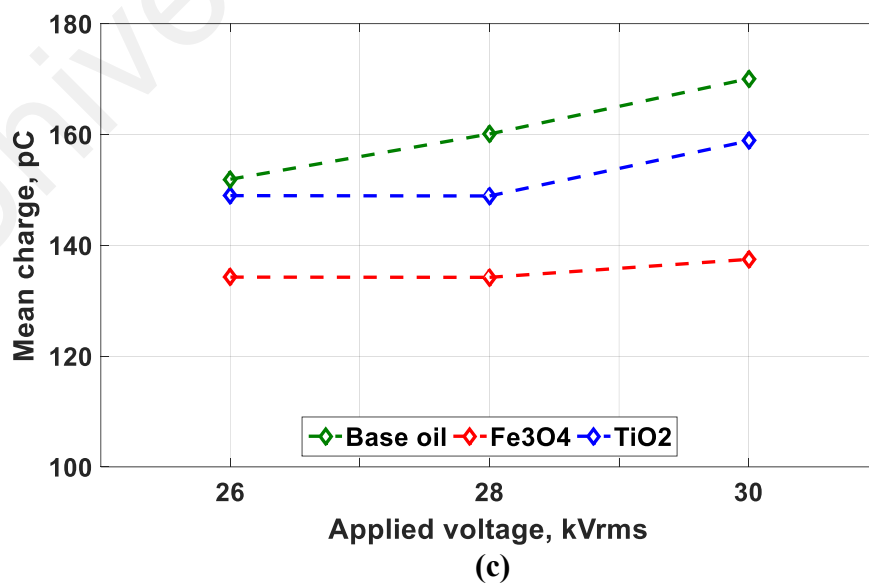
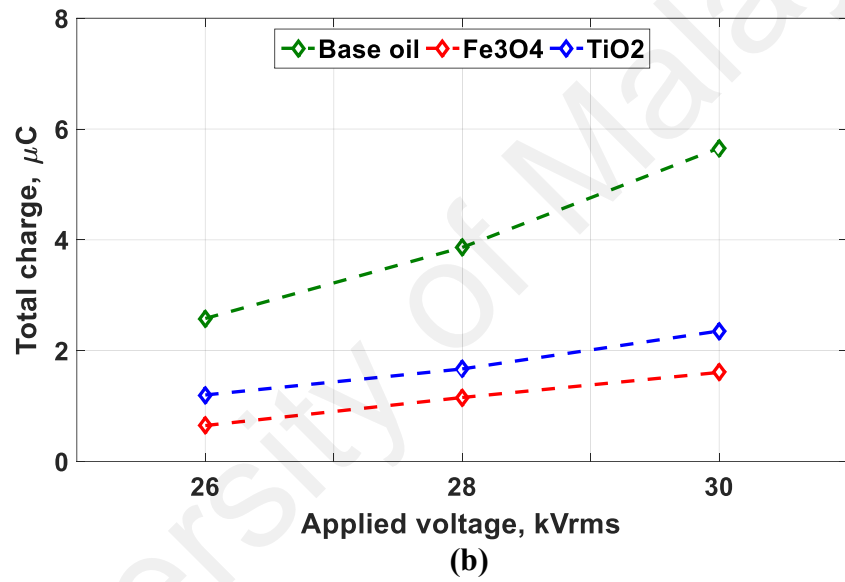
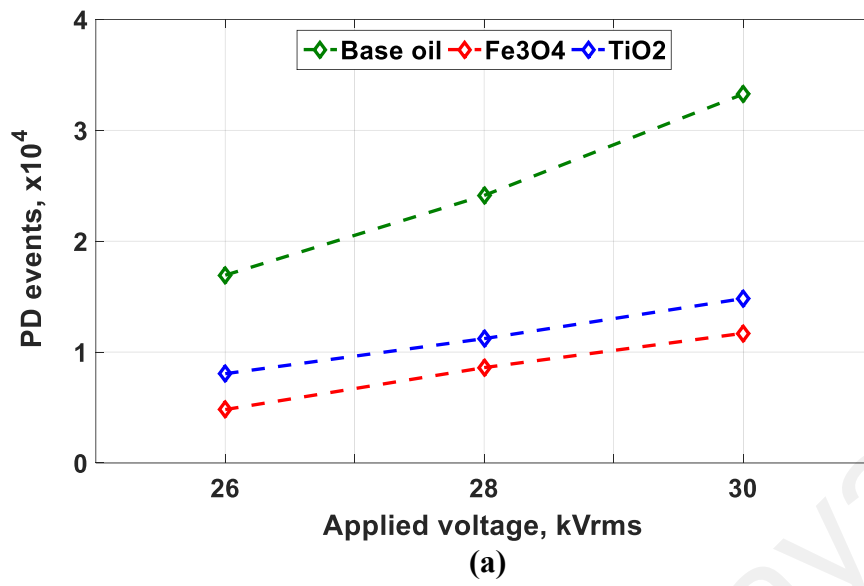


Figure 4.11: PD phase distribution as a function of nanoparticle type.

4.4.2.2 Effect of applied voltage amplitude on PD activity

The PD results obtained for PO, CNF1, and SNF1 as a function of 50 Hz applied voltage amplitude is shown in Figure 4.12. With increased voltage, the PD events, total charge, mean charge, and maximum charge magnitude also increase, but the mean charge for CNF1 is almost constant. When the applied voltage is increased, the electric field is also increased and the ionization process is enhanced, increasing the free electron generation rate. At this stage, PD events are boosted almost linearly with the applied voltage. The total charge also increases with additional applied voltage due to higher PD occurrences (H. Illias et al., 2011). The mean charge magnitude increases as the applied voltage is increased. Furthermore, the maximum charge magnitude increases with additional applied voltage because higher applied voltage magnitude provides a larger voltage drop across the electrodes when a PD occurs. In the case of nanofluids, both show a lower number of PD activities compared to the base oil at different applied voltage amplitudes.



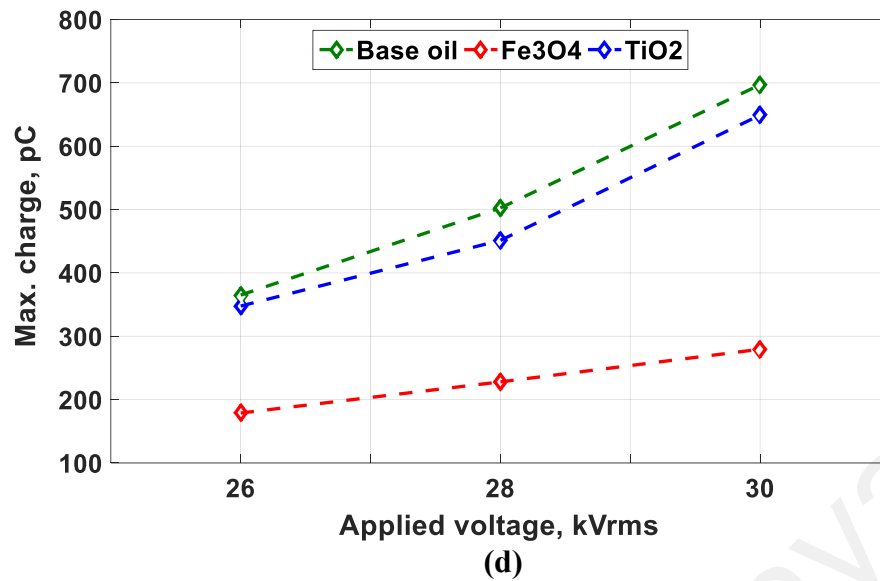
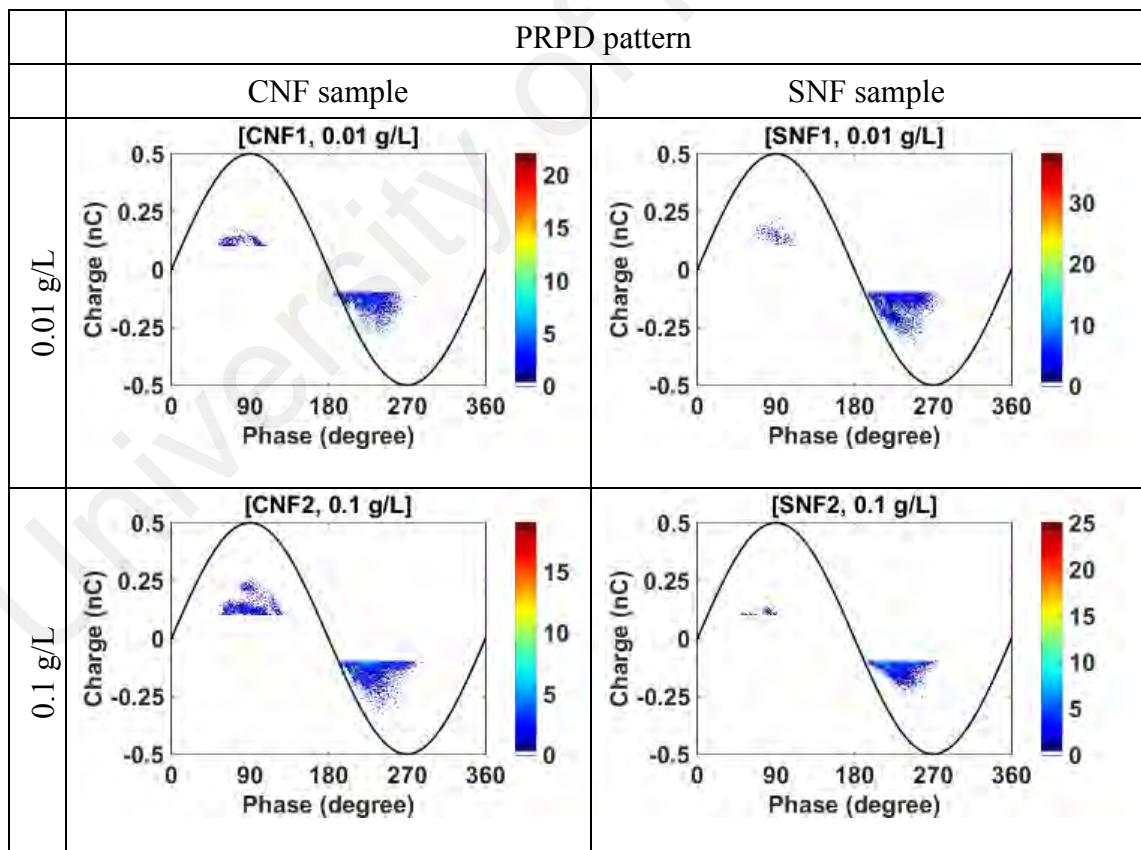


Figure 4.12: PD activities as a function of the applied voltage amplitude in 1500 cycles; (a) PD events, (b) total charge, (c) mean charge, and (d) maximum charge magnitude

4.4.2.3 Effect of nanoparticles concentration on PD activity

The phase-resolved partial discharge (PRPD) patterns obtained from the experiments are presented in Figure 4.13. It can be seen that PDs usually occur between 45° and 100° in the positive cycle and between 180° and 270° in the negative cycle. Since the electron generation rate is enhanced by the larger surface area of the ground electrode, this causes more PDs to occur during the negative cycle. Referring to CNF samples, the intensity and magnitude of PDs increase significantly with increasing concentrations of conductive nanoparticles (CNF1, CNF2, and CNF3 samples). Previous research reported that the magnitude and repetition rates of PDs are slightly higher for Fe_3O_4 compared to semiconductive and insulating nanoparticle types (Cavallini et al., 2015). Increasing Fe_3O_4 concentration up to a certain ratio will also increase the electric dipole-dipole interaction between particles and support their agglomeration and conduction. This consequently leads to the electric field increment between the electrodes, increasing the PD numbers and magnitude.

For SNF samples, the number of PDs and their magnitude decrease with the increasing concentration of semiconductive nanoparticles (SNF1, SNF2, and SNF3). Under certain conditions, such as 1.0 g/L of TiO₂ concentration, no clear PD activities was obtained from the measurement in the positive cycle. This could be due to the increase in resistance against PDs when TiO₂ nanoparticles were added to the suspension. Increasing TiO₂ concentration will also increase dipole–dipole interaction between particles and support the agglomeration process. However, due to the low conductivity of the TiO₂ nanoparticle surface, it leads to insulation mechanism rather than conduction and trapping of the charge with increasing electron trap density (Yuefan Du et al., 2012). In contrast, the reduction of PD activities due to the existence of nanoparticles could be beneficial to the power transformer design, where it can reduce its size and space for liquid insulation.



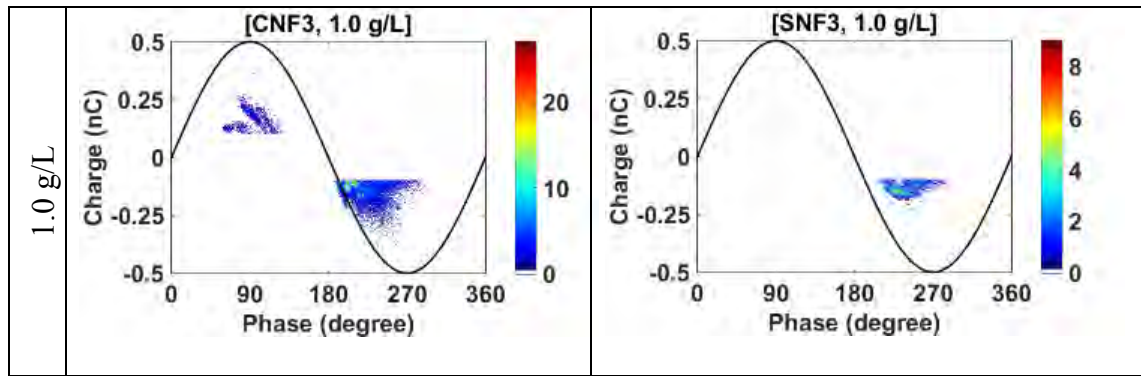


Figure 4.13: PRPD patterns for nanofluid samples with conductive and semiconductive nanoparticles at 26 kVrms applied voltage in 1500 cycles

4.4.3 Discussion

Under applied high voltage magnitude, the electric field is the main contribution to the ionization process, which leads to PD occurrences and breakdown when the insulation material exceeds their dielectric strength. However, the addition of nanoparticles into the base material modifies the electric field distribution between the electrodes, thus enhancing the insulation performance. In general, partial discharge (PD) happens once the electric field stress reaches a certain value, which is the inception field. To explain this mechanism in nanofluids, two conditions are considered: (1) inception and (2) steady-state.

PD inception voltage is usually recorded as the applied voltage at which the first PD occurs. It is also considered as a precursor to the incipient dielectric fault of insulation material (H A Illias, Tunio, Mokhlis, Chen, & Bakar, 2015). This initiation process is random and strongly governed by the local electric field deployed within the electrode-material-electrode system. In the case of nanofluids, the presence of nanoparticles modifies the degree of heterogeneity of the electric field in the nanofluids, which depends on the nanoparticle properties and their dispersion in the base oil (Yuzhen Lv et al., 2018). Local intensity of the electric field can result in localized PD occurrences at the same ionization level and applied voltage. As a result, the fluid interphases near the electrode

ionize high-mobility electrons and low-mobility ions. Therefore, under the influence of electric field force, they are set up to migrate between two electrode polarities. At such conditions, the nanoparticles begin to act as electrons and negative ion scavengers, which generate a potential well, as depicted in Figure 4.14(a).

At PD steady-state condition, assuming the nanoparticles are fully attached and charge-saturated, charges will drive the nanoparticles to move towards the opposite electrode at a very low speed. This is due to dielectrophoretic forces (Negri & Cavallini, 2017), which are responsible for the formation of particle clustering, as illustrated in Figure 4.14(b). This mechanism accelerates the aggregation of nanoparticles along with PD activities, according to their respective concentration levels. For instance, the increase of Fe_3O_4 over a certain amount could cause higher PD activities, hypothetically due to the easy formation of conduction interphases. Within a high electric field, accumulated conductive interphase could be converted into a micro-bridging conductive channel (Zare & Rhee, 2017) and are efficiently utilised by rapid streamer propagation, consequently leading to breakdown (Peppas et al., 2016). This is the main disadvantage of conductive nanoparticles compared to semiconductive or insulating nanoparticles especially in higher concentrations in base oil.

The results of dielectric properties and PD activities of palm oil-based nanofluid insulation under the presence of Fe_3O_4 and TiO_2 are inter-connected. It is well known that dielectric measurement can be used as an efficient tool to assess the insulation performance of the insulating materials (Dabbak, Illias, & Ang, 2017). The presence of nanoparticles in the base oil has a significant effect on the dielectric properties of palm oil. In the case of CNF, the nanofluid is sensitive to polarization and may enhance the dielectric loss. This can also explain why PD can occur easily in CNF compared to SNF. Higher dielectric losses and lower PD resistance of nanofluids are consistent with solid

nanodielectrics, as reported by previous researchers (T Tanaka, 2005), who describe the inter-relationship between the insulation property under low electric field (dielectric measurement) and high electric field (partial discharge). More importantly, the dielectric loss and PD pattern for different nanoparticle types and concentrations are the findings that most need to be addressed. They could potentially influence the insulation performance when nanofluids are applied in a power apparatus in the future.

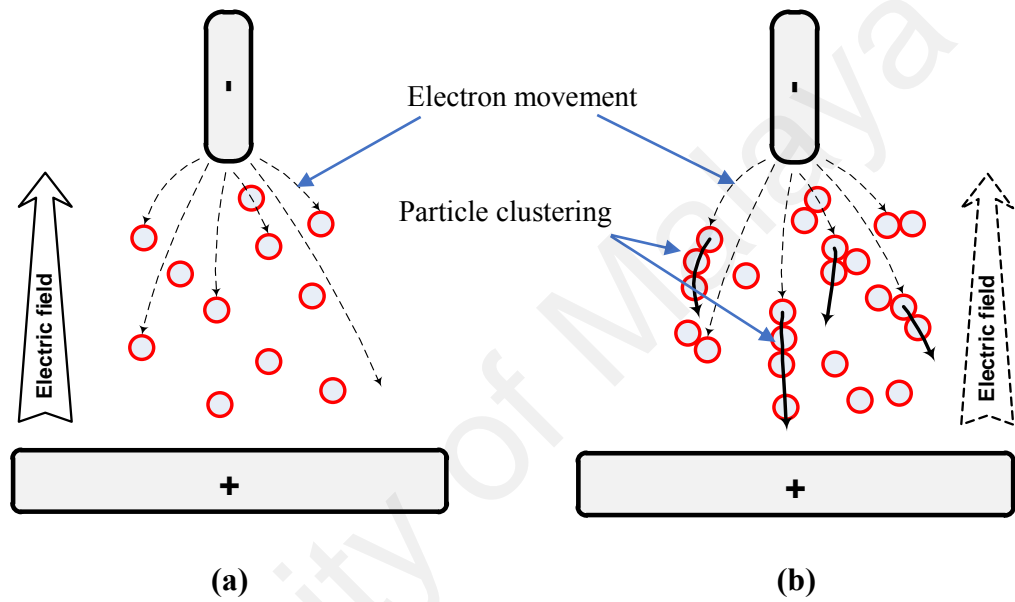


Figure 4.14: The schematic of electron movement for nanofluids between two electrodes; (a) at inception state (b) steady state condition

4.5 Breakdown strength of palm oil-based nanofluid insulation

Breakdown strength has become one of the important parameters to characterise the electrical properties of insulating material. In HV system design, percentile values from the probability of breakdown are used to estimate the probability that the insulation will breakdown when being stressed with high electric fields. The Weibull distribution is an extreme-value distribution, which considers the asymmetry between the low (<10%) and high (>90%) failure rates. Thus, the Weibull statistical method was applied as a tool to provide the degree of withstanding capability of the samples. The two Weibull parameter; scale (α) and shape (β) are widely used in analysing the breakdown performance.

4.5.1 Effect of nanoparticle type on breakdown strength

The measured breakdown strength of palm oil-based nanofluid with conductive and semiconductive type of nanoparticles is shown in Figure 4.15. The result compares Weibull plots of AC breakdown strength for palm oil as base oil and palm oil containing two types of nanoparticles, conductive (Fe_3O_4) and semiconductive (TiO_2) at same concentration. As can be seen from the Table 4.3, comparing two types of nanoparticles, which are conductive and semiconductive, CNF samples demonstrate higher scale parameter, shape parameter and have highest withstand voltage at lower probabilities compared to the PO and SNF. For SNF, the smallest shape parameter indicates that the samples provide more stable breakdown behaviour than the other samples under a high electric field. Referring to the scale parameter value, the addition of 0.01 g/L of TiO_2 into palm oil, on the other hand, slightly reduces the breakdown strength of the material. However, this slight reduction is negligible, considering the uncertainty in Weibull analysis. The breakdown strength is still comparable with that PO and CNF at the same concentration.

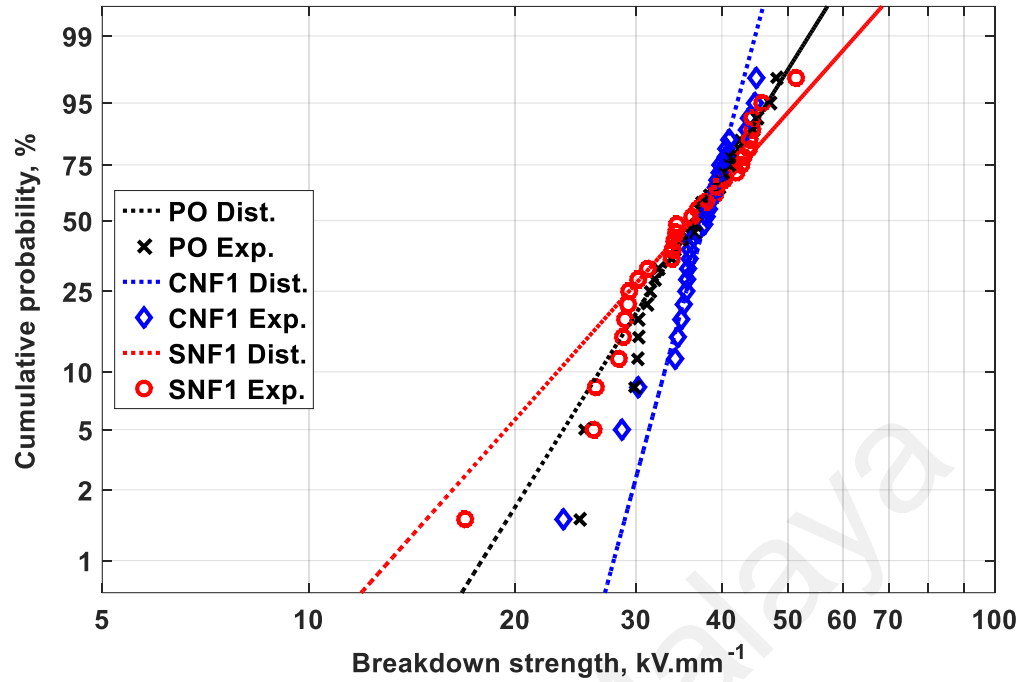


Figure 4.15: Cumulative probability plots of base insulating oil (palm oil), with conductive (Fe_3O_4), and semiconductive (TiO_2) nanoparticles

Table 4.3: Weibull parameter of base insulating oil (palm oil), with conductive (Fe_3O_4), and semiconductive (TiO_2) nanoparticles

Sample	Scale parameter, α (kV.mm ⁻¹)	Shape parameter, β	Withstand voltage, (kV.mm ⁻¹)	
			Lowest, $U_{1\%}$	Highest, $U_{99\%}$
PO	39.001	6.843	18.027	50.117
CNF1	39.252	10.016	27.876	43.445
SNF1	38.846	5.539	13.084	57.234

4.5.2 Effect of nanoparticle weight fraction on breakdown voltage

Figure 4.16 and 4.17 show the Weibull probability plots of the breakdown strength from the experimental results of CNF and SNF samples. It can be seen clearly that CNF samples have decreasing trend of dielectric strength with the increasing amount of Fe_3O_4 nanoparticles. Referring the values of scale parameter, for CNF samples, the breakdown strength is as high as 39.252 kVmm⁻¹ at 0.01 g/L concentration of Fe_3O_4 . The addition of

0.1 g/L of conductive nanoparticles reduces the breakdown strength to 24.916 kVmm⁻¹. Further reduction in breakdown strength is seen when the amount of Fe₃O₄ nanoparticles is increased up to 1.0 g/L. In fact, iron oxide is one of the widely used nanoparticles suspension to increase the breakdown voltage of insulating oils (Fal, Mahian, & Żyła, 2018).

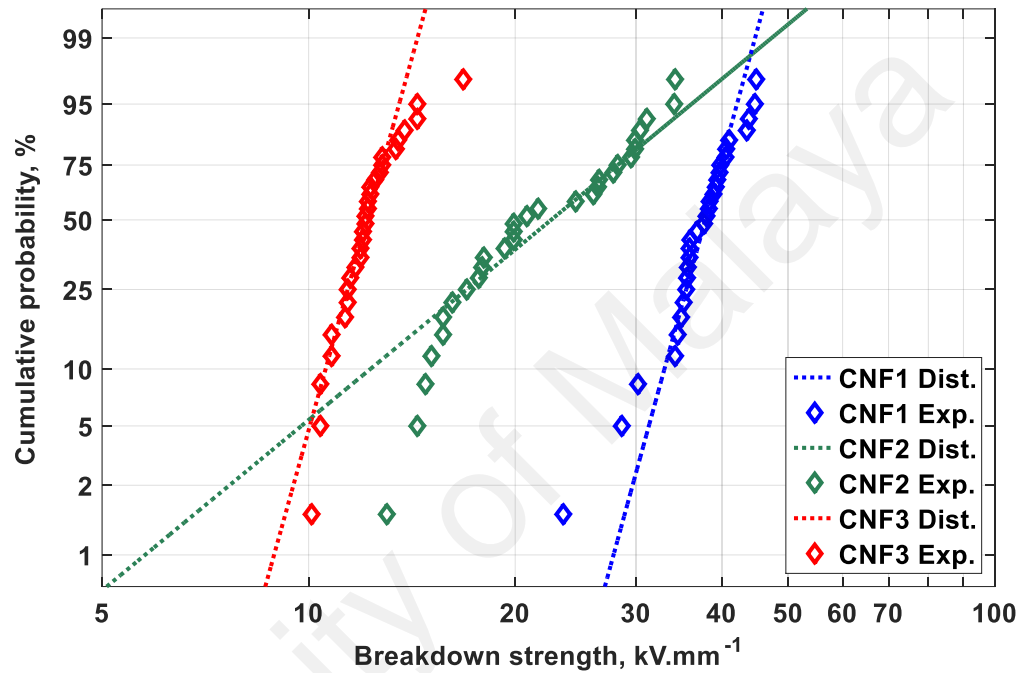


Figure 4.16: Cumulative probability plots of palm oil with conductive nanoparticles (Fe₃O₄)

Table 4.4: Weibull parameter of palm oil-based nanofluid containing with conductive nanoparticles (Fe₃O₄)

Sample	Scale parameter, α (kV.mm ⁻¹)	Shape parameter, β	Withstand voltage, (kV.mm ⁻¹)	
			Lowest, $U_{1\%}$	Highest, $U_{99\%}$
CNF1	39.252	10.016	27.876	43.445
CNF2	24.916	3.929	5.953	41.539
CNF3	12.3	7.975	8.891	14.023

At 0.01 g/L of weight fraction, SNF does not have a significant effect on the dielectric strength in general. Nevertheless, referring to Figure 4.17 and Table 4.5, the breakdown strength of SNF samples demonstrates an increasing trend where it can be seen from the scale parameter as 38.846, 49.171, 51.704 kVmm^{-1} for SNF1, SNF2 and SNF3 respectively. SNF samples show a higher breakdown strength with TiO_2 addition, where the increase in dielectric strength at higher concentration (in this study, 1.0 g/L) shows inferior withstand voltage in highest probability ($U_{99\%}$), which could imply to the limitation of nanoparticles addition into the base oil. The incorporation of nanoparticles amount beyond this limit will reduce the dielectric strength of nanofluid.

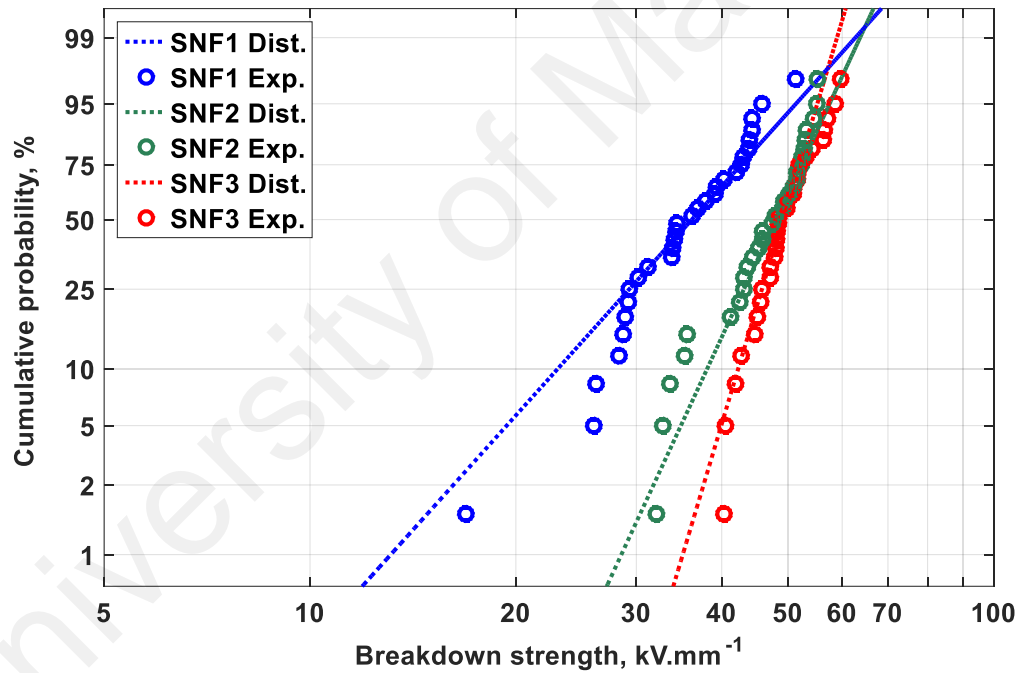


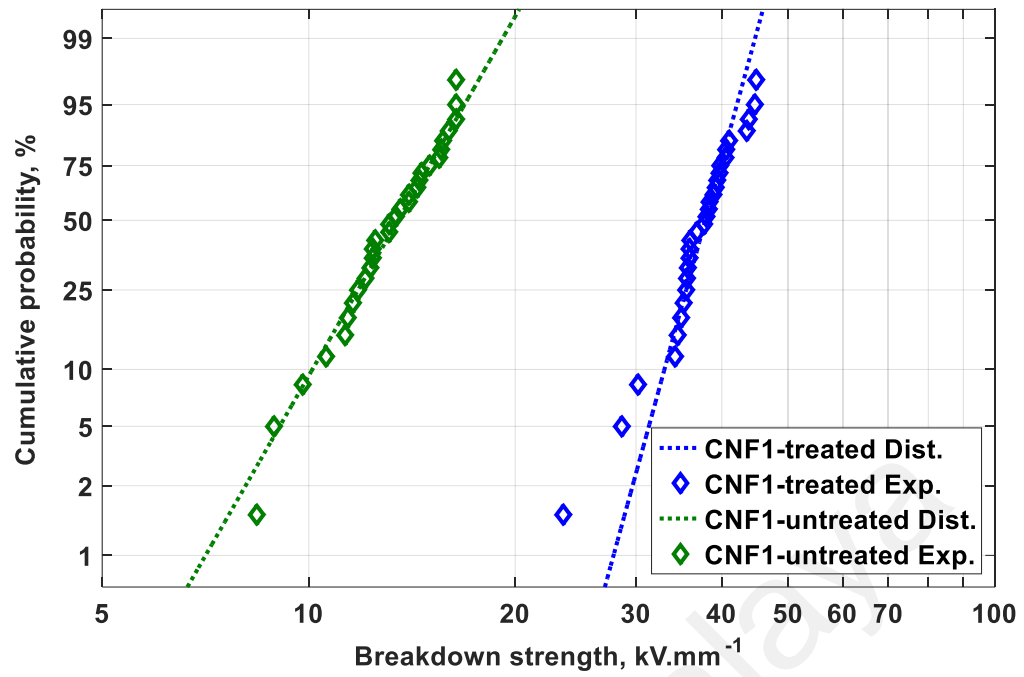
Figure 4.17: Cumulative probability plots of palm oil with semiconductive nanoparticles (TiO_2)

Table 4.5: Weibull parameter of palm oil-based nanofluid containing with semiconductive nanoparticle (TiO₂)

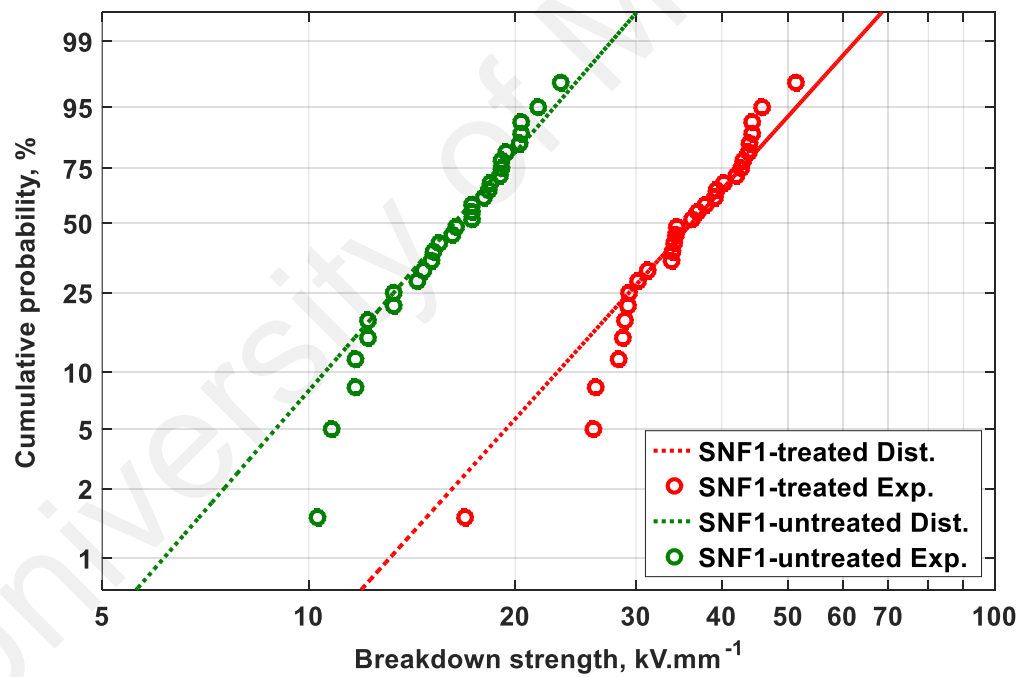
Sample	Scale parameter, α (kV.mm ⁻¹)	Shape parameter, β	Withstand voltage, (kV.mm ⁻¹)	
			Lowest, $U_{1\%}$	Highest, $U_{99\%}$
SNF1	38.846	5.539	13.084	57.234
SNF2	49.171	8.818	28.415	60.903
SNF3	51.704	10.415	35.018	57.321

4.5.3 Effect of nanoparticles treatment on breakdown voltage

Despite the effect of nanoparticle types and concentrations on the dielectric strength of palm oil-based nanofluids, nanoparticles treatment usually decides the acceptance results of the breakdown strength of nanofluid. To confirm the breakdown strength of palm oil with the addition of untreated nanoparticles, another batch of samples was investigated, subjected to nanoparticles directly from the supplier. Figure 4.18 shows the comparison result of CNF and SNF with treated and untreated nanoparticles. Table 4.6 summarizes the Weibull parameters of the examined breakdown strength from Figure 4.18. For instance, nanofluid containing untreated nanoparticles always has lower breakdown strength compared to nanofluid with treated nanoparticles. This is the indication that the use of treatment process via calcination on nanoparticles are necessary in order to achieve the acceptable value of breakdown strength. Referring to the scale parameter, the increment of breakdown strength for CNF and SNF after calcination process is 63.97% and 54.23% respectively.



(a)



(b)

Figure 4.18: Weibull plots comparing breakdown strength of palm oil containing treated and untreated nanoparticles (a) Fe₃O₄ (b) TiO₂

Table 4.6: Weibull parameters for breakdown strength of palm oil containing treated and untreated nanoparticles (a) Fe₃O₄ (b) TiO₂

Sample	Scale parameter, α (kV.mm ⁻¹)	Shape parameter, β	Withstand voltage, (kV.mm ⁻¹)	
			Lowest, $U_{1\%}$	Highest, $U_{99\%}$
CNF1 (treated)	39.252	10.016	27.876	43.445
CNF1 (untreated)	14.143	7.295	7.064	18.261
SNF1 (treated)	38.846	5.539	13.084	57.234
SNF1 (untreated)	17.779	5.54	6.139	25.501

4.5.4 Discussion

Electrical breakdown in a liquid dielectric is initiated by the streamer formation between two electrodes when the electric field intensity exceeds their threshold level. At this level, the molecules of the liquid are ionized and more ions and electrons are created, forming a conductive path known as a streamer. After a streamer is formed, it tends to elongate and transverse in the dielectric liquid from the point of initiation towards the lowest potential in the system, which is usually the grounded electrode. When the streamer reaches the grounded electrode, it forms a bridge or short circuit between the two electrodes. Eventually, a current or arc flows through it, causing a dielectric breakdown (Jadidian, Zahn, Lavesson, Widlund, & Borg, 2012).

Refined, bleached, deodorised palm oil (RBDPO) is a low melting liquid fraction of natural ester, which consists of oleic acid (C18:1) at 48% due to refining and good bleaching processes (Mancini et al., 2015). Oleic acid acts as a natural surfactant when metal oxide nanoparticles are dispersed into a base oil during the sample preparation process. A mechanically-stable palm oil-based nanofluid sample is obtained when oleic

acid is chemisorbed as carboxylate on the nanoparticle surface. Hence, the interfacial zone of the nanofluid as a solid–liquid suspension is enhanced (Wu et al., 2004). The role of the interfacial zone in a nanofluid is to create intermolecular forces, which keeps the molecules from each other according to the Van Der Waals theorem. As a result, the nanoparticle consists of two layers, the affected and aligned layers, which are difficult to polarize, trapping charges and slowing down the electron mobility, as suggested by Mansour et al. (Mansour et al., 2016).

For low volumes (0.01 g/L) of nanoparticles in a base insulating oil, the interfaces have a large space to form an efficient distance of double layers. This is a possible mechanism explaining the reduction of the total amount of polarization for both types of nanoparticles, resulting in a decrease of dielectric constant. The aligned layers also create a rigid intermolecular structure that traps electron and ion mobility between inter-particle zones, resulting in a decrease in the conduction current and consequently an increase in the dielectric breakdown voltage. On the other hand, for higher amounts of nanoparticles (0.1 and 1.0 g/L), the inter-particle distance decreases, reducing the efficient width of double layers and overlapping will potentially occur (Lau et al., 2017). In conjunction with the applied electric field, particles can be easily charged and move to bridging the flow of electrons (Peppas et al., 2016).

For highly-conductive nanoparticles, such as iron oxide, when the amount in natural ester is high, a smaller inter-particle distance affects the electric field enhancement. This is due to the effect of nanoparticle surface conductivity being more dominant. For semi-conductive and dielectric nanofluids, reduction and overlapping of the interfacial zone space does not affect the dielectric response much because they can attract and trap electrons in shallow traps, as well as having very low conductivity values (Yuefan Du et al., 2012; Ibrahim et al., 2016). Nevertheless, if impurities exist on the particle surface,

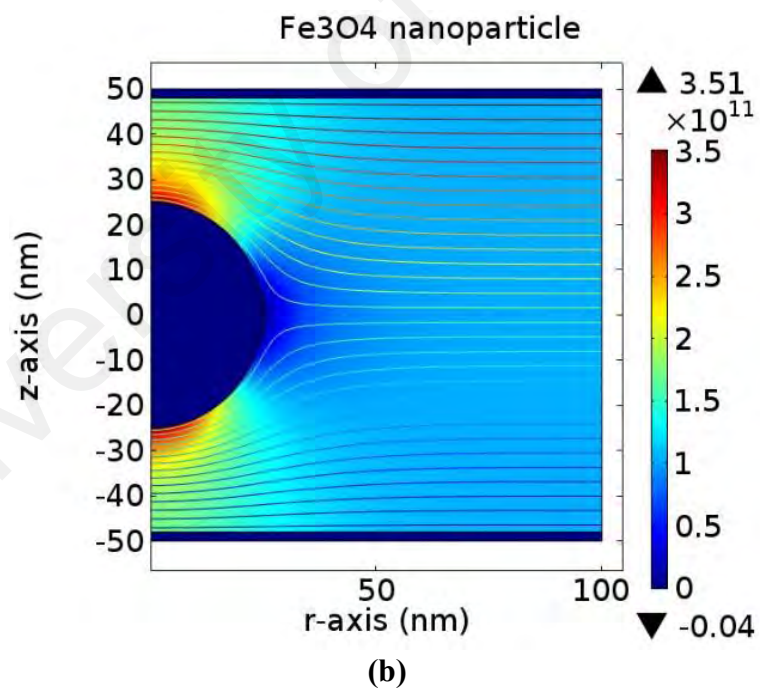
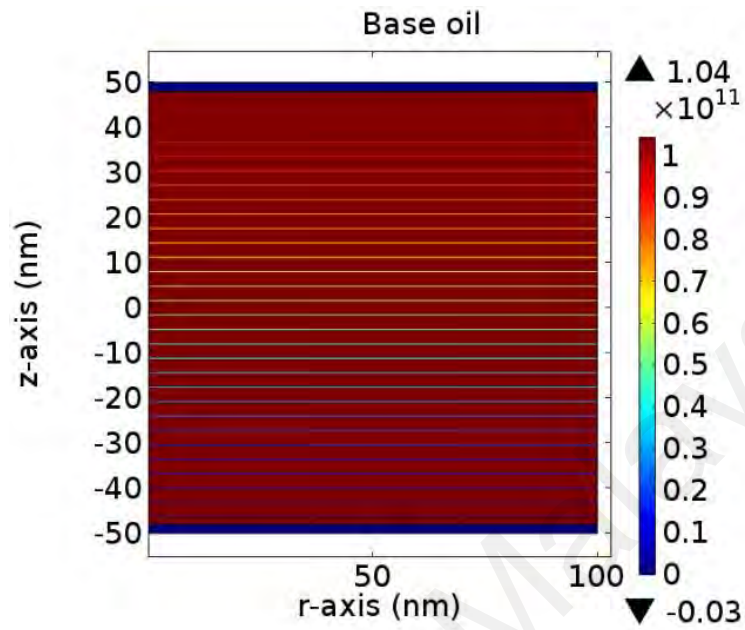
they play an important role in the mechanism, increasing the electrical conductivity of the base material (D. Liu et al., 2016).

The addition of untreated nanoparticles into palm oil alters the AC breakdown strength of the resulting nanofluid in comparison with base oil. This is in line with the recent experimental findings by other researchers in solid nanodielectrics (Rahim et al., 2018). Sartoratto et al. (2005) also reported that the maghemite nanoparticles needed to be dried in a thermo vacuum system in order to reduce water content. In this work, the altered breakdown strength of palm oil containing untreated nanoparticles in comparison with the treated samples cannot be linked to the electrical properties of nanoparticles. This leads to a second possibility – the effect of polar species on the surface of nanoparticles, which affects the breakdown strength of molecular composition (D. Liu, Pourrahimi, Olsson, Hedenqvist, & Gedde, 2015).

4.6 Electric field distribution

In order to understand the enhancement mechanism in this study, a Finite Element Analysis (FEA) model was developed. The simulated electric equipotential lines and the electric field distribution from the FEA model, with and without nanoparticle (Fe_3O_4 and TiO_2), are shown in Figure 4.19. The model consists of a spherical nanoparticle of 50 nm diameter suspended in a natural ester oil, which is immersed between two-plane electrode gap of 100 nm under 50 Hz, 10 kV AC applied voltage. The conductivity values of Fe_3O_4 and TiO_2 were set as 1×10^5 and 1×10^{-11} S/m, respectively, while the permittivity values were set as 80 and 100 according to the literature (Muhammad Rafiq et al., 2016). The results are similar with the previous simulation results obtained from a model of a spherical nanoparticle suspended in transformer oil with various permittivity values (Ibrahim et al., 2016). Other published research has also used FEA software to obtain the

distribution of electric field within nanofluid during streamer discharges (W. Sima, Shi, Yang, & Yu, 2014; Velasco et al., 2018).



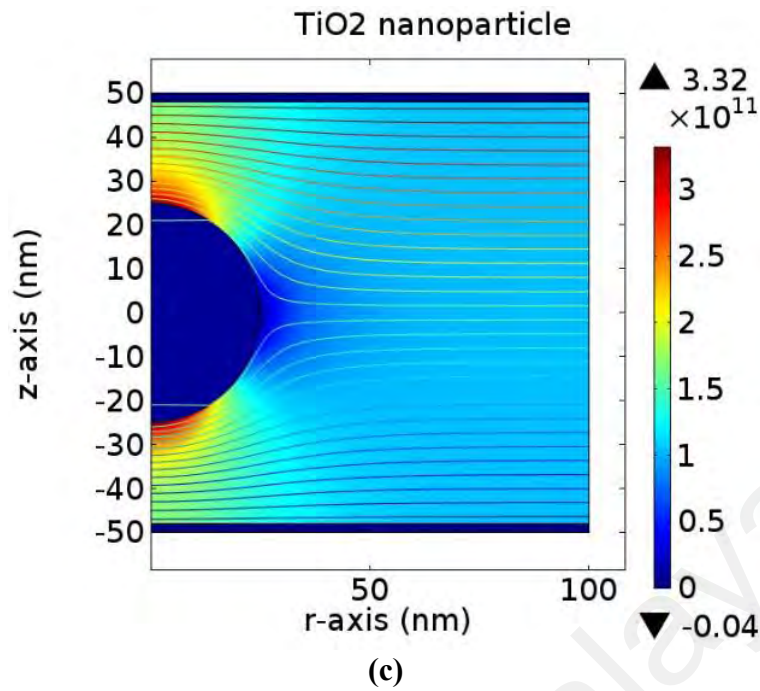


Figure 4.19: Electric field (V/m) distribution and electric equipotential lines for (a) base oil, (b) with Fe_3O_4 and (c) TiO_2 nanoparticle

In Figure 4.19(a), the electric field of the base oil and surrounding area between the electrodes system is uniformly distributed, since the electrical properties of the dielectric are homogenously constant. The maximum value of the electric field is 1.04×10^{11} V/m. When a nanoparticle was added in the oil, the electric field is significantly altered, as shown in Figure 4.19(b),(c). Due to the charging dynamic effect, suspending a nanoparticle into base oil results in a higher deformation of the electric field distribution at the particle-oil interface. This increment can be seen clearly along the z-axis of the cross section plot of the electric field magnitude, as shown in Figure 4.20. The maximum electric field induces or polarizes the electric double layer of conductive particles and semiconductive particles in a very short timescale. This generates positive charges in the upper hemisphere and negative charges in the lower hemisphere, according to the electric field direction. As a result, free electrons initiated from the surroundings due to ionization or charge injection move quickly and are trapped in the positively-charged hemisphere until fully saturated (J. G. Hwang et al., 2010). Fe_3O_4 experiences a higher increment of

the electric field magnitude. Hence, it highly induces positive charges and traps more free electrons than TiO_2 . This mechanism elucidated how those nanoparticles enhance the dielectric and electrical properties of palm oil-based nanofluid as insulation material.

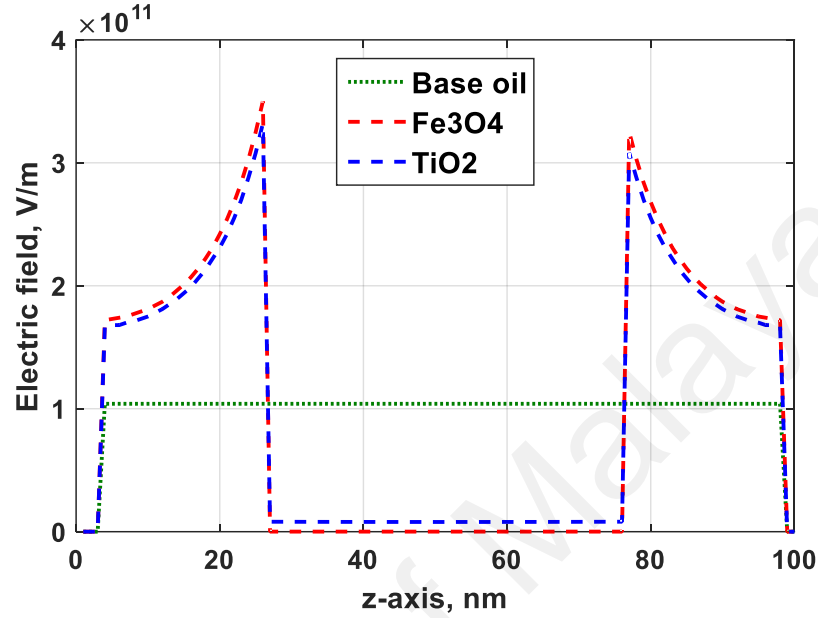


Figure 4.20: Cross section plot of the electric field magnitude from the FEA model in Figure 4.19.

4.7 Summary

The palm oil (PO), which is used in this work, has a good performance as an insulating liquid, where it has a dielectric strength of 39 kVmm^{-1} . It also has a low dielectric constant and loss value at 50 Hz power frequency, which is 2.61 and 0.00428 respectively. The mean value of the conductivity of PO without addition of nanoparticles at DC field conditions is $1.13 \times 10^{-10} \text{ S/m}$. During PD occurrences, PO recorded the number of discharges with 16938 events and $2.58 \mu\text{C}$ of total charge magnitude in 1500 cycles of the applied voltage.

By taking the results of PO as a reference, further observation was made to highlight the best nanofluid sample formulation as high voltage insulating materials as follows:

When conductive nanoparticle (Fe_3O_4) with 0.01 g/L (CNF1) is used in the suspension, it slightly increases the mean dielectric strength of nanofluid by 0.5% (at 39.2 kVmm^{-1}). It has higher dielectric constant and loss value of base oil at 50 Hz power frequency, which is 7.45% (2.83) and 17.53% (0.00519) respectively. The mean value of the conductivity of NE with addition of 0.01 g/L of Fe_3O_4 nanoparticles at DC field condition decreases to 17.79% ($9.29 \times 10^{-11} \text{ S/m}$). During PD occurrences, CNF1 recorded the lowest number of discharges in conductive-based nanofluid series with 4817 events (71.56% of reduction) and $0.64 \mu\text{C}$ of total charge magnitude (75.19% of reduction) in 1500 cycles of the applied voltage.

When semiconductive nanoparticle (TiO_2) with 1.0 g/L (SNF3) is used in the suspension, it increases the mean dielectric strength of nanofluid with the highest percentage by 25% (at 52 kV/mm). It has lower dielectric constant and loss value of base oil at 50 Hz power frequency, which is 8.81% (2.38) and 1.17% (0.00423) respectively. The mean value of the conductivity of NE with addition of 1.0 g/L of TiO_2 nanoparticles at DC field condition decreases to 50% ($5.65 \times 10^{-11} \text{ S/m}$). During PD occurrences, SNF6 also recorded the lowest number of discharges in all nanofluid with 2875 events (83.03% of reduction) and $0.4 \mu\text{C}$ of total charge magnitude (84.5% of reduction) in 1500 cycles of the applied voltage.

CHAPTER 5: CONCLUSIONS AND FUTURE WORK

5.1 Conclusions

In this study, six types of palm oil based nanofluid at different nanoparticles type and weight fraction had been successfully prepared. Characterization on their stability had also been made. The nanoparticle type (in this current work, Fe_3O_4 and TiO_2) and its weight fraction have significant effect to the enhancement of the dielectric and electrical characteristics of palm oil-based nanofluid. The major conclusions on the experimental results are as follows:

The pattern obtained from XRD results confirm that the particles used in this work are crystalline. The preparation process under the ultrasonication method improved the stability of the nanofluids by reducing the aggregation of nanoparticles size in the suspensions. DLS measurement showed that the particle distribution exhibits smaller hydrodynamic particles aggregation size, which is less than 100 nm. Nevertheless, the dispersion stability decreases with the increasing concentration of nanoparticles. Sedimentation analysis demonstrates the nanofluid samples in stable condition within 24 hours. This has become an indicator for the maximum time of storage. Hence, in this work, it can be concluded that the best result to prepare a very stable dispersion of palm oil-based nanofluid is using 0.01 g/L of nanoparticles concentration.

From the measurements of dielectric properties, the incorporation of conductive and semiconductive nanoparticles in 0.01 g/L increases the dielectric constant and decreases the dielectric loss of the base palm oil. As conductive nanoparticle content is increased, the permittivity and losses become higher. Concurrently, the permittivity and dielectric losses become lower in the case of semiconductive nanoparticles. This is due to the difference in interfaces conductivity region, which is dependent on the nanoparticle properties amid higher concentration.

It was found that the addition of nanoparticles into palm oil has a notable influence on the resistance to PD. This applies to both types of conductive and semiconductive nanoparticles. However, dielectrophoretic forces due to PD activities will derive the nanoparticles and clustering could occur in the suspension. This significantly reduces the dielectric insulating performance, especially when the nanoparticle is in a high concentration. In addition, the PD activity increases with the increasing of the applied voltage. Since the influence of dielectrophoretic forces on Fe_3O_4 nanoparticles is more vigorous compared to TiO_2 nanoparticles in terms of formation of interphase conduction as a result of PD activities, it is reasonable to suggest that semiconductive nanoparticle is more appropriate to be applied as nanofluid-based insulation.

The breakdown strength of palm oil-based nanofluids was analyzed based on the ASTM standard. AC breakdown strength showed that increasing the amount of conductive nanoparticles reduced the breakdown strength of the nanofluid significantly. Meanwhile, the increasing weight fraction of semiconductive nanoparticles enhanced the breakdown strength of the base oil. There could be due to several reasons, such as the morphology and existence of the polar impurities that promote conductive region. For the observed AC breakdown behaviour, the mechanisms are governed by decreasing inter-particle distance, where reducing the efficient width of double layers and overlapping will potentially occur.

Finally, a simulation study was carried out to understand the role of conductivity and permittivity of nanoparticle when there is an applied electric field. It was demonstrated that conductive nanoparticle experiences a higher increment of the electric field magnitude. Hence, it highly induces positive charges and traps more free electrons than semiconductive type. This mechanism elucidates how nanoparticles are influencing the dielectric and electrical properties of palm oil.

5.2 Future work

In light of the present work, the potential work to be explored in the future includes:

1. To date, the dispersion of nanoparticles in a base oil is still an issue to be highlighted. Nanoparticles tend to agglomerate rather than appear as isolated particles when incorporated into suspension in a long time. Therefore, an alternative nanofluid preparation, such as one-step method, can be explored to enhance the nanofluid stability and insulating properties.
2. The current work considered the use of Fe_3O_4 , TiO_2 and palm oil as the respective nanoparticle and base oil. It is noted that different nanoparticle-base oil combinations can result in different dielectric properties of the final nanofluids. Therefore, investigation into various nanoparticle-base oil combination can provide valuable information about the dielectric and electrical characteristics of nanofluids.
3. The investigation on partial discharge activity, which is reported in this work, considered stressing the sample for the typical period, which is less than 1 hour. It is recommended that PD studies are performed under longer duration of time to figure out the possible phenomena that might occur under the applied voltage.
4. The electrical properties of nanoparticle such permittivity and its conductivity are changing according to thermal effect. Hence, simulation on how the thermal condition influences the electrical properties of nanoparticle which is dispersed into the base oil and the effects on the nanofluid dielectric responses can be performed.

REFERENCES

- Ab Ghani, S., Muhamad, N. A., Noorden, Z. A., Zainuddin, H., Abu Bakar, N., & Talib, M. A. (2018). Methods for improving the workability of natural ester insulating oils in power transformer applications: A review. *Electric Power Systems Research*, 163, 655–667.
- Abdelmalik, A. A. (2014). Chemically modified palm kernel oil ester: A possible sustainable alternative insulating fluid. *Sustainable Materials and Technologies*, 1–2, 42–51.
- Abeyesundara, D. C., Weerakoon, C., Lucas, J. R., Gunatunga, K. A. I., & Obadage, K. C. (2001). Coconut oil as an alternative to transformer oil. *ERU Symposium*, 1–11.
- Akoh, H., Tsukasaki, Y., Yatsuya, S., & Tasaki, A. (1978). Magnetic properties of ferromagnetic ultrafine particles prepared by vacuum evaporation on running oil substrate. *Journal of Crystal Growth*, 45, 495–500.
- Alj, A., Denat, A., Gosse, J. P., Gosse, B., & Nakamura, I. (1985). Creation of Charge Carriers in Nonpolar Liquids. *IEEE Transactions on Electrical Insulation*, EI-20(2), 221–231.
- Aljure, M., Becerra, M., & Pallon, L. K. H. (2016). Electrical conduction currents of a mineral oil-based nanofluid in needle-plane configuration. *Annual Report - Conference on Electrical Insulation and Dielectric Phenomena, CEIDP, 2016-Decem*, 687–690.
- Aljure, Mauricio, Becerra, M., & Karlsson, M. (2018). Streamer Inception from Ultra-Sharp Needles in Mineral Oil Based Nanofluids. *Energies*, Vol. 11.
- Aluyor, E. O., & Ori-jesu, M. (2009). Biodegradation of mineral oils A review. *African Journal of Biotechnology*, 8(6), 915–920.
- Asano Jr., R., & Page, S. A. (2014). Reducing Environmental Impact and Improving Safety and Performance of Power Transformers With Natural Ester Dielectric Insulating Fluids. *IEEE Transactions on Industry Applications*, 50(1), 134–141.
- Atiya, E. G., Mansour, D. E. A., Khattab, R. M., & Azmy, A. M. (2015). Dispersion behavior and breakdown strength of transformer oil filled with TiO₂ nanoparticles. *IEEE Transactions on Dielectrics and Electrical Insulation*, Vol. 22, pp. 2463–2472.
- Azis, N., Jasni, J., Ab Kadir, M. Z. A., & Mohtar, M. N. (2014). Suitability of palm based oil as dielectric insulating fluid in transformers. *Journal of Electrical Engineering and Technology*, 9(2), 662–669.
- Aziz, N. H., Catterson, V. M., Rowland, S. M., & Bahadoorsingh, S. (2017). Analysis of partial discharge features as prognostic indicators of electrical treeing. *IEEE Transactions on Dielectrics and Electrical Insulation*, 24(1), 129–136.
- Babita, Sharma, S. K., & Gupta, S. M. (2016). Preparation and evaluation of stable nanofluids for heat transfer application: A review. *Experimental Thermal and Fluid*

- Bartnikas, R. (1997). Performance characteristics of dielectrics in the presence of space charge. *IEEE Transactions on Dielectrics and Electrical Insulation*, 4(5), 544–557.
- Berger, L. I. (2000). Dielectric Strength of insulating materials. *Boron*, 1–5.
- Bouaicha, A., Fofana, I., Farzaneh, M., Setayeshmehr, A., Borsi, H., Gockenbach, E., ... Aka, N. T. (2009). Dielectric spectroscopy techniques as quality control tool: a feasibility study. *IEEE Electrical Insulation Magazine*, 25(1), 6–14.
- Brière, G., & Gaspard, F. (1968). Electric conduction in nitrobenzene. *Chemical Physics Letters*, 1(13), 706–708.
- Castellanos, A. (1998). *Electrohydrodynamics* (1st ed.).
- Cavallini, A., Karthik, R., & Negri, F. (2015). The effect of magnetite, graphene oxide and silicone oxide nanoparticles on dielectric withstand characteristics of mineral oil. *IEEE Transactions on Dielectrics and Electrical Insulation*, 22(5), 2592–2600.
- Chang, H., Jwo, C. S., Lo, C. H., Su, C., Tsung, T. T., Chen, L. C., ... Kao, M. J. (2005). Process development and photocatalytic property of nanofluid prepared by combined ASNSS. *Materials Science and Technology*, 21(6).
- Chantrell, R., Popplewell, J., & Charles, S. (1978). Measurements of particle size distribution parameters in ferrofluids. *IEEE Transactions on Magnetics*, 14(5), 975–977.
- Chiesa, M., & Das, S. K. (2009). Experimental investigation of the dielectric and cooling performance of colloidal suspensions in insulating media. *Colloids and Surfaces A: Physicochemical and Engineering Aspects*, 335(1), 88–97.
- Choi, S.-H., & Huh, C.-S. (2013). The Lightning Impulse Properties and Breakdown Voltage of Natural Ester Fluids Near the Pour Point. In *Journal of Electrical Engineering and Technology* (Vol. 8).
- Choi, S. U. S., & Eastman, J. A. (1995). *Enhancing thermal conductivity of fluids with nanoparticles BT - Developments and Applications of Non-Newtonian flows*. New York: ASME.
- Choi, S. U. S., Yu, W., Hull, J. R., Zhang, Z. G., & Lockwood, F. E. (2001). *Nanofluids for vehicle thermal management*. SAE Technical Paper.
- Choudhary, R., Khurana, D., Kumar, A., & Subudhi, S. (2017). Stability analysis of Al₂O₃/water nanofluids. *Journal of Experimental Nanoscience*, 8080, 1–12.
- Dabbak, S. Z., Illias, H. A., & Ang, B. C. (2017). Effect of surface discharges on different polymer dielectric materials under high field stress. *IEEE Transactions on Dielectrics and Electrical Insulation*, 24(6), 3758–3765.
- Darton, R. C., & Sun, K.-H. (1999). The Effect of Surfactant on Foam and Froth Properties. *Chemical Engineering Research and Design*, 77(6), 535–542.

- Dhar, P., Katiyar, A., Maganti, L. S., Pattamatta, A., & Das, S. K. (2016). Superior dielectric breakdown strength of graphene and carbon nanotube infused nano-oils. *IEEE Transactions on Dielectrics and Electrical Insulation*, 23(2).
- Dong, M., Dai, J., Li, Y., Xie, J., Ren, M., & Dang, Z. (2017). Insight into the dielectric response of transformer oil-based nanofluids. *AIP Advances*, 7(2), 25307.
- Du, Y., Lv, Y., Li, C., Chen, M., Zhou, J., Li, X., ... Tu, Y. (2011). Effect of electron shallow trap on breakdown performance of transformer oil-based nanofluids. *Journal of Applied Physics*, 110(10).
- Du, Yuefan, Lv, Y., Li, C., Chen, M., Zhong, Y., Zhou, J., ... Zhou, Y. (2012). Effect of semiconductive nanoparticles on insulating performances of transformer oil. *IEEE Transactions on Dielectrics and Electrical Insulation*, 19(3), 770–776.
- Duy, C. T., Lesaint, O., Denat, A., & Bonifaci, N. (2009). Streamer propagation and breakdown in natural ester at high voltage. *IEEE Transactions on Dielectrics and Electrical Insulation*, , Vol. 16, pp. 1582–1594.
- Edward, J. T. (1970). Molecular volumes and the Stokes-Einstein equation. *Journal of Chemical Education*, 47(4), 261.
- Emara, M. M., Mansour, D. E. A., & Azmy, A. M. (2017). Mitigating the impact of aging byproducts in transformer oil using TiO₂ nanofillers. *IEEE Transactions on Dielectrics and Electrical Insulation*, 24(6), 3471–3480.
- EWT transformer sdn bhd. (n.d.). Oil Immersed Distribution Transformer.
- Fal, J., Mahian, O., & Żyła, G. (2018). Nanofluids in the Service of High Voltage Transformers: Breakdown Properties of Transformer Oils with Nanoparticles, a Review. *Energies*, Vol. 11.
- Fedele, L., Colla, L., Bobbo, S., Barison, S., & Agresti, F. (2011). Experimental stability analysis of different water-based nanofluids. *Nanoscale Research Letters*, 6(1), 300.
- Fernández, I., Ortiz, A., Delgado, F., Renedo, C., & Pérez, S. (2013). Comparative evaluation of alternative fluids for power transformers. *Electric Power Systems Research*, Vol. 98, pp. 58–69.
- Fontes, D. H., Ribatski, G., & Bandarra Filho, E. P. (2015). Experimental evaluation of thermal conductivity, viscosity and breakdown voltage AC of nanofluids of carbon nanotubes and diamond in transformer oil. *Diamond and Related Materials*, 58.
- Frimpong, G. K., Oommen, T. V., & Asano, R. (2011). A survey of aging characteristics of cellulose insulation in natural ester and mineral oil. *IEEE Electrical Insulation Magazine*, Vol. 27, pp. 36–48.
- Ganguly, S., Sikdar, S., & Basu, S. (2009). Experimental investigation of the effective electrical conductivity of aluminum oxide nanofluids. *Powder Technology*, 196(3), 326–330.
- Ghadimi, A., Saidur, R., & Metselaar, H. S. C. (2011). A review of nanofluid stability

properties and characterization in stationary conditions. *International Journal of Heat and Mass Transfer*, 54(17–18), 4051–4068.

Hanai, M., Hosomi, S., Kojima, H., Hayakawa, N., & Okubo, H. (2013). Dependence of TiO₂ and ZnO nanoparticle concentration on electrical insulation characteristics of insulating oil. *2013 Annual Report Conference on Electrical Insulation and Dielectric Phenomena*, 780–783.

Hao, Y., Yu, N., Qi, G., Qin, J., & Zhang, R. (2019). Study on the Influence of Antioxidants on Transformer Oil Related Indicators. *IOP Conference Series: Earth and Environmental Science*, 223(1), 012032.

Herchl, Marton, Tomco, Kopcansky, Timko, Koneracka, & Kolcunova. (2008). Breakdown and partial discharges in magnetic liquids. *Journal Of Physics-Condensed Matter*, 20(20), 204110.

Hoof, M., & Patsch, R. (1994). Analyzing partial discharge pulse sequences-a new approach to investigate degradation phenomena. *Proceedings of 1994 IEEE International Symposium on Electrical Insulation*, 327–331.

Hwang, J. G., O'Sullivan, F., Zahn, M., Hjortstam, O., Pettersson, L. A. A., & Liu, R. (2008). Modeling of Streamer Propagation in Transformer Oil-Based Nanofluids. *Electrical Insulation and Dielectric Phenomena, 2008. CEIDP 2008. Annual Report Conference On*, pp. 361–366.

Hwang, J. G., Zahn, M., O'Sullivan, F. M., Pettersson, L. A. A., Hjortstam, O., & Liu, R. (2010). Effects of nanoparticle charging on streamer development in transformer oil-based nanofluids. *Journal of Applied Physics*, 107(1), 014310.

Hwang, Y., Lee, J.-K., Lee, J.-K., Jeong, Y.-M., Cheong, S. -i., Ahn, Y.-C., & Kim, S. H. (2008). Production and dispersion stability of nanoparticles in nanofluids. *Powder Technology*, 186(2).

Hwang, Y., Lee, J. K., Lee, C. H., Jung, Y. M., Cheong, S. I., Lee, C. G., ... Jang, S. P. (2007). Stability and thermal conductivity characteristics of nanofluids. *Thermochimica Acta*, 455(1–2), 70–74.

Ibrahim, M. E., Abd-Elhady, A. M., & Izzularab, M. A. (2016). Effect of nanoparticles on transformer oil breakdown strength: experiment and theory. *IET Science, Measurement & Technology*, 10(8), 839–845.

IEEE Guide for Acceptance and Maintenance of Natural Ester Fluids in Transformers. (2008). *IEEE Std C57.147-2008*, pp. 1–31.

Illias, H., Chen, G., & Lewin, P. (2011). Partial discharge behavior within a spherical cavity in a solid dielectric material as a function of frequency and amplitude of the applied voltage. *IEEE Transactions on Dielectrics and Electrical Insulation*, 18(2), 432–443.

Illias, H A, Tunio, M. A., Mokhlis, H., Chen, G., & Bakar, A. H. A. (2015). Experiment and modeling of void discharges within dielectric insulation material under impulse voltage. *IEEE Transactions on Dielectrics and Electrical Insulation*, Vol. 22, pp.

- Illias, Hazlee Azil. (2011). *Measurement and simulation of partial discharges within a spherical cavity in a solid dielectric material*. University of Southampton.
- Jadidian, J., Zahn, M., Lavesson, N., Widlund, O., & Borg, K. (2012). Effects of impulse voltage polarity, peak amplitude, and rise time on streamers initiated from a needle electrode in transformer oil. *IEEE Transactions on Plasma Science*, 40(3 PART 2), 909–918.
- Jaroszewski, M., & Rakowiecki, K. (2017). Partial discharge inception voltage in transformer natural ester liquid - Effect of the measurement method in the presence of moisture. *IEEE Transactions on Dielectrics and Electrical Insulation*, 24(4), 2477–2482.
- Jin, H., Andritsch, T., Tsekmes, I. A., Kochetov, R., Morshuis, P. H. F., & Smit, J. J. (2014). Properties of mineral oil based silica nanofluids. *IEEE Transactions on Dielectrics and Electrical Insulation*, 21(3).
- Jin, Huifei, Morshuis, P. H. F., Mor, A. R., & Andritsch, T. (2014). An investigation into the dynamics of partial discharge propagation in mineral oil based nanofluids. *Dielectric Liquids (ICDL), 2014 IEEE 18th International Conference On*, pp. 1–4.
- Jin, Huifei, Morshuis, P., Mor, A. R., Smit, J. J., & Andritsch, T. (2015). Partial discharge behavior of mineral oil based nanofluids. *IEEE Transactions on Dielectrics and Electrical Insulation*, Vol. 22, pp. 2747–2753.
- Jwo, C.-S., Chang, H., Kao, M.-J., & Lin, C.-H. (2007). Photodecomposition of volatile organic compounds using TiO₂ nanoparticles. *Journal of Nanoscience and Nanotechnology*, 7(6), 1947–1952.
- Kanoh, T., Iwabuchi, H., Hoshida, Y., Yamada, J., Hikosaka, T., Yamazaki, A., ... Koide, H. (2008). Analyses of electro-chemical characteristics of Palm Fatty Acid Esters as insulating oil. *2008 IEEE International Conference on Dielectric Liquids*, pp. 1–4.
- Kao, K. C. (1976). Theory of High-Field Electric Conduction and Breakdown in Dielectric Liquids. *IEEE Transactions on Electrical Insulation*, EI-11(4), 121–128.
- Karthik, R., Negri, F., & Cavallini, A. (2016). Influence of ageing on dielectric characteristics of silicone dioxide, tin oxide and ferro nanofluids based mineral oil. *Proceeding of IEEE - 2nd International Conference on Advances in Electrical, Electronics, Information, Communication and Bio-Informatics, IEEE - AEEICB 2016*.
- Kemp, R., Sanchez, R., Mutch, K. J., & Bartlett, P. (2010). Nanoparticle Charge Control in Nonpolar Liquids: Insights from Small-Angle Neutron Scattering and Microelectrophoresis. *Langmuir*, 26(10), 6967–6976.
- Kiyoshi Wakimoto. (2015). Features of Eco-Friendly Transformers Using Palm Fatty Acid Ester (PFAE), a New Vegetable-Based Insulation Oil. *Meiden Review*, (163), 39–45.

- Kopčanský, P., Tomčo, L., Marton, K., Koneracká, M., Timko, M., & Potočová, I. (2005). The DC dielectric breakdown strength of magnetic fluids based on transformer oil. *Journal of Magnetism and Magnetic Materials*, 289, 415–418.
- Kotia, A., Borkakoti, S., Deval, P., & Ghosh, S. K. (2017). Review of interfacial layer's effect on thermal conductivity in nanofluid. *Heat and Mass Transfer*, 53(6), 2199–2209.
- Kurimský, J., Rajňák, M., Cimbala, R., Rajnič, J., Timko, M., & Kopčanský, P. (2019). Effect of magnetic nanoparticles on partial discharges in transformer oil. *Journal of Magnetism and Magnetic Materials*, 165923.
- Lau, K. Y., Piah, M. A. M., & Ching, K. Y. (2017). Correlating the breakdown strength with electric field analysis for polyethylene/silica nanocomposites. *Journal of Electrostatics*, 86, 1–11.
- Lau, K. Y., Vaughan, a S., Chen, G., Hosier, I. L., & Holt, a F. (2013). On the dielectric response of silica-based polyethylene nanocomposites. *Journal of Physics D: Applied Physics*, 46(9), 095303.
- Lee, J.-C., Lee, W.-H., Lee, S.-H., & Lee, S. (2012). Positive and negative effects of dielectric breakdown in transformer oil based magnetic fluids. *Materials Research Bulletin*, 47(10), 2984–2987.
- Lewis, T. J. (2005). Interfaces: nanometric dielectrics. *Journal of Physics D: Applied Physics*, 38(2), 202.
- Li, B., Wang, X., Yan, M., & Li, L. (2003). Preparation and characterization of nano-TiO₂ powder. *Materials Chemistry and Physics*, 78(1), 184–188.
- Li, D., Hong, B., Fang, W., Guo, Y., & Lin, R. (2010). Preparation of Well-Dispersed Silver Nanoparticles for Oil-Based Nanofluids. *Industrial & Engineering Chemistry Research*, 49(4), 1697–1702.
- Li, J., Zhang, Z., Zou, P., Grzybowski, S., & Zahn, M. (2012). Preparation of a vegetable oil-based nanofluid and investigation of its breakdown and dielectric properties. *Electrical Insulation Magazine, IEEE*, 28(5), 43–50.
- Li, Jian, Du, B., Wang, F., Yao, W., & Yao, S. (2016). The effect of nanoparticle surfactant polarization on trapping depth of vegetable insulating oil-based nanofluids. *Physics Letters A*, 380(4), 604–608.
- Li, Jian, Wang, Y., Wang, F., Liang, S., Lin, X., Chen, X., & Zhou, J. (2017). A study on ionization potential and electron trap of vegetable insulating oil related to streamer inception and propagation. *Physics Letters A*, 381(44), 3732–3738.
- Li, Junhao, Si, W., Yao, X., & Li, Y. (2009). Partial discharge characteristics over differently aged oil/pressboard interfaces. *IEEE Transactions on Dielectrics and Electrical Insulation*, 16(6), 1640–1647.
- Li, X., Zhu, D., & Wang, X. (2007). Evaluation on dispersion behavior of the aqueous copper nano-suspensions. *Journal of Colloid and Interface Science*, 310(2), 456–

- Liao, R., Lv, C., Yang, L., Zhang, Y., Wu, W., & Tang, C. (2013). The insulation properties of oil-impregnated insulation paper reinforced with nano-TiO₂. *Journal of Nanomaterials*, 2013.
- Liu, D., Pourrahimi, A. M., Olsson, R. T., Hedenqvist, M. S., & Gedde, U. W. (2015). Influence of nanoparticle surface treatment on particle dispersion and interfacial adhesion in low-density polyethylene/aluminium oxide nanocomposites. *European Polymer Journal*, 66, 67–77.
- Liu, D., Pourrahimi, A. M., Pallon, L. K. H., Sánchez, C. C., Olsson, R. T., Hedenqvist, M. S., ... Gedde, U. W. (2016). Interactions between a phenolic antioxidant, moisture, peroxide and crosslinking by-products with metal oxide nanoparticles in branched polyethylene. *Polymer Degradation and Stability*, 125, 21–32.
- Liu, Donglin, Zhou, Y., Yang, Y., Zhang, L., & Jin, F. (2016). Characterization of high performance AIN nanoparticle-based transformer oil nanofluids. *IEEE Transactions on Dielectrics and Electrical Insulation*, 23(5), 2757–2767.
- Liu, J., Zhou, L., Wu, G., Zhao, Y., Liu, P., & Peng, Q. (2012). Dielectric frequency response of oil-paper composite insulation modified by nanoparticles. *IEEE Transactions on Dielectrics and Electrical Insulation*, 19(2), 510–520.
- Liu, M. S., Lin, M. C. C., Tsai, C. Y., & Wang, C. C. (2006). Enhancement of thermal conductivity with Cu for nanofluids using chemical reduction method. *International Journal of Heat and Mass Transfer*, 49(17–18), 3028–3033.
- Liu, Q., & Wang, Z. D. (2013). Breakdown and withstand strengths of ester transformer liquids in a quasi-uniform field under impulse voltages. , *IEEE Transactions On Dielectrics and Electrical Insulation*, Vol. 20, pp. 571–579.
- Lo, C.-H., Tsung, T.-T., & Chen, L.-C. (2005). Shape-controlled synthesis of Cu-based nanofluid using submerged arc nanoparticle synthesis system (SANSS). *Journal of Crystal Growth*, 277(1), 636–642.
- Lv, Y., Ge, Y., Li, C., Wang, Q., Zhou, Y., Qi, B., ... Yuan, J. (2016). Effect of TiO₂ nanoparticles on streamer propagation in transformer oil under lightning impulse voltage. *IEEE Transactions on Dielectrics and Electrical Insulation*, 23(4).
- Lv, Y. Z., Zhou, Y., Li, C. R., Wang, Q., & Qi, B. (2014). Recent progress in nanofluids based on transformer oil: Preparation and electrical insulation properties. *IEEE Electrical Insulation Magazine*, 30(5), 23–32.
- Lv, Yu-zhen, Li, C., Sun, Q., Huang, M., Li, C., & Qi, B. (2016). Effect of Dispersion Method on Stability and Dielectric Strength of Transformer Oil-Based TiO₂ Nanofluids. *Nanoscale Research Letters*, 11(1), 515.
- Lv, Yuzhen, Du, Y., Li, C., Qi, B., Zhong, Y., & Chen, M. (2013). TiO₂ nanoparticle induced space charge decay in thermal aged transformer oil. *Applied Physics Letters*, 102(13), 132902.

- Lv, Yuzhen, Ge, Y., Wang, L., Sun, Z., Zhou, Y., Huang, M., ... Qi, B. (2018). Effects of Nanoparticle Materials on Prebreakdown and Breakdown Properties of Transformer Oil. *Applied Sciences*, Vol. 8.
- Lv, Yuzhen, Rafiq, M., Li, C., & Shan, B. (2017). Study of Dielectric Breakdown Performance of Transformer Oil Based Magnetic Nanofluids. *Energies*, 10(7), 1025.
- M., H., Salamah, Z. U., Iqtiyani, I. N., & Hang, S. C. (2016). Global electricity demand, generation, grid system, and renewable energy polices: a review. *Wiley Interdisciplinary Reviews: Energy and Environment*, 6(3), e222.
- Mahanta, D. K., & Laskar, S. (2017). Electrical insulating liquid: A review. *Journal of Advanced Dielectrics*, 07(04), 1730001.
- Mahbubul, I. M., Chong, T. H., Khaleduzzaman, S. S., Shahrul, I. M., Saidur, R., Long, B. D., & Amalina, M. A. (2014). *Effect of Ultrasonication Duration on Colloidal Structure and Viscosity of Alumina – Water Nano fluid*.
- Mancini, A., Imperlini, E., Nigro, E., Montagnese, C., Daniele, A., Orru, S., & Buono, P. (2015). Biological and nutritional properties of palm oil and palmitic acid: Effects on health. *Molecules*, 20(9), 17339–17361.
- Mansour, D.-E. A., Elsaed, A. M., & Izzularab, M. A. (2016). The role of interfacial zone in dielectric properties of transformer oil-based nanofluids. *IEEE Transactions on Dielectrics and Electrical Insulation*, 23(6).
- Martin, D., Krause, O., & McPherson, L. (2016). Analysis of the field ageing of natural ester transformer dielectrics: Ten years of data. *Proceedings of the 2016 Australasian Universities Power Engineering Conference, AUPEC 2016*.
- Martin, D., & Wang, Z. D. (2008). Statistical analysis of the AC breakdown voltages of ester based transformer oils. *IEEE Transactions on Dielectrics and Electrical Insulation*, 15(4), 1044–1050.
- Martins, M. A. G. (2010). Vegetable oils, an alternative to mineral oil for power transformers- experimental study of paper aging in vegetable oil versus mineral oil. *IEEE Electrical Insulation Magazine*, Vol. 26, pp. 7–13.
- Matharage, B. S. H. M. S., Fernando, M. A. R. M., Bandara, M. A. A. P., Jayantha, G. A., & Kalpage, C. S. (2013). Performance of coconut oil as an alternative transformer liquid insulation. *IEEE Transactions On Dielectrics and Electrical Insulation*, Vol. 20, pp. 887–898.
- McShane, C. P., Corkran, J., Rapp, K., & Luksich, J. (2006). Natural Ester Dielectric Fluid Development. *Transmission and Distribution Conference and Exhibition, 2005/2006 IEEE PES*, pp. 18–22.
- Mehta, D. M., Kundu, P., Chowdhury, A., Lakhiani, V. K., & Jhala, A. S. (2016). A review on critical evaluation of natural ester vis-a-vis mineral oil insulating liquid for use in transformers: Part 1. *IEEE Transactions on Dielectrics and Electrical Insulation*, 23(2).

- Mentlik, V., Trnka, P., Hornak, J., & Totzauer, P. (2018). Development of a Biodegradable Electro-Insulating Liquid and Its Subsequent Modification by Nanoparticles. *Energies*, Vol. 11.
- Mergos, J. A., Athanassopoulou, M. D., Argyropoulos, T. G., & Dervos, C. T. (2012). Dielectric properties of nanopowder dispersions in paraffin oil. *IEEE Transactions on Dielectrics and Electrical Insulation*, 19(5), 1502–1507.
- Miao, J., Dong, M., Ren, M., Wu, X., Shen, L., & Wang, H. (2013). Effect of nanoparticle polarization on relative permittivity of transformer oil-based nanofluids. *Journal of Applied Physics*, 113(20), 204103.
- Missana, T., & Adell, A. (2000). On the Applicability of DLVO Theory to the Prediction of Clay Colloids Stability. *Journal of Colloid and Interface Science*, 230(1), 150–156.
- Mohamad, A. N., Azis, N., Jasni, J., Ab Kadir, Z. M., Yunus, R., & Yaakub, Z. (2018). Physiochemical and Electrical Properties of Refined, Bleached and Deodorized Palm Oil under High Temperature Ageing for Application in Transformers. *Energies*, Vol. 11.
- Mohamad, N., Azis, N., Jasni, J., Ab Kadir, M., Yunus, R., Yaakub, Z., ... Yaakub, Z. (2018). Ageing Study of Palm Oil and Coconut Oil in the Presence of Insulation Paper for Transformers Application. *Materials*, 11(4), 532.
- Murshed, S. M. S., Leong, K. C., & Yang, C. (2005). Enhanced thermal conductivity of TiO₂—water based nanofluids. *International Journal of Thermal Sciences*, 44(4), 367–373.
- Nazari, M., Rasoulifard, M. H., & Hosseini, H. (2016). Dielectric breakdown strength of magnetic nanofluid based on insulation oil after impulse test. *Journal of Magnetism and Magnetic Materials*, 399, 1–4.
- Negri, F., & Cavallini, A. (2015). Analysis of conduction currents in nanofluids. *2015 IEEE Conference on Electrical Insulation and Dielectric Phenomena (CEIDP)*, pp. 27–30.
- Negri, F., & Cavallini, A. (2017). Effect of dielectrophoretic forces on nanoparticles. *IEEE Transactions on Dielectrics and Electrical Insulation*, 24(3), 1708–1717.
- Nor, S. F. M., Azis, N., Jasni, J., Kadir, M. Z. A. A., Yunus, R., & Yaakub, Z. (2017). Investigation on the electrical properties of palm oil and coconut oil based TiO₂ nanofluids. *IEEE Transactions on Dielectrics and Electrical Insulation*, 24(6), 3432–3442.
- Okamoto, T., & Tanaka, T. (1986). Novel Partial Discharge Measurement Computer-Aided Measurement Systems. *IEEE Transactions On Dielectric and Electrical Insulation*, EI-21(6), 1015–1019.
- Oommen, T. V. (2002). Vegetable oils for liquid-filled transformers. *IEEE Electrical Insulation Magazine*, 18(1), 6–11.

- Oommen, T. V., Claiborne, C. C., & Mullen, J. T. (2002). Biodegradable electrical insulation fluids. *Proceedings: Electrical Insulation Conference and Electrical Manufacturing and Coil Winding Conference*, 465–468.
- Palm, E. B. H. and N. N. and M. S. and M. B. and S. A. M. and H. P. and R. K. and M. S. T. and M. M. and B. (2013). Shelf stability of nanofluids and its effect on thermal conductivity and viscosity. *Measurement Science and Technology*, 24(10), 105301.
- Patsch, R., & Berton, F. (2002). Pulse Sequence Analysis - a diagnostic tool based on the physics behind partial discharges. *Journal of Physics D: Applied Physics*, 35(1), 25–32.
- Peppas, G. D., Bakandritsos, A., Charalampakos, V. P., Pyrgioti, E. C., Tucek, J., Zboril, R., & Gonos, I. F. (2016). Ultrastable Natural Ester-Based Nanofluids for High Voltage Insulation Applications. *ACS Applied Materials and Interfaces*, 8(38).
- Pompili, M., & Bartnikas, R. (2012). On partial discharge measurement in dielectric liquids. *IEEE Transactions on Dielectrics and Electrical Insulation*, 19(5), 1476–1481.
- Pourrahimi, A. M., Olsson, R. T., & Hedenqvist, M. S. (2017, November 13). The Role of Interfaces in Polyethylene/Metal-Oxide Nanocomposites for Ultrahigh-Voltage Insulating Materials. *Advanced Materials*, p. 1703624.
- Primo, V. A., Garcia, B., & Albarracin, R. (2018). Improvement of transformer liquid insulation using nanodielectric fluids: A review. *IEEE Electrical Insulation Magazine*, 34(3), 13–26.
- Quinchia, L. A., Delgado, M. A., Franco, J. M., Spikes, H. A., & Gallegos, C. (2012). Low-temperature flow behaviour of vegetable oil-based lubricants. *Industrial Crops and Products*, 37(1), 383–388.
- Rafiq, M., Li, C., Lv, Y., Yi, K., & Sun, Q. (2016). Breakdown characteristics of mineral oil based magnetic nanofluids. *ICHVE 2016 - 2016 IEEE International Conference on High Voltage Engineering and Application*.
- Rafiq, Muhammad, Lv, Y., & Li, C. (2016). A Review on Properties, Opportunities, and Challenges of Transformer Oil-Based Nanofluids. *Journal of Nanomaterials*, 2016.
- Rahim, N. H., Lau, K. Y., Kamarudin, S. N. H., Muhamad, N. A., Mohamad, N., & Rahman, W. A. W. A. (2018). Effect of Nanofiller Calcination on Breakdown Performance of Silica Based Polyethylene Nanocomposites. *2018 IEEE 7th International Conference on Power and Energy (PECon)*, 91–95.
- Rajab, A., Umar, K., Hamdani, D., Aminuddin, S., Suwarno, Abe, Y., ... Hikita, M. (2011). Partial discharge phase distribution of palm oil as insulating liquid. *Telkomnika*, 9(1), 151–160.
- Raymon, A., Pakianathan, P. S., Rajamani, M. P. E., & Karthik, R. (2013). Enhancing the critical characteristics of natural esters with antioxidants for power transformer applications. *IEEE Transactions on Dielectrics and Electrical Insulation*, 20(3), 899–912.

- Rudnick, L. (2013). *Synthetics, Mineral Oils, and Bio-Based Lubricants*.
- Saenkhumwong, W., & Suksri, A. (2015). Investigation on Voltage Breakdown of Natural Ester Oils Based-On ZnO Nanofluids. *Advanced Materials Research*, 1119, 175–178.
- Sarojini, K. G. K., Manoj, S. V., Singh, P. K., Pradeep, T., & Das, S. K. (2013). Electrical conductivity of ceramic and metallic nanofluids. *Colloids and Surfaces A: Physicochemical and Engineering Aspects*, 417, 39–46.
- Sartoratto, P. P. C., Neto, A. V. S., Lima, E. C. D., Rodrigues de Sá, A. L. C., & Morais, P. C. (2005). Preparation and electrical properties of oil-based magnetic fluids. *Journal of Applied Physics*, 97(10), 10Q917.
- Segal, V., Nattrass, D., Raj, K., & Leonard, D. (1999). Accelerated thermal aging of petroleum-based ferrofluids. *Journal of Magnetism and Magnetic Materials*, 201(1), 70–72.
- Segal, Vladimir, Hjortsberg, A., Rabinovich, A., Nattrass, D., & Raj, K. (1998). AC (60 Hz) and impulse breakdown strength of a colloidal fluid based on transformer oil and magnetite nanoparticles. *IEEE International Symposium On Electrical Insulation*, 1998. 2, 619–622.
- Sha, Y., Zhou, Y., Nie, D., Wu, Z., & Deng, J. (2014). A study on electric conduction of transformer oil. *IEEE Transactions on Dielectrics and Electrical Insulation*, 21(3), 1061–1069.
- Shin, S. K., & Kim, T. S. (2006). Levels of polychlorinated biphenyls (PCBs) in transformer oils from Korea. *Journal of Hazardous Materials*, 137(3), 1514–1522.
- Sima, W., Shi, J., Yang, Q., & Yu, F. (2014). Surface modification of nanoparticle and its charging dynamics during streamer discharge in transformer oil. *Nanoscience and Nanotechnology Letters*, 6(5).
- Sima, Wenxia, Shi, J., Yang, Q., Huang, S., & Cao, X. (2015). Effects of conductivity and permittivity of nanoparticle on transformer oil insulation performance: experiment and theory. *IEEE Transactions On Dielectrics and Electrical Insulation*, Vol. 22, pp. 380–390.
- Sinan, S. S., Shawaludin, S. N., Jasni, J., Azis, N., Kadir, M. Z. A. A., & Mohtar, M. N. (2014). Investigation on the AC breakdown voltage of RBDPO Olein. *2014 IEEE Innovative Smart Grid Technologies - Asia (ISGT ASIA)*, pp. 760–763.
- Singh, A. K., & Raykar, V. S. (2008). Microwave synthesis of silver nanofluids with polyvinylpyrrolidone (PVP) and their transport properties. *Colloid and Polymer Science*, 286(14), 1667–1673.
- Smalo, H. S., Astrand, P. O., & Ingebrigtsen, S. (2010). Calculation of ionization potentials and electron affinities for molecules relevant for streamer initiation and propagation. *IEEE Transactions on Dielectrics and Electrical Insulation*, 17(3), 733–741.

- Smith, R. C., Hui, L., Nelson, J. K., & Schadler, L. S. (2009). Interfacial charge behavior in nanodielectrics. *Electrical Insulation and Dielectric Phenomena, 2009. CEIDP '09. IEEE Conference On*, 650–653.
- Suttiponparnit, K., Jiang, J., Sahu, M., Suvachittanont, S., Charinpanitkul, T., & Biswas, P. (2010). Role of Surface Area, Primary Particle Size, and Crystal Phase on Titanium Dioxide Nanoparticle Dispersion Properties. *Nanoscale Res Lett*, 6(1), 27.
- Tagmouti, S., Bouzit, S. E., Costa, L. C., Graça, M. P. F., & Outzourhit, A. (2015). Impedance Spectroscopy of Nanofluids based on Multiwall Carbon Nanotubes. *Spectroscopy Letters*, 48(10), 761–766.
- Tanaka, T. (2005). Dielectric nanocomposites with insulating properties. *Dielectrics and Electrical Insulation, IEEE Transactions On*, 12(5), 914–928.
- Tanaka, Toshikatsu, Kozako, M., Fuse, N., & Ohki, Y. (2005). Proposal of a multi-core model for polymer nanocomposite dielectrics. *IEEE Transactions on Dielectrics and Electrical Insulation*, 12(4), 669–681.
- Top, T. V, Massala, G., & Lesaint, O. (2002). Streamer propagation in mineral oil in semi-uniform geometry. *IEEE Transactions on Dielectrics and Electrical Insulation*, 9(1), 76–83.
- Unge, M., Singha, S., Van Dung, N., Linhjell, D., Ingebrigtsen, S., & Lundgaard, L. E. (2013). Enhancements in the lightning impulse breakdown characteristics of natural ester dielectric liquids. *Applied Physics Letters*, 102(17), 172905.
- Velasco, J., Frascella, R., Albarracín, R., Burgos, C. J., Dong, M., Ren, M., & Yang, L. (2018). Comparison of Positive Streamers in Liquid Dielectrics with and without Nanoparticles Simulated with Finite-Element Software. *Energies*, Vol. 11.
- Wang, M., Vandermaar, A. J., & Srivastava, K. D. (2002). Review of condition assessment of power transformers in service. *IEEE Electrical Insulation Magazine*, 18(6), 12–25.
- Wang, Q., Rafiq, M., Lv, Y., Li, C., & Yi, K. (2016). Preparation of three types of transformer oil-based nanofluids and comparative study on the effect of nanoparticle concentrations on insulating property of transformer oil. *Journal of Nanotechnology*, 2016.
- Wilhelm, H., Feitosa, L., Silva, L., Cabrino, A., & Ramos, L. (2015). Evaluation of in-service oxidative stability and antioxidant additive consumption in corn oil based natural ester insulating fluid. *IEEE Transactions on Dielectrics and Electrical Insulation*, 22(2), 864–868.
- Wu, N., Fu, L., Su, M., Aslam, M., Wong, K. C., & Dravid, V. P. (2004). Interaction of Fatty Acid Monolayers with Cobalt Nanoparticles. *Nano Letters*, 4(2), 383–386.
- Yu, W., & Xie, H. (2012). A Review on Nanofluids: Preparation, Stability Mechanisms, and Applications. *Journal of Nanomaterials*, 2012, 1–17.
- Z Liu, Q. L. and Z. D. W. (2016). Effect of electric field configuration on streamer and

partial discharge phenomena in a hydrocarbon insulating liquid under AC stress. *Journal of Physics D: Applied Physics*, 49(18), 185501.

Zaengl, W. S. (2003). Dielectric spectroscopy in time and frequency domain for HV power equipment. I. Theoretical considerations. *IEEE Electrical Insulation Magazine*, 19(5), 5–19.

Zare, Y., & Rhee, K. Y. (2017). Development of a Model for Electrical Conductivity of Polymer/Graphene Nanocomposites Assuming Interphase and Tunneling Regions in Conductive Networks. *Industrial & Engineering Chemistry Research*, 56(32), 9107–9115.

Zawrah, M. F., Khattab, R. M., Girgis, L. G., El Daidamony, H., & Abdel Aziz, R. E. (2016). Stability and electrical conductivity of water-base Al₂O₃ nanofluids for different applications. *HBRC Journal*, 12(3), 227–234.

Zhang, J., Wang, F., Li, J., Ran, H., & Huang, D. (2017). Influence of copper particles on breakdown voltage and frequency-dependent dielectric property of vegetable insulating oil. *Energies*, 10(7), 938.

Zhang, Z., Li, J., Zou, P., & Grzybowski, S. (2010). Electrical properties of nano-modified insulating vegetable oil. *Electrical Insulation and Dielectric Phenomena (CEIDP), 2010 Annual Report Conference On*, pp. 1–4.

Zhong, Y., Lv, Y., Li, C., Du, Y., Chen, M., Zhang, S., ... Chen, L. (2013). Insulating properties and charge characteristics of natural ester fluid modified by TiO₂ semiconductive nanoparticles. *IEEE Transactions on Dielectrics and Electrical Insulation*, 20(1).

LIST OF PUBLICATIONS AND PAPERS PRESENTED

List of journal papers:

1. Makmud, M. Z. H., Illias, H. A., Chee, C. Y., & Sarjadi, M. S. (2018). Influence of Conductive and Semi-Conductive Nanoparticles on the Dielectric Response of Natural Ester-Based Nanofluid Insulation. *Energies*, 11(2), 333. **(ISI-Indexed)**
2. Makmud, Mohamad, Illias, H., Chee, C., & Dabbak, S. (2019). Partial Discharge in Nanofluid Insulation Material with Conductive and Semiconductive Nanoparticles. *Materials*, 12(5), 816. **(ISI-Indexed)**

List of conference paper:

1. Makmud, M. Z. H., Illias, H. A., & Chee, C. Y. (2017). Partial Discharge Behaviour within Palm Oil-based Fe₂O₃ Nanofluids under AC Voltage. *IOP Conference Series: Materials Science and Engineering*, 210(1), 12034.
2. Makmud, M. Z. H., Illias, H. A., & Chee, C. Y. (2018). Partial Discharge Behaviours of Natural Ester-based Conductive Nanoparticles. *2018 MyHVnet Colloquium*, Selangor, Malaysia.